

# **Characterisation of photo-switching in fluorescent molecules at low temperatures**

Dissertation  
zur Erlangung des Doktorgrades  
an der Fakultät für Mathematik, Informatik und Naturwissenschaften  
Fachbereich Physik  
der Universität Hamburg

vorgelegt von  
Vi Quint Duong

Hamburg  
2023

---

Provando e riprovando

---

Gutachter\*innen der Dissertation:

Prof. Dr. Rainer Kaufmann  
Prof. Dr. Arwen Pearson

Zusammensetzung der Prüfungskommission:

Prof. Dr. Daniela Pfannkuche  
Prof. Dr. Rainer Kaufmann  
Prof. Dr. Arwen Pearson  
Prof. Dr. Kay Grünewald  
Prof. Dr. Thomas Marlovits

Vorsitzende\*r der Prüfungskommission:

Prof. Dr. Daniela Pfannkuche

Datum der Disputation: 19.10.2023

Vorsitzender Fach-Promotionsausschuss PHYSIK:

Prof. Dr. Markus Drescher

Leiter des Fachbereichs PHYSIK:

Prof. Dr. Wolfgang J. Parak

Dekan der Fakultät MIN:

Prof. Dr.-Ing. Norbert Ritter

# Contents

1. Abstract	1
2. Zusammenfassung	2
3. Introduction	3
4. Fundamental principles	5
4.1. Fluorescence	5
4.1.1. Fluorescence intermittence	5
4.2. Resolution limit	6
4.3. Super-resolution microscopy	8
4.3.1. STED microscopy	8
4.3.2. Structured illumination	10
4.3.3. Single molecule localisation microscopy	10
4.3.4. SOFI	11
4.4. Vitrification	12
4.5. Photo-physics under cryogenic conditions	14
4.6. Cryogenic super-resolution fluorescence microscopy	14
4.6.1. Cryo-SMLM	15
4.6.2. Cryo-SOFI	16
4.6.3. SR-cryo-CLEM	16
5. Methods	17
5.1. Fluorescence cryogenic microscope	17
5.1.1. Mechanical instabilities of the setup	18
5.2. Bespoke cryogenic fluorescence microscope	19
5.3. Plunge freezing	21
5.3.1. Shigella samples	21
5.3.2. Non-vitrified samples	21
6. Developed algorithms and software	22



7. Results	26
7.1. Autocorrelation analysis of blinking and fluctuating fluorescent states of single Alexa Fluor 647 molecules in vitrified PBS . . . . .	26
7.1.1. Categorization of time profiles . . . . .	27
7.1.2. Analysis of Alexa Fluor 647 molecules in vitrified PBS . . . . .	29
7.2. Autocorrelation analysis of different organic dyes in vitrified PBS in comparison . . . . .	32
7.3. Categorization of organic dyes in vitrified PBS in comparison . . . . .	33
7.4. Determination of on and off times for the FB category . . . . .	36
7.5. Investigation of the effect of different environments on blinking and fluctuating fluorescent states for single Alexa Fluor 647 molecules . . . . .	39
7.5.1. Autocorrelation based comparison of different environments for Alexa Fluor 647 molecules . . . . .	39
7.5.2. Categorization comparison of Alexa Fluor 647 molecules in different environments . . . . .	41
7.5.3. Determination of on- and off-times of single Alexa Fluor 647 molecules for the FB category . . . . .	42
7.6. Influence of heavy water on photo-physics of organic dyes . . . . .	43
7.7. Qualitative analysis of multiple fluorescent states in individual single molecule time traces . . . . .	46
7.8. Qualitative analysis of changes in single molecule switching on a time interval of hours . . . . .	51
7.9. UV recovery of different organic dye molecules . . . . .	52
7.10. Using fast fluorescence fluctuations for super-resolution cryo-FM imaging of shigella labelled with Alexa Fluor 647 . . . . .	55
7.11. Investigation of blinking in "super blinking nanoparticles" . . . . .	56
7.12. Investigation of blinking and bleaching of fluorescent proteins in vitrified cells . . . . .	57
8. Discussion	60
8.1. Autocorrelation and category analysis of blinking and fluctuating fluorescent states in single organic dyes . . . . .	60
8.2. Qualitative analysis of multiple fluorescent states in individual single molecule time traces . . . . .	62
8.3. Determination of on and off times for the FB category . . . . .	63
8.4. Influence of heavy water on photo-physics of organic dyes . . . . .	64
8.5. UV recovery of different organic dye molecules . . . . .	65
8.6. Using fast fluorescence fluctuations for super-resolution cryo-FM imaging of shigella labelled with Alexa Fluor 647 . . . . .	65
8.7. Investigation of blinking in "super blinking nanoparticles" . . . . .	66

---

8.8. Investigation of blinking and bleaching of fluorescent proteins in vitrified cells . . . . .	66
9. Conclusion	68
10. Outlook	69
Bibliography	70
A. Danksagung	79
B. Erklärung	80

# 1. Abstract

Super-resolution microscopy (SRM) enables the generation of light microscopy images below the diffraction limit. To study biological structures with highest spatial resolution, they have to be immobilized to avoid movement during data acquisition. Classical chemical fixation methods are widespread but can lead to structural artefacts. On the contrary, cryo-immobilization methods achieve structural preservation in a near-native state. Fast freezing techniques (vitrification) are already successfully used to immobilized samples in a near-native state for electron cryo-microscopy. This opens up the path to cryo-SRM. Even though there are already successful attempts in cryo-SRM the underlying photo-physical processes at low temperature are different from ambient temperature and largely unknown. In this thesis several fluorescent organic dyes are investigated for their suitability for cryo-SRM. It was found that all investigated dyes show fluorescence fluctuation in the 10 millisecond time range which can be used by cryogenic super-resolution optical fluctuation imaging (cryo-SOFI) for a resolution enhancement of up to threefold. Furthermore, fluorescence intermittence at longer time ranges was observed, which can be used for cryogenic single molecule localization microscopy (cryo-SMLM) leading to a spatial resolution of 10-20 nm. These findings show that one dye can be used for different resolution enhancements depending on their mode of switching between the fluorescent state and non-fluorescent state(s).

## 2. Zusammenfassung

Die superauflösende Mikroskopie (SRM) ermöglicht die Erzeugung von lichtmikroskopischen Bildern unterhalb der Beugungsgrenze. Um biologische Strukturen mit höchster räumlicher Auflösung untersuchen zu können, müssen sie immobilisiert werden, damit sie sich während der Datenerfassung nicht bewegen. Klassische chemische Fixierungsmethoden sind weit verbreitet, können aber zu strukturellen Artefakten führen. Im Gegensatz dazu erreichen Kryo-Immobilisierungsmethoden eine Strukturhaltung in einem nahezu natürlichen Zustand. Vitrifikation, eine Immobilisierungsmethode, in der die Proben so schnell eingefroren werden, dass die Wassermoleküle keine kristalline Struktur ausbilden können, wurde bereits erfolgreich eingesetzt, um Proben für die Elektronenkryomikroskopie in einem nahezu nativen Zustand zu immobilisieren. Dies eröffnet den Weg zum Kryo-SRM. Obwohl es bereits erfolgreiche Versuche im Kryo-SRM gibt, sind die zugrundeliegenden photophysikalischen Prozesse bei niedrigen Temperaturen anders als bei Umgebungstemperatur und weitgehend unbekannt. In dieser Arbeit wurden verschiedene organische Fluoreszenzfarbstoffe auf ihre Eignung für Kryo-SRM untersucht. Es wurde festgestellt, dass alle untersuchten Farbstoffe Fluoreszenzfluktuationen im Zeitbereich von 10 Millisekunden aufweisen, die mit Hilfe der kryogenen superauflösenden optischen Fluktuationsbildgebung (cryo-SOFI) für eine bis zu dreifache Auflösungsverbesserung genutzt werden können. Darüber hinaus wurden Fluoreszenzunterbrechungen bei längeren Zeitspannen beobachtet, die für die kryogene Einzelmolekül-Lokalisierungsmikroskopie (cryo-SMLM) verwendet werden können, was zu einer räumlichen Auflösungsverbesserung auf 10-20 nm führt. Diese Ergebnisse zeigen, dass ein und derselbe Farbstoff für unterschiedliche Auflösungsverbesserungen verwendet werden kann, je nachdem, wie er zwischen einem fluoreszierenden und mehreren nicht fluoreszierenden Zuständen wechselt.

### 3. Introduction

To take a look into the microscopic world of a cell some device has to be used to magnify the object of interest. Microscopes can give an insight into a complete new environment that was "hidden" from our eyes. But even with the most advanced light microscope the resolution is limited by diffraction and is defined by the Abbe diffraction limit<sup>1</sup> which is roughly 200 nm for visible light. To achieve even higher resolution electrons instead of photons can be used to create an image. Since the wavelength of electrons can be much smaller than photons much higher resolution can be achieved and it is possible to resolve at atomic scale.<sup>2</sup> Fast freezing techniques (vitrification) provide methods to immobilize biological samples which freeze the samples rapidly preventing the formation of crystalline ice and are kept at -196°C. With this, the samples are embedded in amorphous ice, preserving them in their near native state.<sup>3</sup> This method is preventing structural artefacts which can be caused by chemical fixation. By using electron cryo-microscopy (cryo-EM) resolutions in the Ångstrom scale can be achieved for protein structures.<sup>4,5</sup> Even though the high resolution of cryo-EM enables the structural analysis of proteins in its biological context it might be hard to actually find the proteins or events of interest, if imaging inside cells. This can be resolved by combining the specific labelling of fluorescence cryo-microscopy (cryo-FM) to localize the proteins or events and the structural information at high resolution of cryo-EM.<sup>6,7</sup> The resolution of conventional cryo-FM is limited to 350-450 nm.<sup>8</sup> However, with the introduction of super-resolution microscopy (SRM) for imaging vitrified samples under cryo-conditions, this limit can be circumvented. By using cryo-SRM in cryo-CLEM the resolution gap between cryo-FM and cryo-EM can be reduced and the proteins or events of interest can be better localized. First proof of the feasibility of cryo-SRM and correlation with cryo-EM was already shown.<sup>9-11</sup> However, the photo-physical properties of the dyes used for cryo-SRM are still unknown and conflicting.<sup>9,11,12</sup>

For cryogenic single molecule localization microscopy (cryo-SMLM) the photo-physical behaviour of dyes especially the fluorescence intermittance (blinking) is crucial for the resolution enhancement. Long off or dark states and short and bright fluorescent states are ideal for cryo-SMLM. Challenges for the investigation of the photo-physical properties are poor mechanical and thermal stability of microscopes causing drift and inhibiting long term studies and the sample preparation itself. The sample preparation and the handling under cryogenic conditions is a challenging task. Furthermore, the medium used to solve changes the photo physics of the dyes. Additionally, the carbon film of the sample

carrier introduces additional background signal reducing the signal to noise ratio.

The aim of this thesis is to investigate the photo-physical properties of different fluorescent organic dyes at low temperature. For this, a workflow is established in this thesis to automatically process the data of the dyes as much as possible. Furthermore, the suitability for cryogenic super-resolution optical fluctuation imaging (cryo-SOFI) and cryo-SMLM is investigated. It was found that one dye shows different blinking behaviour at different time scales. At shorter time scale the blinking is really fast and are close to fluctuation with can be used by the cryo-SOFI algorithm to get an resolution enhancement. The blinking at longer time scales are also longer in duration and can be used by the cryo-SMLM algorithm to get an even higher resolution enhancement. A deeper understanding would further improve the resolution enhancement for biological samples.

## 4. Fundamental principles

### 4.1. Fluorescence

Fluorescent molecules can be excited by a photon with enough energy  $h\nu_{Ex}$  from the ground state  $S_0$  to a higher excited singlet state like  $S_1$  or  $S_2$  which takes femtoseconds. From this excited state it relaxes via internal conversion (IC) (picoseconds) to the lowest vibrational state. From there it can relax into the ground state  $S_0$  again by emitting a photon with less energy  $h\nu_F$  (nanoseconds) and is called fluorescence. The difference between  $h\nu_{Ex}$  and  $h\nu_F$  is called Stokes shift. By using appropriate filters and dichroic mirrors the fluorescence signal from the dyes can be separated from the excitation laser and other background signals that do not have the same wavelength as the dyes emission wavelength. Leading to a higher contrast. From the excited state  $S_1$  it is also possible that the molecule reach a triplet state via intersystem crossing (ISC). Since this transition is quantum mechanically forbidden the rate is much lower and has to fulfil certain criteria. It stays here for  $\mu\text{s}$  to minutes before it returns either nonradiative or radiative which is called phosphorescence.<sup>13</sup> These processes are shown in Fig. 4.1.

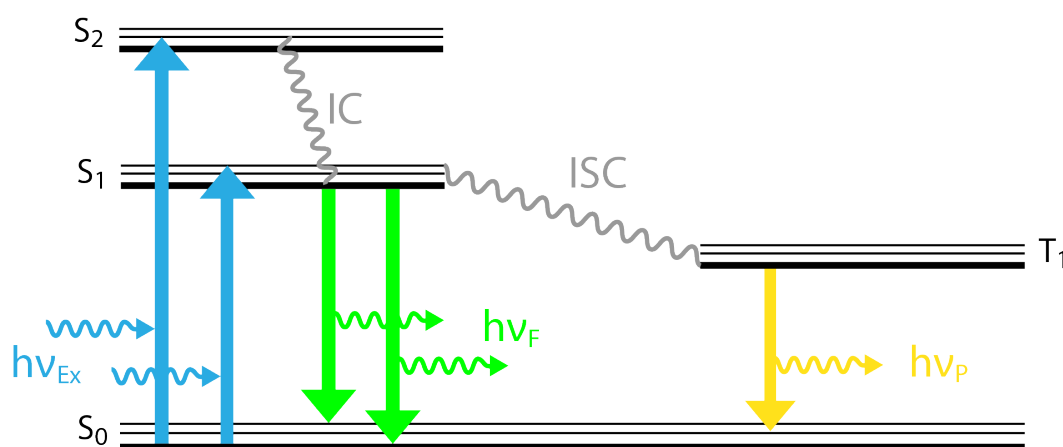


**Fig. 4.1.** Schematic illustration of the fluorescence and phosphorescence process.

#### 4.1.1. Fluorescence intermittence

Fluorophores irradiated with light might start to "blink" on the single molecule level. This is caused by the intersystem crossing (ISC) to a triplet state, which has a longer lifetime of typically micro- to milliseconds compared to the fluorescent state. It is also

possible that the molecules transition via the triplet state into a long-lived dark state with a life time of milliseconds to several hundreds of seconds.<sup>14</sup> It was shown that this state is not a triplet state since it is temperature independent.<sup>1516</sup> In Fig. 4.2 a extended Jabłoński diagram illustrates the transition to a long-lived state and ultimately also the irreversible bleaching is shown. The molecule can reach this dark state by either reduction or oxidation and can return to the ground state by the inverse, reduction or oxidation. From this dark state it is also possible for the molecule to transition into the irreversible bleached state.

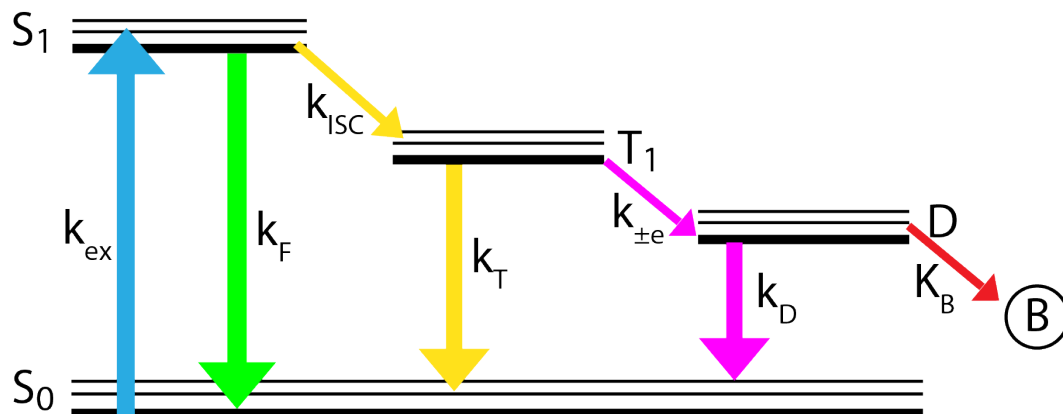


**Fig. 4.2.** Extended Jabłoński showing the possible route from fluorescent state over the triplet state and a long-lived dark state to irreversible photo bleaching. Based on two different publications.<sup>1516</sup>

## 4.2. Resolution limit

In light microscopy the resolution can not resolve features below the diffraction limit. If the light passes a circular aperture the light will be diffracted at the aperture and generate a diffraction pattern in the far field called airy pattern and the innermost part is called airy disk, which is shown in Fig. 4.3.

A point like emitter below the diffraction limit which is imaged by an optical system will reach the detector blurred. The function by which the emitter is blurred is called point spread function (PSF). The intensity distribution  $I_{image}(x_2, y_2)$  of the imaged fluorophores  $P_F(x_1, y_1)$  through an optical system is given by:

$$I_{image}(x_2, y_2) = PSF \otimes P_F(x_1, y_1) \quad (4.1)$$

From (4.1) follows that the resolution limit of a system is defined by the smallest distance it can resolve between to point sources. If the distance falls below this limit the overlap of the airy disk is to high and the point sources can not be differentiated any more. There are different definition for the resolution limit. For the definitions the numerical aperture NA has to be introduced which is defined as:



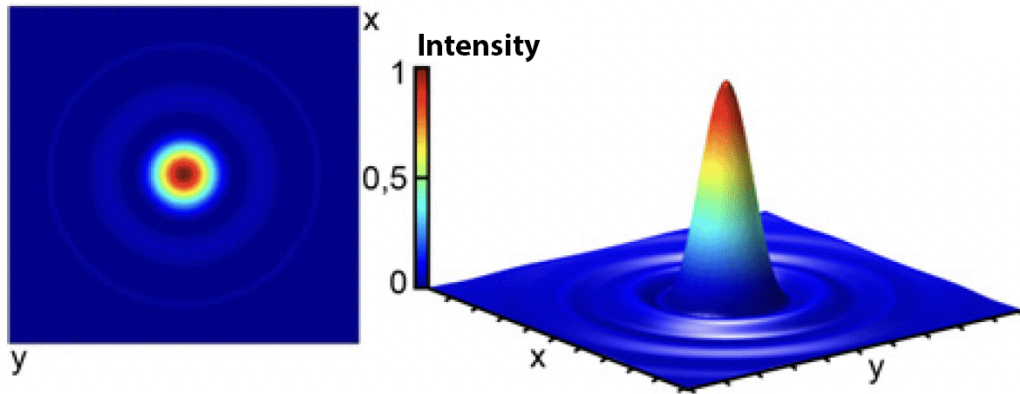


**Fig. 4.3.** PSF of a point source passing through a circular aperture. The intensity is normalized and colour coded. Modified from Kaufmann.<sup>17</sup>

$$NA = \sin \alpha \quad (4.2)$$

with  $n$  the refractive index of the medium,  $\alpha$  half of angle of the cone of light entering the lens.

The distance between two point sources can be resolved if the 0. and 1. order of the diffraction pattern can be resolved. This is the Abbe criterion and is defined with:<sup>1</sup>

$$D = 0.5 \frac{\lambda}{NA} \quad (4.3)$$

with  $\lambda$  the used wavelength.

A different definition is given by the Rayleigh criterion:<sup>18</sup> Two point sources can still be resolved if the maximum of one airy disk falls into the first minimum of the other airy disk.

$$D = 0.61 \frac{\lambda}{NA} \quad (4.4)$$

Sparrow gave another definition for the resolution limit of a system with the Sparrow criterion:<sup>19</sup> The minimal distance of two point sources is given by the distance where the intensity at the midpoint between the peaks shows a minimum. This is suitable for similar bright point sources with similar wavelengths and is defined with:

$$D = 0.47 \frac{\lambda}{NA} \quad (4.5)$$

The above defined criteria are shown in Fig. 4.4.

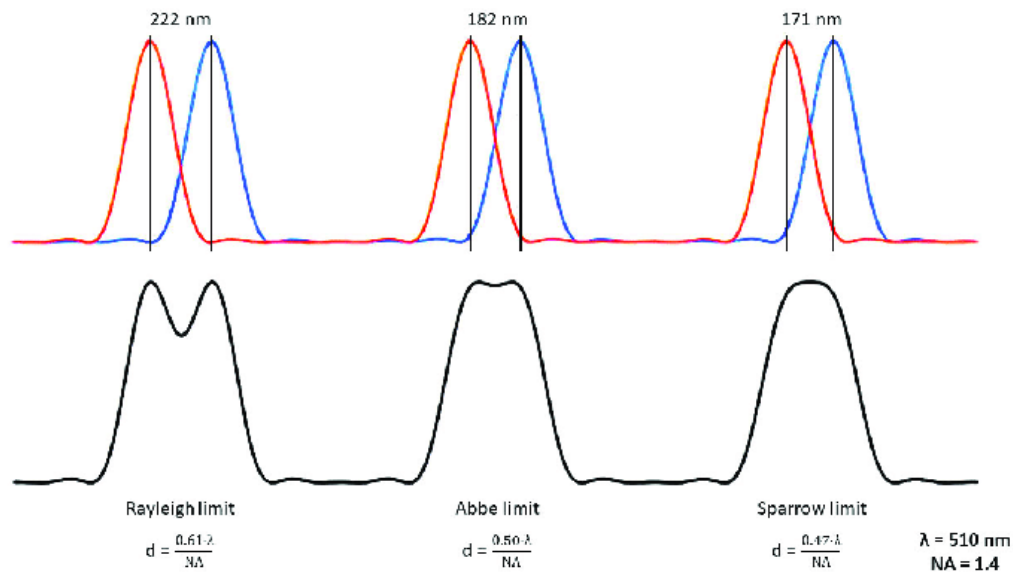


**Fig. 4.4.** Illustrations of the three criteria. With resolution limit examples for a wavelength of 510 nm and  $NA = 1.4$ .<sup>20</sup>

### 4.3. Super-resolution microscopy

There are different possibilities to improve the resolution of a fluorescence microscope. Based on the resolution limit mentioned above one possibility would be to reduce the wavelength as used in x-ray or electron microscopy. However, reducing the wavelength comes with several problems. The transmission for shorter wavelengths drops significantly and the high energy photons damages the biological sample especially the DNA. Another possibility is to increase the NA, which is limited to 0.9 for air objective lenses and to 1.4 for immersion objective lenses. Additionally, there is no immersion objective lens for cryogenic conditions.<sup>8</sup>

A different way is to use methods which "circumvent" the resolution limit. Those methods are described in the following. A schematic overview for the methods is shown in Fig. 4.5.

#### 4.3.1. STED microscopy

Stimulated emission depletion (STED)<sup>22</sup> bases on saturable and reversible optical transitions between two different states of a fluorophore. A STED microscope works like a confocal microscope by scanning the sample. Additionally, most of the fluorophores are deactivated in the focal area with a torus shaped STED laser which has a minimum in its center. The number of fluorophores, which are still in their radiative state depends on the intensity of the STED laser. This enables the volume of the fluorescent molecules to be smaller than the PSF of the system. Therefore circumventing the resolution limit. The Abbe criterion can be appended for STED microscopy as follow:<sup>23</sup>

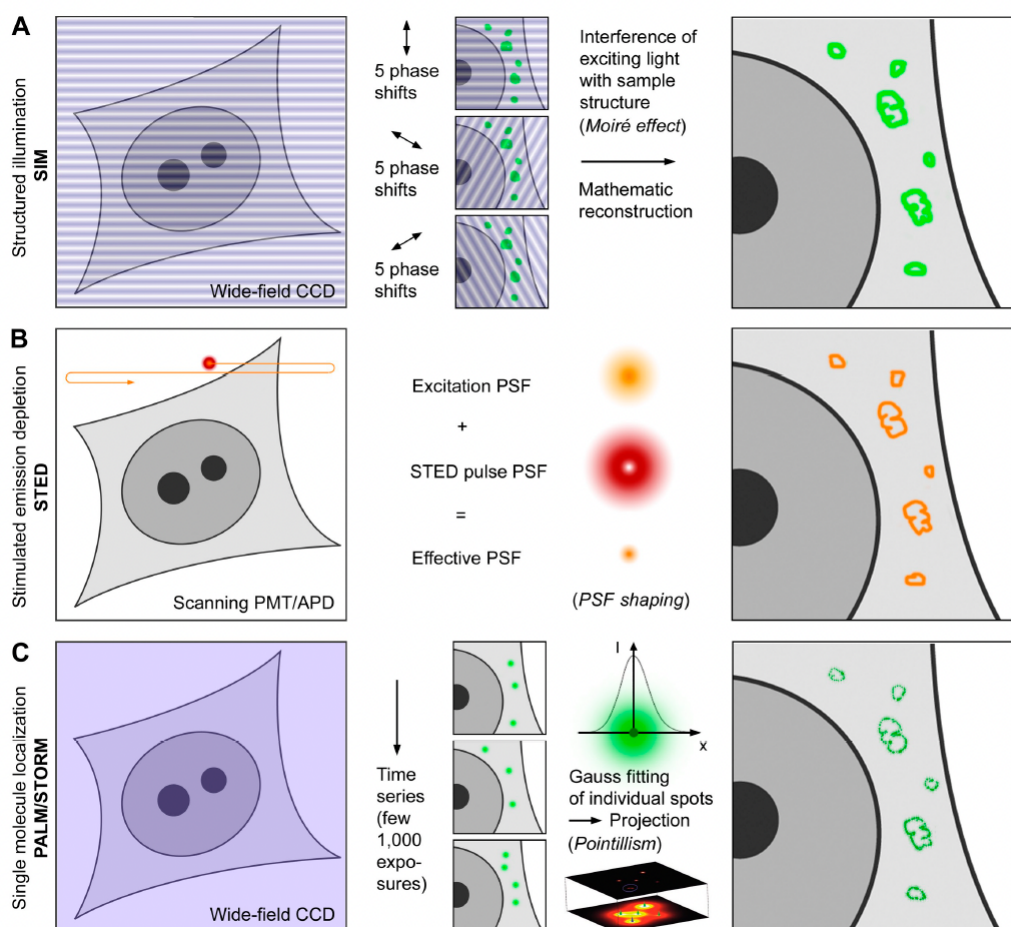


**Fig. 4.5.** Schematic showing the super-resolution principles. A: In SIM the sample is illuminated with a periodic pattern which combines with sample structures below the diffraction limit to generate moiré fringes. This allows a reconstruction of a high-resolution image from typically 15 raw images. The resolution improvement is limited to double the resolution. B: In STED microscopy the sample is scanned by two overlapping laser beams, which are pulsed with a time delay to each other. The first laser excites the fluorophores, while the second laser returns the fluorophores in the ground state by stimulated emission. The second laser has a torus shaped which has a minimum in its center, leading to a volume of molecules remaining in the fluorescent state which is smaller than the diffraction limit. C: Single molecule localization microscopy utilize the temporal separation the fluorophores which is achieved by either photoactivation, photoswitching, triplet state shelving, or blinking. With this only a low number of the molecules are in the fluorescent state. The detected fluorophores are diffraction limited and be localized with a very high accuracy by a fit. By collecting a time series with a few thousand raw images, each with a different subset of fluorescent molecules, a density map of the single molecule position is generated.<sup>21</sup>

$$\delta d \geq \frac{\lambda}{2n \sin \alpha \sqrt{1 + \frac{I}{I_{sat}}}} \quad (4.6)$$

with  $I_{sat}$  the saturation intensity where the fluorescence probability of molecule is reduced by 50%.

### 4.3.2. Structured illumination

Another method to increase the spatial resolution of fluorescence microscopes is structured illumination microscopy (SIM).<sup>24,25</sup> Instead of a homogeneous illumination a periodic pattern for the excitation of the fluorophores is used. This pattern interferes with the fine structures of the fluorescent sample and create coarser interference patterns - moiré fringes. The higher spatial frequencies, which could not be transferred by the objective lens before are shifted to lower frequencies, enabling a transfer of those informations. The acquired raw images are processed by computer algorithms to generate a high-resolution image by shifting the moiré information back to the high frequency places. The maximum resolution enhancement is limited by factor of two since the excitation pattern is also diffraction limited.

### 4.3.3. Single molecule localisation microscopy

Burns *et al.*,<sup>26</sup> Betzig *et al.*<sup>27</sup> and Bornfleht *et al.*<sup>28</sup> showed that it is possible that the localisation of a point source can be more precise than the optical resolution limit of the system. For the reconstruction of more complex structure a appropriate number molecules have to be localised. To get a subdiffraction image of the structure the molecules have to be separated. This can be achieved by switching the molecules between two different fluorescent states which can be separated by the optical system. There are different ways to achieve this, which are briefly explained in the following and are all part of the single molecule localization microscopy (SMLM) family.

#### 4.3.3.1. Photoactivation

For this method photoactivatable molecules like photoactivatable green fluorescent protein (PAGFP) are used. They change into a fluorescent state upon irradiation with a certain wavelength and are used in methods like photoactivated localization microscopy (PALM)<sup>29</sup> and fluorescence photoactivation localization microscopy (FPALM).<sup>30</sup> For these methods one wavelength is used to excite the fluorophores. At the beginning of the recording ideally no fluorophore should be active. A different wavelength is then used to activate only a small amount of the fluorophores. The intensity of the activation laser determines the numbers of activated molecules per time interval. The number of fluores-

cent fluorophore is chosen in such a way that their PSFs do not overlap. After a certain time the activated fluorophores will eventually irreversibly photobleach and will not be fluorescent any more. In this way (under ideal conditions) every fluorophore is detected only once.

#### 4.3.3.2. Photoswitching

Stochastic optical reconstruction microscopy (STORM)<sup>31</sup> uses the reversible transition of fluorophore between a dark and a bright state. The working principle is similar to the above mentioned method with photoactivatable fluorophores, also using a different wavelength than the excitation laser to switch the fluorophores between the two states. The difference is the reversible transition of the fluorophores leading to the multiple detection of one fluorophore.

#### 4.3.3.3. Photoswitching of conventional fluorophores

The above mentioned methods need special fluorophores or certain fluorophore pairs and an additional laser to activate or switch the fluorophores. There is another group of methods which use conventional fluorophores and does not necessarily need an additional activation/switching laser of another wavelength to achieve super-resolution. The separation of the fluorophores is achieved by using reversible dark states, which can be facilitated if the intensity of the excitation laser is high enough. The lifetime of these dark states can be influenced by the laser intensity, environment or with an additional laser wavelength. Spectral precision distance / position determination microscopy (SPDM)<sup>32</sup> and reversible photobleaching microscopy (RPM)<sup>33</sup> only use one laser wavelength for excitation and reversible photobleaching. Direct stochastic optical reconstruction microscopy (dSTORM)<sup>34</sup> and ground state depletion imaging microscopy (GSDIM)<sup>35</sup> use an additional laser with a different wavelength with a lower intensity to influence the reversible photobleaching. The transition back to the ground state is stochastic which means that the fluorescence signal from the fluorophores can be temporally and spatially separated.

#### 4.3.4. SOFI

Besides the three most commonly used super-resolution methods introduced above, a resolution enhancement can also be achieved by utilising the temporal fluctuations caused by the above mentioned fluorescence blinking without isolating and localizing individual molecules. This technique is called super-resolution optical fluctuation imaging (SOFI) and was developed by Dertinger *et al.*<sup>36</sup>

In a conventional fluorescence image the signal is given by the superposition of the emission of different, nearby emitters. To achieve a resolution enhancement for a SOFI-image

of the  $n$ th-order the  $n$ th-order cumulant, which is quantity related to the  $n$ th-order correlation function, filters the original pixel time series based on its fluctuation in such a way that only highly correlated fluctuations are left over. This means, only emitters within the pixel are contributing to the brightness of the pixel, since the fluorescence signal contribution of emitters in neighbouring pixels will yield lower correlation values and therefore lead to higher resolution.

## 4.4. Vitrification

Suitable imaging methods to investigate biological samples at high spatial resolution often require immobilization of the sample. One possibility is to use chemical fixation but it can lead to structural changes in the sample and therefore generate artefacts which in turn lead to misinterpretations of biological functions and mechanisms. An artefact free alternative offer fast freezing techniques (vitrification). The vitrification process is shown in Fig. 4.7. It allows the immobilization of biological samples in a near native state, without generating artefacts in the sample preparation process.<sup>3</sup> This has the additional advantage that the amorphous ice does not diffract the electrons in transmission electron cryomicroscopy (cryo-TEM) thus does not create diffraction artefacts. For this sample holders ("EM grids") with thin aqueous films need to be frozen very fast to avoid crystallization of the water molecules and yield amorphous, vitreous ice.<sup>3</sup> Liquid nitrogen can not be used as cryogen, since its heat transfer rate is not high enough to avoid crystallization.<sup>37</sup> Instead a liquid propane-ethane mixture at liquid nitrogen temperature is used, which can provide a cooling rate of over  $10^4$  K/s which ensures the vitrification of the sample.<sup>38</sup> The plunge freezing process (as shown in Fig. 4.6) can vitrify only thin samples up to 5-15  $\mu\text{m}$ .<sup>39</sup>

With high-pressure freezing samples up to 200  $\mu\text{m}$  can be vitrified.<sup>41</sup> This enables the study of larger cells and organelles in their near-native state with electron cryo-tomography (cryo-ET) and obtain high resolution images but the sample thickness for cryo-ET is limited to maximum of about 500-800 nm, for cryo-TEM the limit is about 1 $\mu\text{m}$ .<sup>42</sup> Thicker sample are confined to lower resolution whereas thin samples allows higher resolution<sup>43</sup> One way to solve this is to generate sections of the vitreous biological sample. By using focused ion beam (FIB) milling<sup>44</sup> to mill 150-500 nm thick lamella which can be subsequently observed in a cryo-TEM.<sup>45</sup> Cryo-EM can be combined with fluorescence cryo-microscopy (cryo-FM) to correlative light and electron cryo-microscopy (cryo-CLEM). This enables the combination of the high specificity of fluorescent labelling with the very high resolution from cryo-EM on the same sample. Combined with super-resolution cryo-FM the large resolution gap between cryo-FM and cryo-EM can be narrowed.

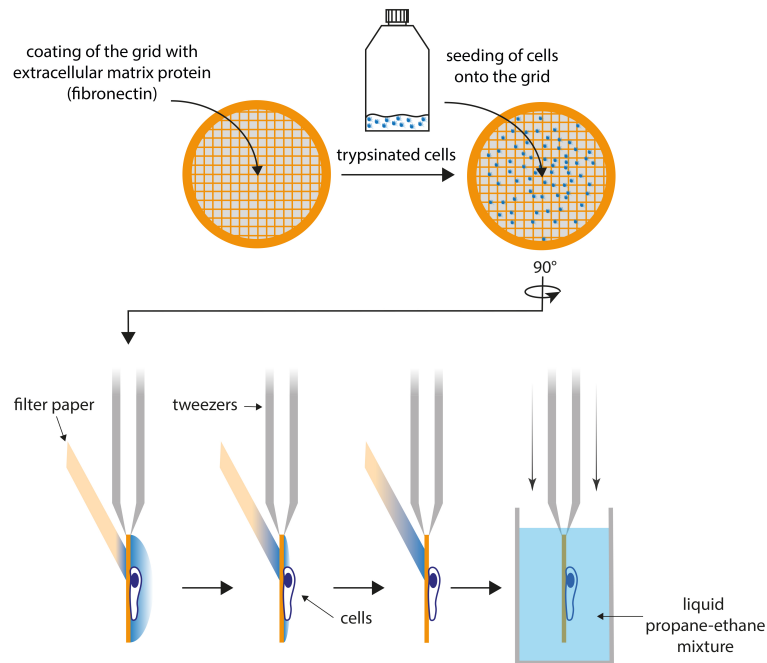


**Fig. 4.6.** Schematic overview of sample preparation for cryo-FM. Detached cells are seeded on a carbon coated gold grid, which was incubated with an extracellular matrix protein. The fluorescent labelling can be done before or after seeding of the cells. After the adhesion of the cells, the grid is transferred from the well to the plunge freezer. Excess medium is removed with a filter paper ('blotting'). The sample is vitrified in a mixture of liquid propane and ethane, which is cooled with LN 2.<sup>40</sup>

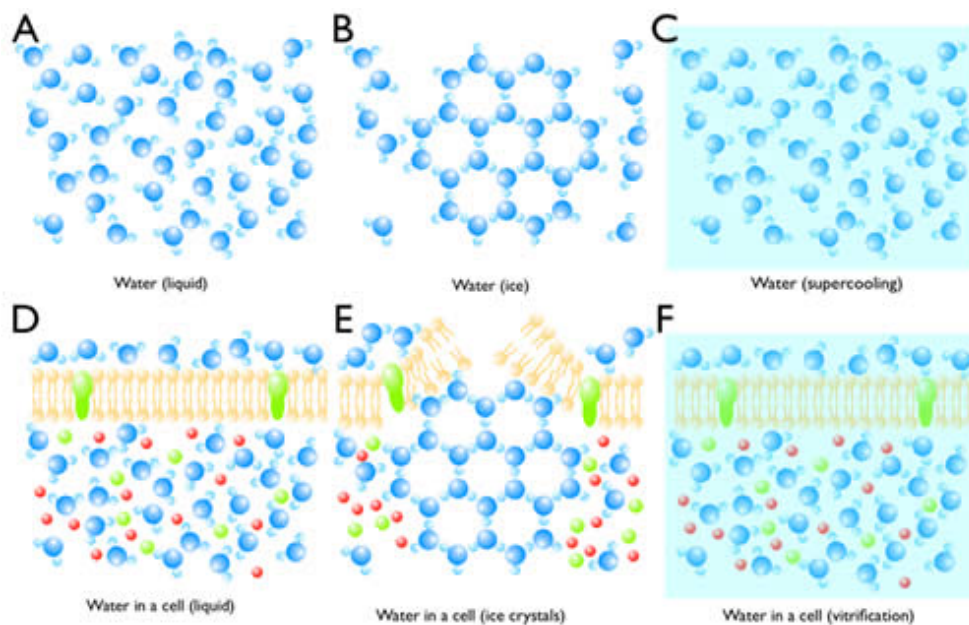


**Fig. 4.7.** Crystallization and vitrification of water. (A) Water molecules are highly mobile in liquid. (B) When the temperature reaches 0°C, water starts to crystallize if there is a seed. (C) Water can be super-cooled to -40°C at atmospheric pressure. (D) Water in a cell is also highly mobile despite the presence of molecules in the cytosol. (E) Ice crystals can break the cell membrane and also displace molecules and cellular structures. (F) By fast freezing methods, water vitrifies, thereby preserving the native state of a cell.<sup>46</sup>

## 4.5. Photo-physics under cryogenic conditions

Under cryogenic conditions the behaviour of fluorophores changes. Photobleaching is reduced since two major mechanisms leading to irreversible bleaching of fluorophores are suppressed. The diffusion of small reactive molecules like oxygen leading to bleaching through photo-oxidation is stopped.<sup>47</sup> Furthermore, the quenching by chemical reactions is also reduced since reaction rates are exponentially reduced by cooling. This leads to an increase in fluorescence yield.<sup>48</sup> Quenching by energy transfer on the other hand is temperature independent.<sup>49</sup> At low temperature the effects on the fluorescence spectrum and the absorption spectrum are similar. The absorbance is higher, caused by the enlarged absorption cross-section. Additionally, the spectrum can be narrowed and fine-structuring can be observed.<sup>47,50,51</sup> The narrowing of the spectra can be utilized to distinguish fluorophores in cryo-FM which would have overlapping spectra at room temperature.<sup>48</sup> In some cases, the whole spectrum can be blue-shifted<sup>50</sup> or red-shifted,<sup>51</sup> depending on the molecular structure or state of the fluorescent molecule. Additionally, the fluorescence might be reduced because of the polarisation dependent excitation and fixed dipoles of the fluorophores.<sup>52</sup> The fluorescence yield could be further reduced due to a high population of the excited triplet state and long triplet lifetime. The above mentioned reduced diffusion of oxygen can substantially reduce the recovery rate of the fluorescent ground state therefore keeping the fluorophore in a long lived dark state.<sup>15,53</sup> Which also leads to reduced signal to noise ratio of the fluorescent signal.

Additionally, transformational changes, which are a crucial step to photodecomposition of the molecules, are hindered.<sup>54</sup> Photoswitching on the other hand can still be observed for many fluorophores at low temperatures but might be changed compared to room temperature.<sup>55</sup> The photoswitching at low temperature are caused by photoinduced protonation.<sup>56</sup> Furthermore, the number of photons emitted by the fluorophores can be increased up to two orders of magnitude compared to room temperature.<sup>57</sup>

## 4.6. Cryogenic super-resolution fluorescence microscopy

Super-resolution under cryogenic conditions is a new field and most of the boundary conditions are still unknown<sup>48</sup> and as mentioned above the photophysical behaviour of the fluorophores changes under cryogenic conditions.

Most importantly for super-resolution techniques is that photo-switching can be still observed at low temperatures but might be drastically changed compared to room temperatures.<sup>55</sup> Additionally, the high laser intensity used for most of the super-resolution methods to induce photo-switching might locally devitrify the sample resulting in the formation of crystalline ice and might destroy the biological sample<sup>9,11</sup>

A lack of a commercial immersion objective lens for cryogenic conditions limits the NA to below 1.0 and therefore a reduced detection efficiency.<sup>8</sup> Additionally, the NA might be



even lower if a high working distance between the sample and objective lens is required.<sup>58</sup> Some groups have built a cryo-microscopes which use immersion lenses with an NA of 1.2-2.17. Le Gros *et al.*<sup>59</sup> built a setup with an objective lens operating at cryogenic temperatures and uses liquid propane as optical medium. The plunge freezer is built into the cryo stage. However, the the stage cannot be attached to an standard fluorescence microscope. Nahmani *et al.*<sup>60</sup> and Faoro *et al.*<sup>61</sup> have setups with an immersion objective lens with a NA of about 1.2 which operates at or near ambient conditions.<sup>58</sup> The objective lens is optically coupled with water to a coverslip which again is optically coupled with a cryo-medium which has a refractive close to water to the sample. This cryo-medium does not boil a room temperature and do not freeze a  $-140^{\circ}\text{C}$ . The objective lens provides the heating for the cryo-medium to not freeze solid and a cold finger removes the heat which is connected to the sample. The thermal conductance has to be set up carefully that over the less than a millimetre of optical pathway the water is still liquid and the cryo-medium and the sample are at  $-140^{\circ}\text{C}$ . Also, the devitrification point of water is close by at  $-135^{\circ}\text{C}$ .<sup>3</sup>

The advantages of cryo-SR-FM are, bridging the resolution gap in cryo-CLEM, reduced irreversible photo-bleaching.<sup>6,47,62</sup> The challenges are the lack of a commercially available immersion objective lens which limits the and the mechanical instability of most commercial and experimental setups.<sup>63</sup>

#### 4.6.1. Cryo-SMLM

Maximum resolution for cryo-SMLM is only achieved with high laser intensities used for the photo-switching of the used fluorescent molecules but this causes devitrification of the sample.<sup>9,11</sup> The laser has to be kept at below  $100\text{ W/cm}^2$  to prevent devitrification of the sample.<sup>64</sup> It is possible to use cryo-protectants (10% Ficoll PM 70 and 10% ethylene glycol) to achieve higher laser intensities of  $300\text{ W/cm}^2$  for cryo-SMLM but this is only suitable for osmotically robust cells like bacteria,<sup>9</sup> but not for mammalian cells. Additionally, cryo-protectants decrease the contrast in cryo-EM. An alternative could be formvar-coated EM grids, which absorb less light (heat) and allow for higher laser intensities of  $1.75\text{ kW/cm}^2$  and therefore enable improved photo-switching and consequently higher resolution in cryo-SMLM.<sup>11</sup> However, the formvar-coating reduces the compatibility with cryo-EM because of the higher electron absorption, reducing contrast and resolution. Mechanical instabilities of the cryo-SMLM imaging setup can be overcome by drift correction using fiducial markers or bright fluorescent background structures. However, the remaining error was in the order of the average single molecule localization precision.<sup>10,11</sup> SMLM offers, besides resolution improvement, additional single molecule information that can be used for further quantitative analysis. This makes cryo-SMLM ideal for the investigation of protein arrangements and distribution in the structural context.<sup>63</sup>

### 4.6.2. Cryo-SOFI

As mentioned above, to achieve the maximum resolution for cryo-SMLM high laser intensities has to be used which causes devitrification of the sample.<sup>9,11</sup>

Cryo-SOFI offers a low-dose (100 W/cm<sup>2</sup>) super-resolution method suitable for correlative light and electron cryo-microscopy<sup>64</sup> and is based on the SOFI principle.<sup>36</sup> This method does not need a special sample preparation, is fully compatible with conventional cryo-EM samples, and since it uses the same sample preparation method as the already established cryo-EM protocols, it does not effect the quality of the cryo-EM images.<sup>64</sup>

As mentioned above the SOFI principle makes use of the fluorescent intensity fluctuation over time. Since the fluorescence of the neighbouring molecules is independent of each other, only the intensity fluctuation from the same molecule is highly correlated. In principle, using the  $n$ th-order cumulant results in an image with a resolution improvement of  $n$ -fold for reweighted cross-cumulants compared to a conventional fluorescence image.<sup>64</sup> The resolution improvement of SOFI is theoretically not limited by diffraction but is limited by the signal-to-noise ratio (SNR) of the intensity fluctuations in biological samples. The SNR is defined by the number of photons per single-molecule blink vs. background signal.<sup>36</sup> Resolution improvement for biological samples of two to three times are possible, which is about 135 nm.<sup>64</sup> Theoretically higher orders of correlation would yield higher resolution but with higher order the impact of optical aberrations that result in an asymmetric PSF and errors in the correction of mechanical instabilities, is bigger on the resulting image.<sup>64</sup> Still, compared with cryo-SMLM, the resolution of cryo-SOFI reaches a similar range, but with a lower laser intensity.<sup>64</sup>

### 4.6.3. SR-cryo-CLEM

Cryogenic correlative light and electron microscopy (cryo-CLEM) especially fluorescence microscopy makes it possible to locate structures and events of interest in the electron microscope of biological samples in a near native state and was introduced 2007.<sup>6,7</sup> Combined with cryogenic electron tomography it is a powerful tool to observe the interiors of cells in their near native states and in near atomic detail.<sup>58</sup>

Because of the nature of electron microscopes only cell samples with a thickness below 500 nm can be directly imaged. One way to image the interior of thick cells like the nucleus is focused ion beam (FIB) milling to create thin lamellae cut through cells.<sup>44,45,65</sup> However, lamellae are typically 150 nm thick<sup>58</sup> and with a resolution of at best 250 nm laterally and 500 nm axially of a conventional cryo-FM it is impossible to tell where to mill the cell that contains the structure or protein of interests. This problem can be solve by using cryo-SMLM which currently can achieve a resolution of 20 nm lateral and 50 nm axial.<sup>66</sup>

## 5. Methods

### 5.1. Fluorescence cryogenic microscope

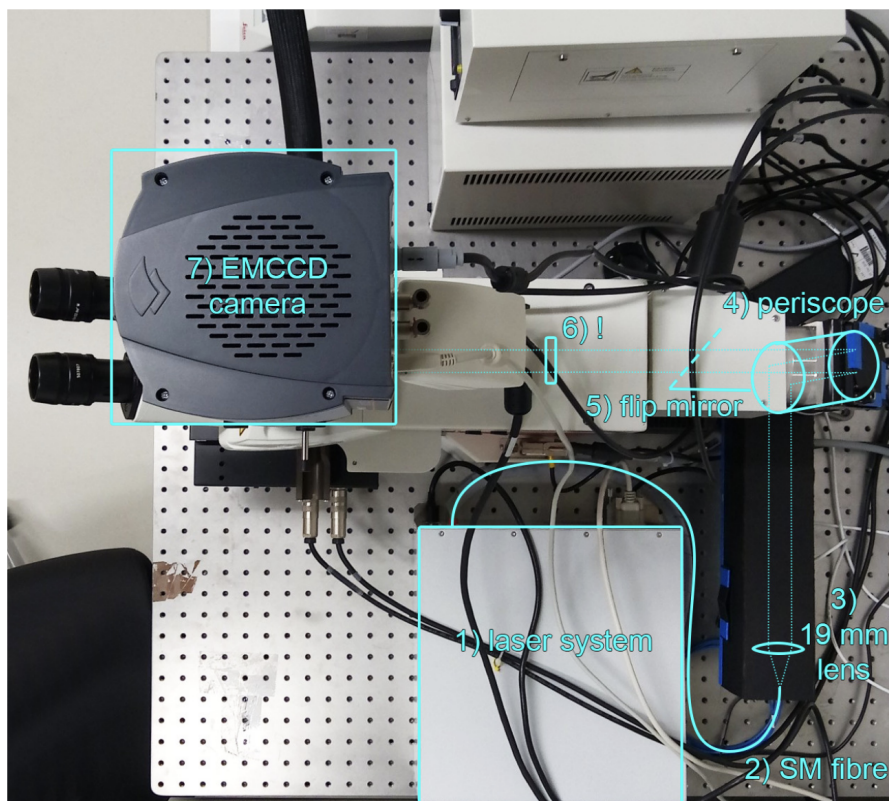


**Fig. 5.1.** Schematic illustration of modifications required to implement cryo-SOFI on conventional cryo-FM system. Additional required components are: 1) lasers with wavelength appropriate for imaging of fluorescent molecules of interest and sufficient power for reaching desired laser intensity for cryo-SOFI; 2) single mode (SM) fibre to couple laser light conveniently and safely into the system; 3) lens to collimate laser output of the fibre into a parallel beam of desired width; 4) periscope to bring beam at required port of the microscope body; 5) flip mirror to change between laser and conventional illumination; 6) in case a diffusor is in the beam path, it needs to be removed; 7) sensitive camera with high quantum efficiency. From Moser *et al.*<sup>64</sup>

For the investigation of the fluorophores a modified Leica cryo-CLEM microscope which was upgraded with a laser system containing the laser lines 405 nm, 488 nm, 561 nm and 640 nm and a Andor iXon 897 EMCCD camera was used (for more details see<sup>64</sup>). The standard issued halogen lamp was used for navigation on the grid.

The used objective lens is a Leica HCX PL APO 50x / 0.90 CLEM. Modified with an heat foil to prevent condensation on the back of the objective lens.

All the time series for the photo-physical investigations were taken with a 128x128 pixel ROI and an EM gain of 300. The integration time was 10 ms and the laser intensity for all used wavelength were set to 100W/cm<sup>2</sup>. The effective pixel size on the camera was 160 nm.

The stage was cooled with liquid nitrogen to ensure that the samples are kept vitrified. For this liquid nitrogen was pumped into the sample chamber, which was kept at -192°C to avoid pumping at maximum flow rate which would can lead to the increase of mechanical instabilities.

### 5.1.1. Mechanical instabilities of the setup

The microscope used to study the dyes was a commercially available microscope which has some mechanical and thermal instabilities which was noticeable during the recording of the time series. Those instabilities can move the molecule in the x-y-axis out of the ROI therefore leading to a reduction in fluorescence intensity. This can be corrected after the measurement with a drift correction algorithm. A much bigger problem is the drift in z-direction since there is no possibility to correct it afterwards. Those were sorted out during the manual categorization of the TPs. TPs with z-drift can be recognized by a slow intensity change over time where the highest and lowest intensity is moving parallel. Those TPs excluded from the data processing process.

## 5.2. Bespoke cryogenic fluorescence microscope

One part of this thesis was to start the design process of a bespoke cryogenic fluorescence microscope which reduces mechanical and thermal instabilities. The current setup is shown in Fig. 5.2. My part was designing the sample chamber and the insulation.

This is achieved by reducing the length of the mechanical arm between the sample and objective lens. Instead of using a C-shape like commercial inverted light microscopes which is a lot more unstable the objective lens in the bespoke microscope is directly mounted on the cold sample chamber. The sample chamber is completely made of copper Kupfer Cu-ETP, Werkstoff CW004A – E-Cu57 and is passively cooled by a copper rod directly mounted to the chamber extending into the dewar below filled with liquid nitrogen as shown in Fig. 5.3. The rod, which is submerged in the liquid nitrogen cools the whole sample chamber without any active pumping, thus reducing any thermal fluctuation. At the same time cold nitrogen gas is formed and flows through a hole in the insulation into the chamber keeping the chamber free of ice contamination. The foam insulation (ebazell 80 from ebalta) is carrying the whole sample chamber and rod and also closes any gap between the dewar keeping any air outside. The sample holder is mounted on top of a positioner, which also cools the sample by thermal coupling. The objective lens is kinematically mounted via a ceramic plate (Macor) to the chamber. This ensures that the objective lens is always in the same position since macor have a low thermal expansion coefficient, and is thermally isolated from the chamber to keep the objective lens at operation temperature.

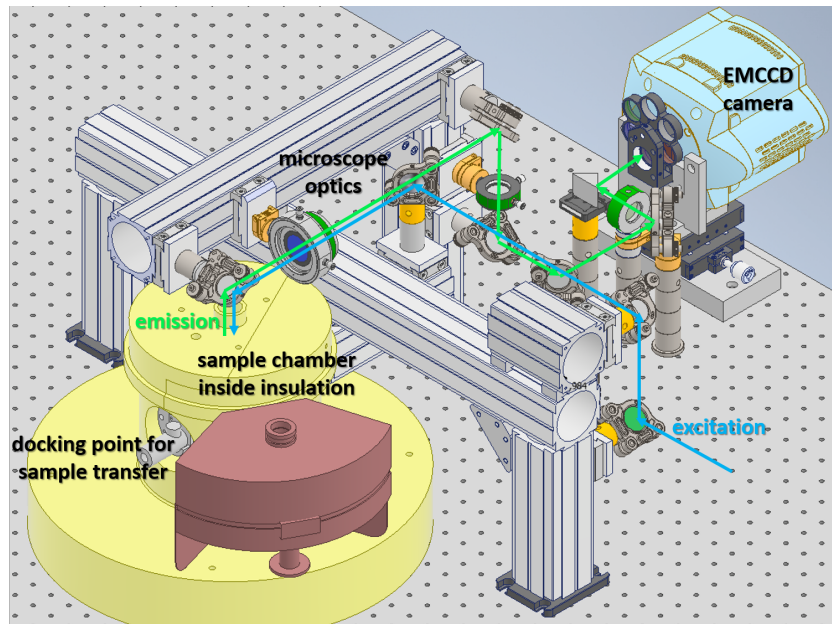


**Fig. 5.2.** Schematic of the bespoke setup of the group. On the left in yellow is the insulation which is covering the sample chamber and is shown in more detail in Fig. 5.3. Mounted on rails is the optical system. The excitation pathway and the emission is depicted in cyan and green respectively. On the right is the EMCCD camera.

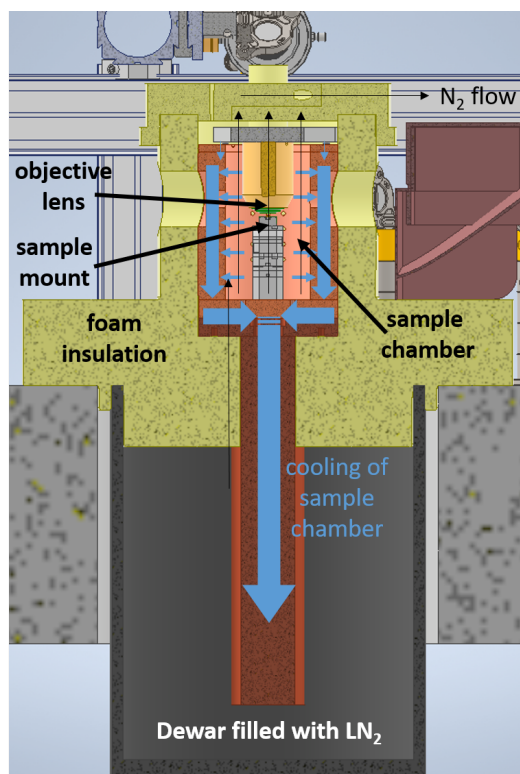


**Fig. 5.3.** Schematic cross section of the sample chamber. The copper sample chamber is surrounded by the foam insulation which carries the whole chamber. A copper rod directly connected to the chamber goes through the insulation directly into the dewar filled with liquid nitrogen. Small holes in the insulation let a constant stream of cold nitrogen flow into the sample chamber to prevent ice contamination. The sample carrier is mounted on top of a positioner. The objective lens is coupled to a ceramic plate which is kinematically mounted to the rim of the chamber ensuring that the objective lens is always in the same position.

## 5.3. Plunge freezing

Liquid nitrogen can not be used as cryogen to vitrify the samples since the Leidenfrost effect would prevent the rapid freezing of the sample. To achieve amorphous ice the sample has to be frozen with a cooling rate of at least 10,000 K/s which is possible with a propane-ethane-mixture (60% propane and 40% ethane) cooled by liquid nitrogen. This mixture has the advantage that it stays liquid compared to pure liquefied ethane.<sup>38</sup>

Depending on the sample type some steps have to be added but primarily TEM grids are used as sample carrier. For only organic dyes the Protochips C-Flat coated with holey carbon film with hole diameter of 2  $\mu\text{m}$  and a spacing of 1  $\mu\text{m}$  and 200 mesh density was used. To prepare the grids they were glow discharged with 25 mA negative polarity for 60 s to make the surface hydrophilic. The grids are moved quickly to the already prepared manual plunger and put into the device. A drop of 3.5  $\mu\text{L}$  is applied to the grid and the excess liquid is removed with a filter paper for about one second. The grid is then quickly plunged into the liquid propane-ethane mixture and carefully stored in a grid box in a liquid nitrogen storage dewar.

### 5.3.1. Shigella samples

The TEM grids are prepared like mentioned above. Instead of the dye solution a drop of 2.5  $\mu\text{L}$  of the shigella was applied to the grid. Additionally, a drop of 2.5  $\mu\text{L}$  of 1/20 100 nm Tetraspeck beads solution was added onto the grid. The excess fluid was removed before freezing. The Tetraspecks enables the drift correction done by software since they are non-blinking and therefore give a steady reference point for the drift correction algorithm.

### 5.3.2. Non-vitrified samples

The TEM grids are prepared like the normal samples. Instead of using a manual plunger the grid is being hold by inverted tweezers and 3,5  $\mu\text{L}$  sample solution is applied to the grid. The excess fluid is removed with filter paper. The Grid is then slowly dipped into liquid nitrogen. This way the solution is forming crystalline ice instead of amorphous ice. This enables additional studies of the influence of the environment on the photo-physics of the fluorescent dyes.

## 6. Developed algorithms and software

In this chapter the the algorithms and software are described, which have been developed within this PhD project to analyse the photo-physical properties of single fluorescent molecules under cryogenic conditions.

The image stacks are recorded and saved as .tiff files. To streamline the process and remove possible bias a script was written to automate the process as much as possible.

For this a script called FPAnalysisGUI was written by me to load the image stack into Matlab and generate a maximum projection with a Gaussian blur. The maximum projection allows the detection of all molecule that switched on at some point during the recording and also reducing a selection bias for when the on-state of the molecule was. The Gaussian blur makes it easier for the human eye to see the molecule. The GUI is shown in Fig. 6.1.

The fluorophores can now be selected in the maximum project via a crosshair and afterwards the background is chosen manually. This way bright pixel close to the selected fluorophore can be avoided. To obtain the time profile (TP) a region of interest (ROI) of 5x5 pixel is created around the the chosen fluorophore and the intensity of the ROI is summed up. The background selection is also done in a ROI of 5x5 pixel. The background is used for a background correction for possible bleaching. A section of the GUI shows the obtained TP directly to manually check whether the selection was done correctly. Upon clicking on the save button the script saves all data needed for further analysis.

The next script developed for the analysis workflow is called onOffRatioCalculatorCorr\_v4. It automatically goes through the selected folder with the acquired TPs and determines the on-frames and off-frames of all TPs. For this the threefold standard deviation calculated from the background is used as threshold. All frames with an intensity above the threshold are regarded as in the on-state. The length of each on-state and off-state are also recorded.

catTPGUI then enables a fast way to manually categorized the TPs. An example is shown in Fig. 6.2. For this the TP is displayed. Also the OOR is calculated based on the on-frames and off-frames obtained from the previous script. Using the later shown examples for categories as orientation the TPs are categorized. This creates a list (catList) for the following scripts to further handle the TPs.

From this point on the data can be processed in different ways.

timeAC\_all calculates the AC curves for each TP from one sample and saves it in one matrix. The mean of the mean of the first four  $\tau$  ( $\tau_4$ ) for all acquired ACs is also calcu-



lated. From here it is possible to plot all the ACs in one graph. With the same script the ACs for each individual category can be calculated and saved.

catCount displays the occurrence of each category by simple counting each category from catList.

To acquire the on-times and off-times a method is used where the intensity histogram of the measure TP ( $TP_{\text{measured}}$ ) is fitted with a quasi Monte Carlo method. For this the intensity histogram of the TP is calculated. Afterwards, TPs are simulated ( $TP_{\text{simulated}}$ ) with different parameters. The resulting intensity histogram are compared with the histogram acquired from the actual TP. The TP simulation is based on Marcel Leuteneggers's `sofiSimulate`.<sup>67</sup> The algorithm was modified with additional noise to account for the readnoise of the camera, which, even for the used EMCCD camera, is not neglectable at the very low photon counts of the performed experiments in this project.

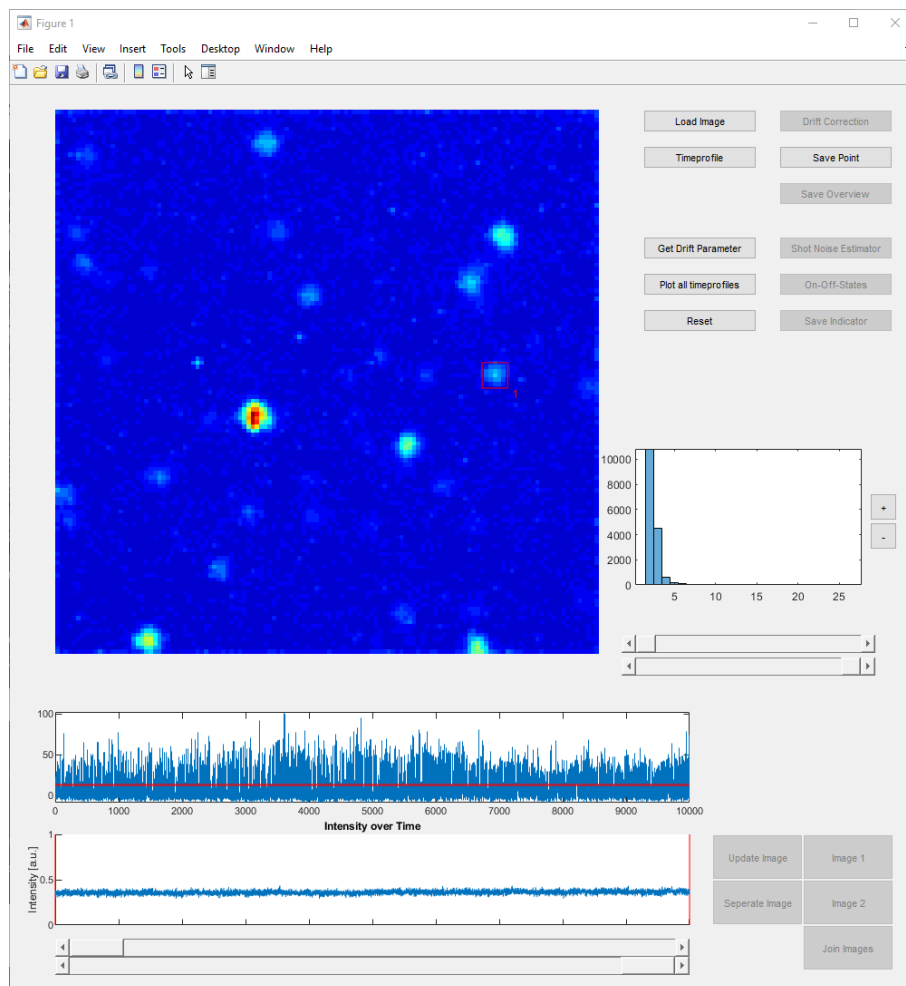


**Fig. 6.1.** GUI of the developed analysis software tool to pick the fluorophores. A large display shows the maximum projection of the image stack with the Gaussian to easily identify the molecules. The buttons on the right offers different operations. "Load image", "Drift Correction" "Get Drift Parameter" "Reset" are self-explanatory. The "Time Profile" starts the process of selecting the fluorophores and background with a crosshair. "Plot all timeprofiles" displays all the already saved time profiles. The histogram on the right shows the intensity of the image. The buttons and slider changes the contrast of the displayed maximum projection. The TP of the chosen molecule is displayed underneath the maximum projection. Beneath this, the average intensity of each entire frame in the time series is displayed. The disabled buttons (excluding the "Drift Correction") are not in use any more.

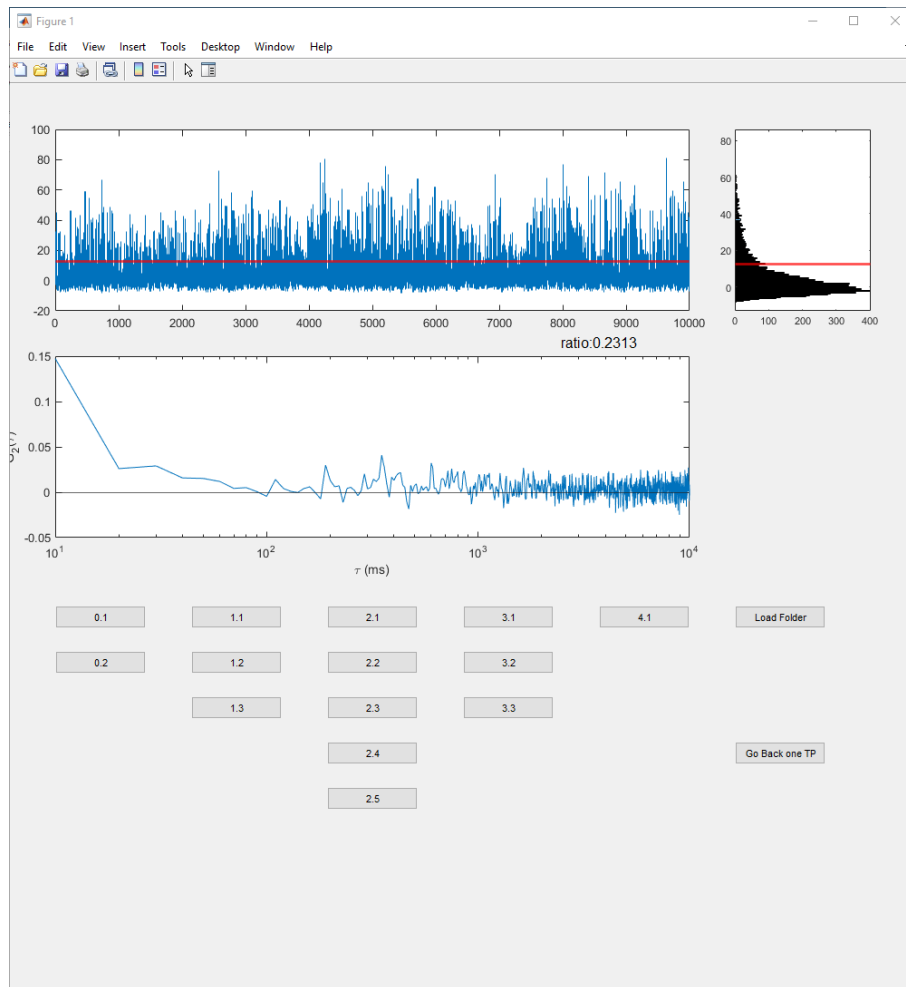


**Fig. 6.2.** GUI developed to categorize the TP. Shown on top is the TP, on the right side the intensity histogram from the TP, below the autocorrelation curve from the TP. Beneath are the buttons to select the category, coded with a number. There are more categories shown that were not used for further analysis and cover rare behaviours.

## 7. Results

### 7.1. Autocorrelation analysis of blinking and fluctuating fluorescent states of single Alexa Fluor 647 molecules in vitrified PBS

Alexa Fluor 647 (Alexa647) is a commercial organic far-red dye and is a commonly used dye for staining cells. The number represents the excitation maxima in nanometres. Alexa647 has been chosen as a reference since it is a commonly used dye for room temperature single molecule localization microscopy (SMLM).

To investigate the suitability of Alexa647 in vitrified phosphate-buffered saline (PBS) (Alexa647<sub>PBS\_V</sub>) for cryogenic super-resolution optical fluctuation imaging (cryo-SOFI) the autocorrelation (AC) of all time profiles (TPs) were studied. The AC correlates the signal of the TPs with itself to a later time point. For SOFI this is interesting since only intensity fluctuation from the same molecule are highly correlated, since the fluorescence of the neighbouring molecules are independent of each other.<sup>64</sup> Therefore, the AC behaviour of the molecules are crucial for a resolution improvement.

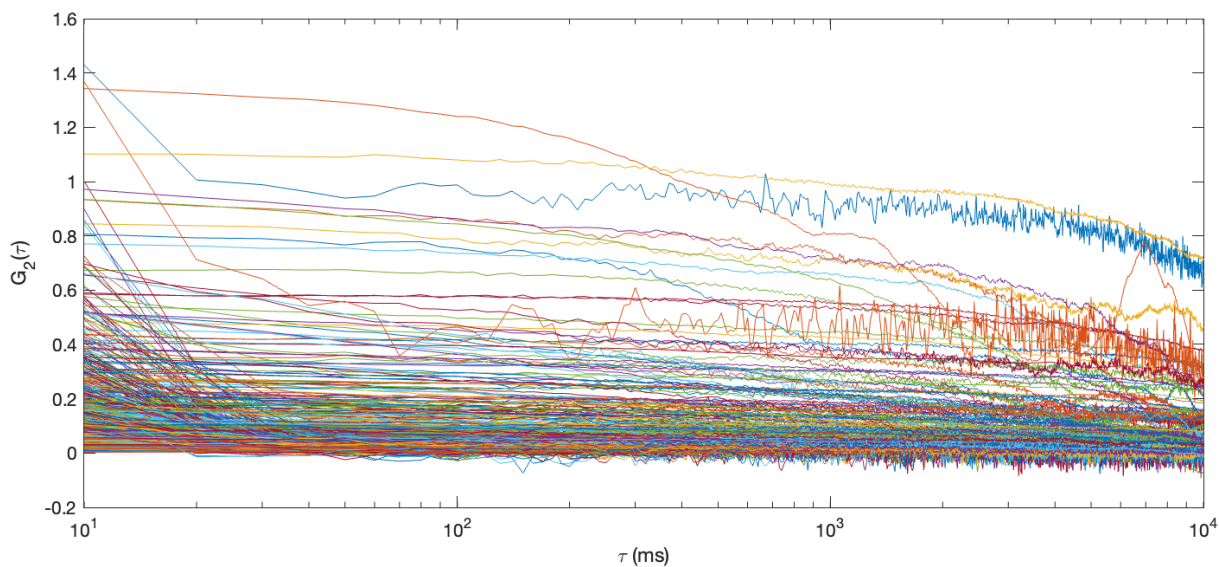
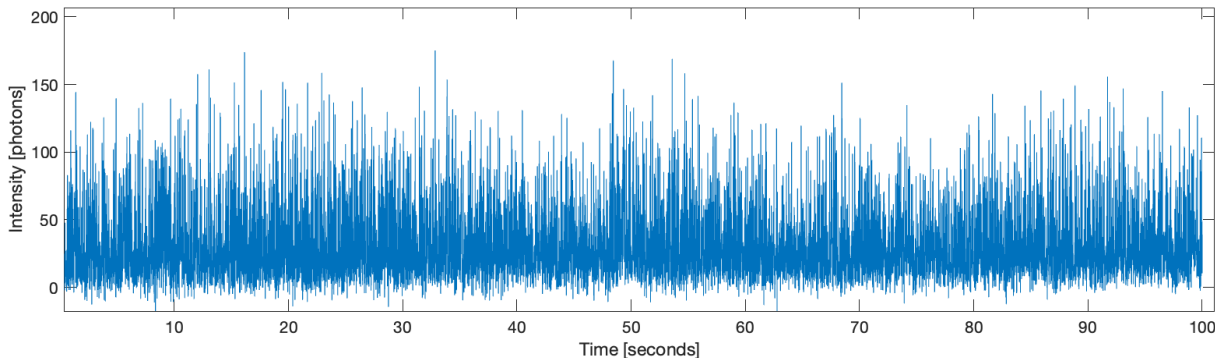


**Fig. 7.1.** AC of all TPs for Alexa647<sub>PBS\_V</sub>. Different AC behaviour can be seen, ranging from fast declining AC curves (indicating FB) to long plateaus (indicating long on-times ( $t_{on}$ )), but also including AC curves fluctuating around 0 (indicating no blinking or switching). The logarithmic x-axis shows  $\tau$  in ms. The temporal resolution is 10 ms.

All AC curves obtained from the TPs are shown in Fig. 7.1. There are also the TPs included which are not blinking, since they also somehow contribute to the generated image and therefore have to be taken into account. It shows the amplitude of the AC curve over different time delays  $\tau$ . Different AC behaviour can be seen, ranging from fast declining AC curves in the 10 ms range, which indicates fast blinking (FB), to long plateaus, indicating long  $t_{\text{on}}$ , but also including AC curves fluctuating around 0, which indicates no blinking or switching. Looking at the AC curves indicate that there are times which are smaller than the temporal resolution of the used camera, which is 10 ms.

### 7.1.1. Categorization of time profiles

The obtained TPs were manually categorized into different blinking behaviour: fast blinking (FB), multi state blinking (MSB) and rare blinking (RB). Examples of the blinking behaviour are shown in the following figures.



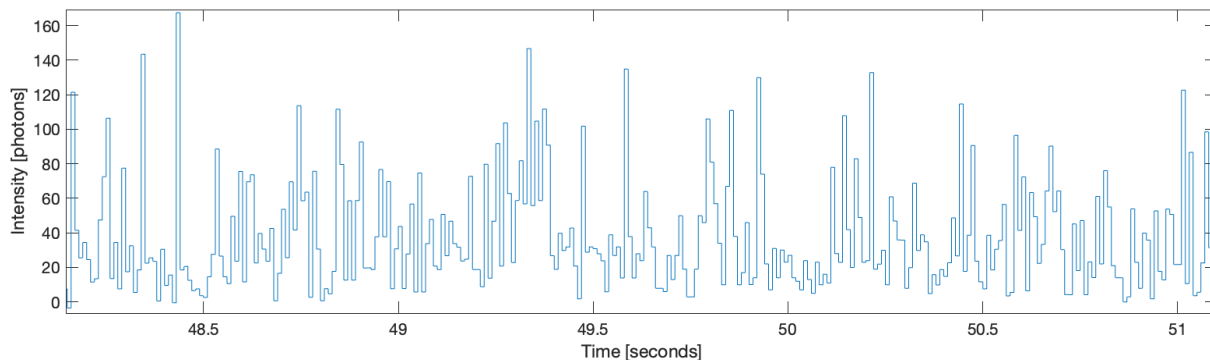
**Fig. 7.2.** One example of a TP for the fast blinking category. The off-state is around 0 intensity and the on-state is only several frames long and returns to the off-state again. The TP is background corrected and the temporal resolution is 10 ms.

Fig. 7.2 shows one TP from the FB category. The TP visualizes the fluorescence intensity course over a time period of 100 s with a temporal resolution of 10 ms.

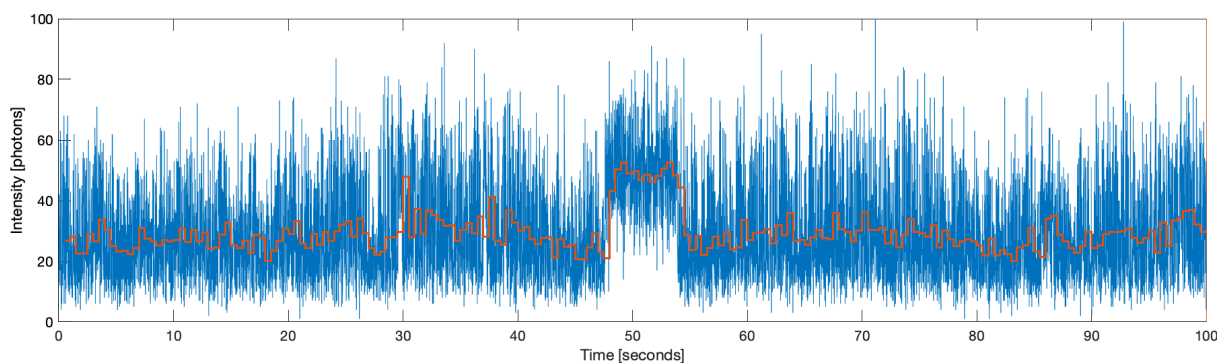
It is observable that this molecule has a shorter  $t_{\text{on}}$  than off-time ( $t_{\text{off}}$ ) since the average of the TP is close to the background. The molecule is mostly in the off-state and switches to the on-state for only one to several frames.

Fig. 7.3 shows a zoomed in section of Fig. 7.2. The short on-states can be clearly distinguished from the longer off-states.

Fig. 7.4 and Fig. 7.5 show two TP as examples for the MSB category. In this category the TP shows two distinct intensity levels. It can also switch between those two levels. It should be noted, that in what appear to be an on-state and off-state at longer temporal binning (e.g. 500 ms, orange TP in Fig. 7.4 and Fig. 7.4) the intensity is fluctuating. A longer temporal binning is overlay in orange. Both TPs generate different AC curves which can result in non homogeneous AC behaviour for the MSB category as shown later in Fig. 7.8



**Fig. 7.3.** Zoomed in section from Fig. 7.2 showing a time period of about 3 s. The TP is background corrected and the temporal resolution is 10 ms.



**Fig. 7.4.** One example of a TP for the multi state blinking category. Blue: TP with temporal resolution of 10 ms. Orange: Same TP with a temporal resolution of 500 ms as overlay. There are two clear intensity levels. Even in the "off-state" FB can be observed which is above the noise level. Also in the "on-state" FB can be observed. The temporal resolution is 10 ms.

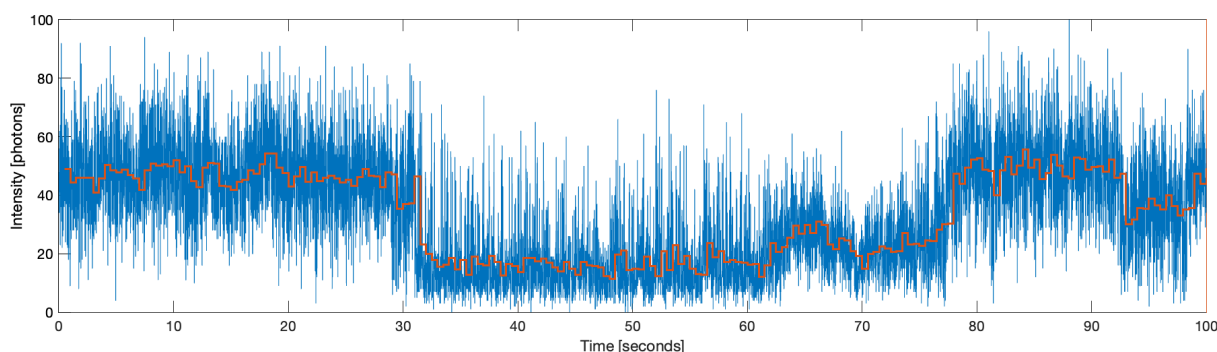


**Fig. 7.5.** Another example of a TP for the multi state blinking category. Blue: TP with temporal resolution of 10 ms. Orange: Same TP with a temporal resolution of 500 ms as overlay. There are two clear intensity levels. Besides FB in the two clearly separated "on-state" and "off-state" as in Fig. 7.4, here also "intermediate states" with FB can be observed. The temporal resolution is 10 ms.

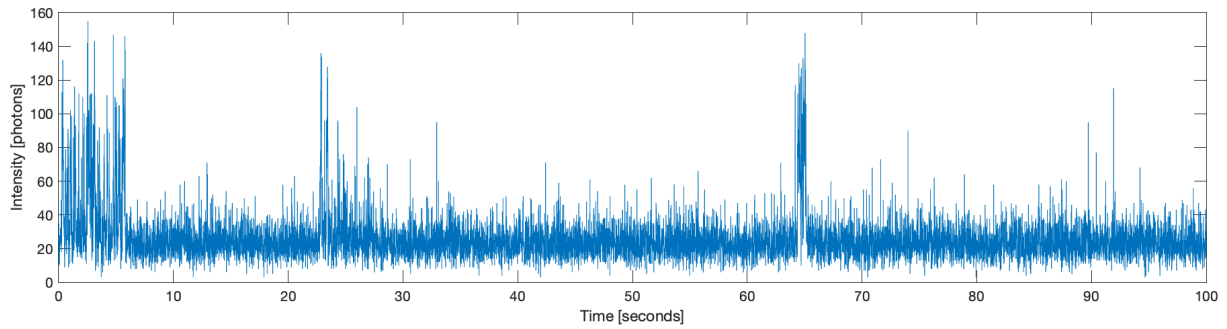


**Fig. 7.6.** One example of a TP for the rare blinking category. The molecule is  $t_{\text{off}}$  is quite long and the on-states are rare and only for a short time. The intensity is also quite high and distinct. The temporal resolution is 10 ms.

Fig. 7.6 shows one TP example from the RB category. The molecule is most of the time in the off-state. Only occasionally the molecule switches into the on-state and mostly for only a few to several frames. The intensity during the on-state is also quite high compared to the on-state of the FB or MSB category.

### 7.1.2. Analysis of Alexa Fluor 647 molecules in vitrified PBS

The above shown categorization of the time profiles were performed for  $\text{Alexa647}_{\text{PBS}_V}$  manually. The AC curves of each category are shown together in one figure below.

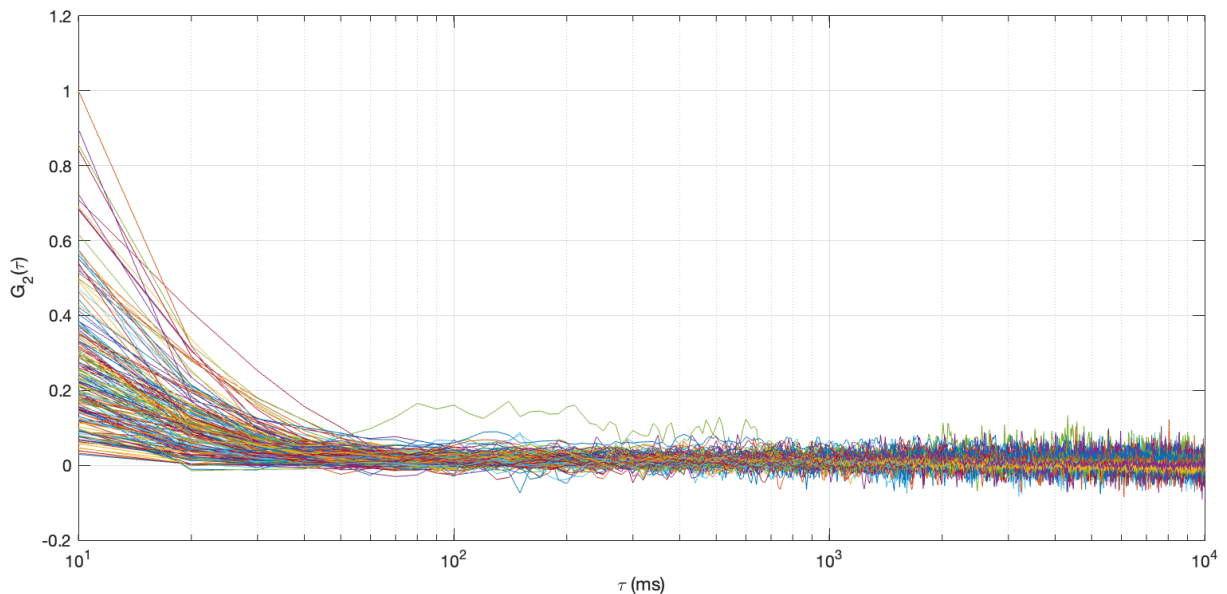


**Fig. 7.7.** AC from the same  $\text{Alexa647}_{\text{PBS}_V}$  sample as Fig. 7.1 but only showing the AC curves from the FB category. Only one type of AC behaviour can be seen. The highest correlation can be seen in the 10 ms range and nearly all of the AC curves declines to nearly 0 after 60 ms, indicating FB. The logarithmic x-axis shows  $\tau$  in ms. The temporal resolution is 10 ms.

In Fig. 7.7 the AC curves from  $\text{Alexa647}_{\text{PBS}_V}$  categorized as FB are shown. There is only one AC behaviour. The AC curves are declining fast in the 10 ms range to nearly 0. The

latest at around 60 ms. This indicates that the  $t_{\text{on}}$  are short and therefore indicates that these are only FB molecules. Since the temporal resolution of the camera is 10 ms, the  $t_{\text{on}}$  can not be determined directly.

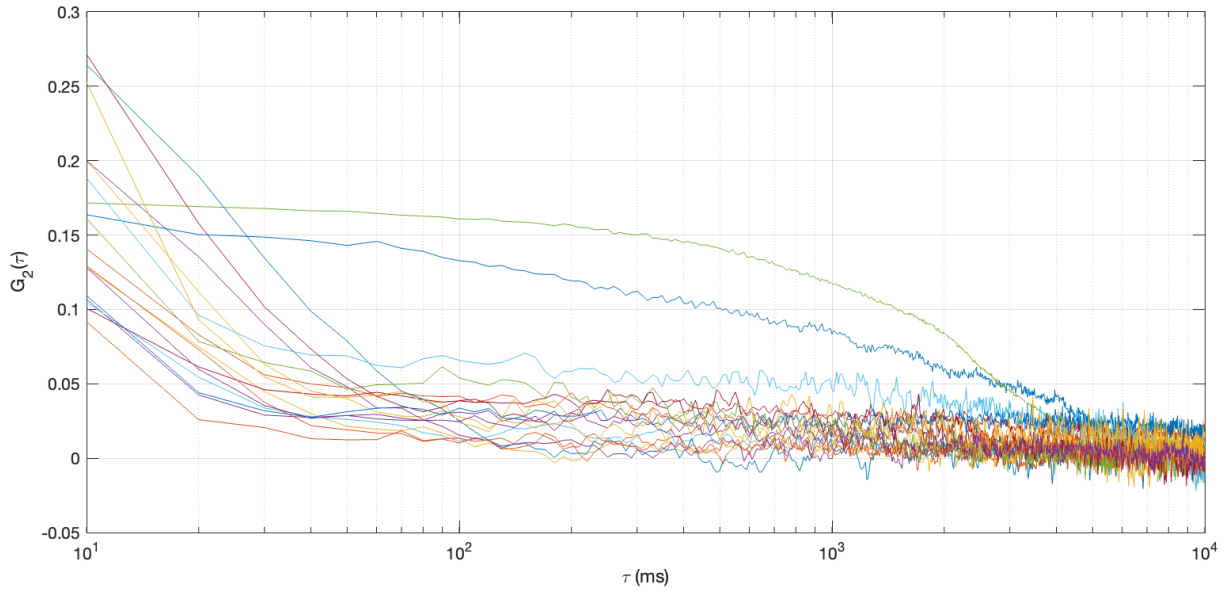


**Fig. 7.8.** AC from the same Alexa647<sub>PBS\_V</sub> sample as Fig. 7.1 but only showing the AC curves from the MSB category. The majority of the AC curves declines to nearly 0 after around 80 ms. Only two have a plateau until 4,000 ms. The logarithmic x-axis shows  $\tau$  in ms. The temporal resolution is 10 ms.

The AC behaviour of the MSB category shown in Fig. 7.8 is similar to FB. The AC curves declines fast to 0 in the 10 ms range but compared to FB they reach 0 around 80 ms, indicating short  $t_{\text{on}}$ . Two AC curves show a different behaviour. They have a plateau which drops to 0 around 4,000 ms, which indicates, as mentioned above, a long  $t_{\text{on}}$ . To explain why there are two different AC curve behaviour in the MSB category the above mentioned TPs in Fig. 7.4 and Fig. 7.5 are from the MSB category but yield different AC curves, which are shown in Fig. 7.9 and Fig. 7.10.

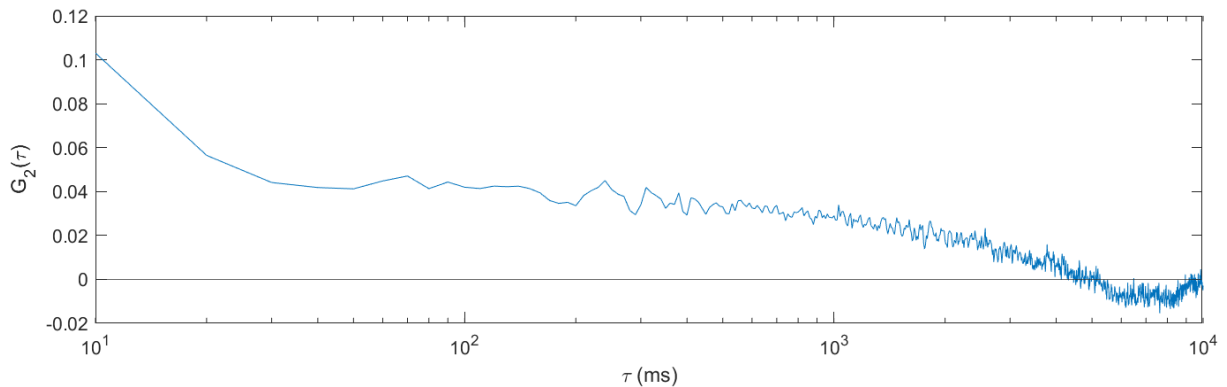


**Fig. 7.9.** AC curve from Fig. 7.4, which is from the MSB category. The amplitude is higher in the 10 ms range and drops to a plateau which ranges from 40 ms to about 1,000 ms and slowly declines further to 0. The logarithmic x-axis shows  $\tau$  in ms. The temporal resolution is 10 ms.



Compared to the TP (Fig. 7.4), which is mostly in the "off-state", the AC curve (Fig. 7.9) shows a higher correlation in the 10 ms range indicating FB and a lower plateau in the time range of 40 ms to about 1,000 ms indicating a slower switching behaviour which both can be seen in the TP.

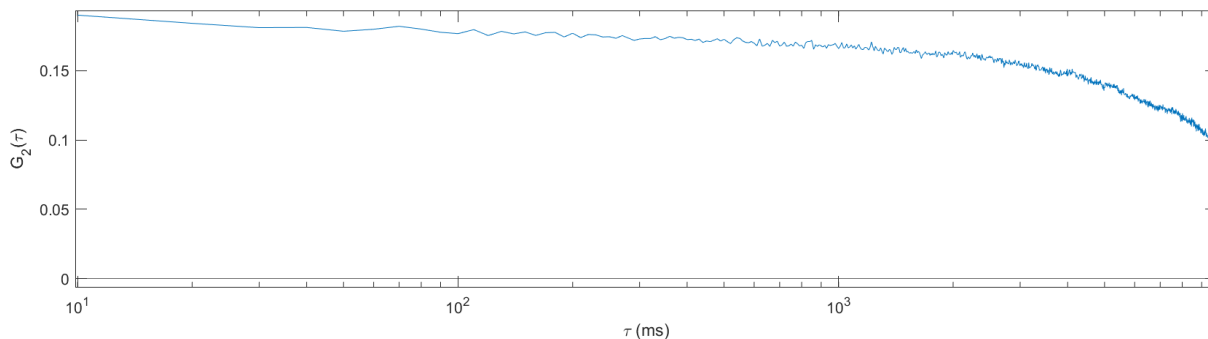


**Fig. 7.10.** AC curve from Fig. 7.5, which is from the MSB category. The AC curve shows a plateau which really slowly declines and declines faster at around 3,000 ms. The logarithmic x-axis shows  $\tau$  in ms. The temporal resolution is 10 ms.

Looking at the TP in Fig. 7.5, which is longer in the "on-state", and the AC curve in Fig. 7.10 FB and longer on-states can be observed which is reflected in the long plateau ranging from the shortest  $\tau$  to beyond 10,000 ms.

Those two AC curves shows that the MSB category can yield to different AC behaviour which are reflected in Fig. 7.8.

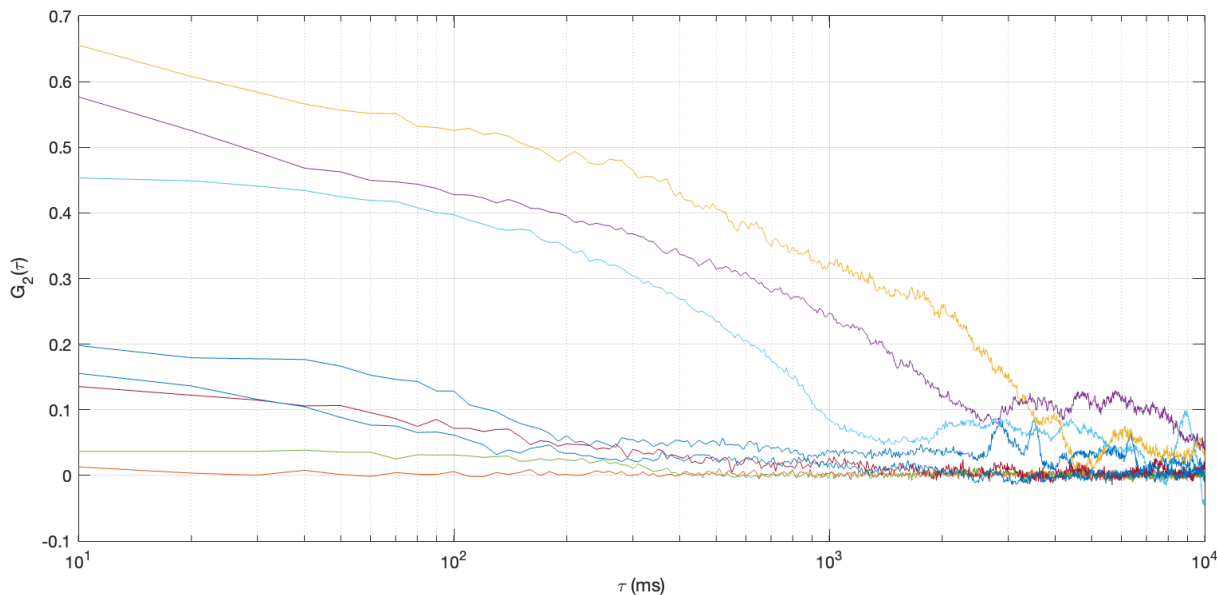


**Fig. 7.11.** AC from the same Alexa647<sub>PBS\_V</sub> sample as Fig. 7.1 but only showing the AC curves from the RB category. Three different behaviours can be seen. One with a higher amplitude declining to 0 around 1,000 to 5,000 ms. The other has a lower amplitude and declines to 0 around 200 ms. Two ACs are just flat around 0. The logarithmic x-axis shows  $\tau$  in ms. The temporal resolution is 10 ms.

The AC behaviour of the RB category shown in Fig. 7.11 is similar to the two AC curves from MSB with the different behaviour and are divided into three groups. One have

a higher amplitude and a plateau which declines to 0 between 1,000 to 5,000 ms. The other group has lower amplitude and also a plateau but declines earlier to 0 at around 200 ms. The last two AC curves are fluctuating around 0. The first two groups show that the  $t_{on}$  are longer, the first group longer than the second group. The third group of AC curves don't have any correlation and do not contribute to the signal in the SOFI image recreation.

This shows that the different blinking behaviour can be clearly distinguished by the time profiles themselves and the resulting AC curves also show a clear distinction in the behaviour for each category. Those differences in AC behaviour will result in different contribution to the signal, which lead to different pixel brightness.

## 7.2. Autocorrelation analysis of different organic dyes in vitrified PBS in comparison

In this section different organic dyes are compared with each other. For this, the mean value of the correlations coefficient  $G(\tau)_{m4}$  of the first four  $\tau$  are used as a benchmark.

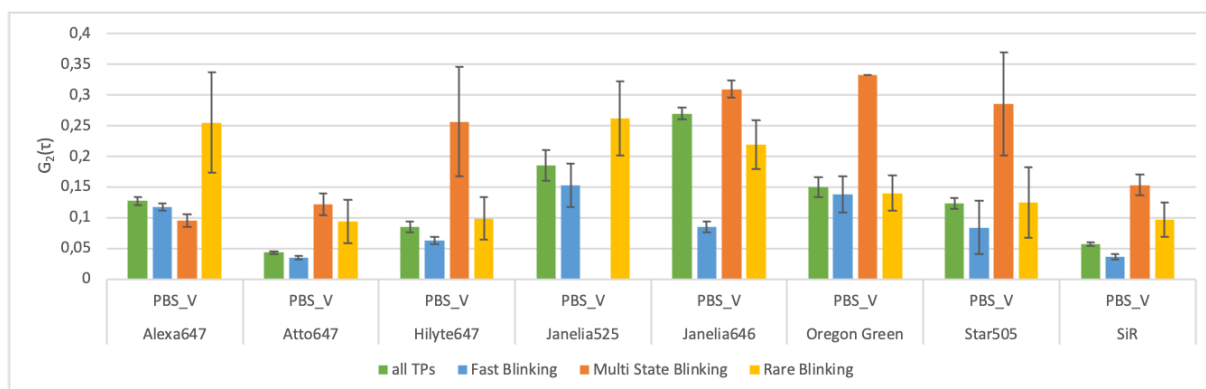


**Fig. 7.12.** Mean of the first four  $\tau$  of the AC of all investigated dyes in vitrified PBS. Different blinking categories are colour-coded: green = all TPs, blue = FB TPs, orange = MSB TPs and yellow = RB TPs. The error bars show the standard error of the mean (SEM).

Shown in Fig. 7.12 are all investigated dyes vitrified in PBS. They are colour-coded as described in the figure description. Generally, the higher the  $G(\tau)_{m4}$  value the higher the amplitude of the AC curves, therefore a higher correlation in the 10 ms time range which leads to a brighter pixel. Noise would have a lower or no correlation and therefore a low amplitude resulting in a darker or black pixel. By looking at the  $G(\tau)_{m4}^{allTPs}$ , colour-coded in green, Janelia Fluor 646 ( $JF646_{PBS\_V}$ ), Janelia Fluor 525 ( $JF525_{PBS\_V}$ ) and Oregon Green ( $OG_{PBS\_V}$ ) have the highest  $G(\tau)_{m4}$  values. Just looking at the  $G(\tau)_{m4}$  of all TPs does not give the needed information to conclude which dyes is the most suitable for cryo-SOFI.

Therefore, to see how high the contribution of each category to the  $G(\tau)_{m4}$  of all TPs is, a ratio can be used to estimate it and is shown in Fig. 7.13 and defined as followed:

$$G(\tau)_{ratio}^{category} = G(\tau)_{m4}^{category} / \tau_4^{allTPs} \quad (7.1)$$

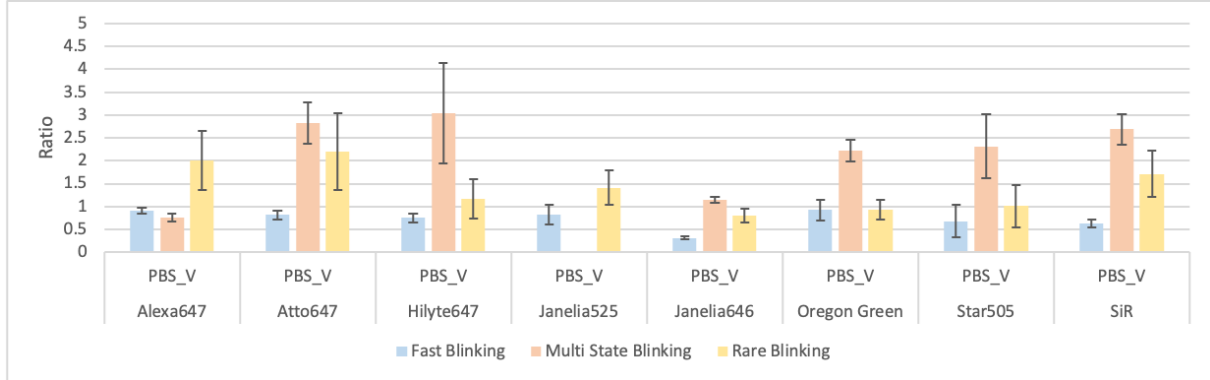


**Fig. 7.13.** Ratio of  $G(\tau)_{m4}$  of each category to  $G(\tau)_{m4}^{allTPs}$  for all dyes vitrified in PBS. The different categories are colour-coded: blue =  $G(\tau)_{m4}^{FB} / \tau_4^{allTPs}$ , orange =  $G(\tau)_{m4}^{MSB} / \tau_4^{allTPs}$  and yellow =  $G(\tau)_{m4}^{RB} / \tau_4^{allTPs}$ . The error bars show the SEM.

For the FB category the highest ratio  $G(\tau)_{ratio}^{FB}$  (shown in Fig. 7.13, color-coded in blue) achieved are from  $OG_{PBS\_V}$ ,  $Alexa647_{PBS\_V}$ , followed by  $JF525_{PBS\_V}$  and  $Atto647_{PBS\_V}$ . Combined with the  $G(\tau)_{m4}$  from the FB category from Fig. 7.12, where the highest  $G(\tau)_{m4}$  are  $JF525_{PBS\_V}$ ,  $OG_{PBS\_V}$  and  $Alexa647_{PBS\_V}$ , would suggest that  $JF525_{PBS\_V}$ ,  $OG_{PBS\_V}$  and  $Alexa647_{PBS\_V}$  are the most suitable for cryo-SOFI.

$G(\tau)_{ratio}^{MSB}$  is shown in Fig. 7.13, colour-coded in orange, are up to 3 times the  $G(\tau)_{m4}^{allTPs}$  and therefore not the main influence of  $G(\tau)_{m4}^{allTPs}$ . Only for  $Alexa647_{PBS\_V}$  and  $JF646_{PBS\_V}$  it is close to 1. From this figure it is not apparent if  $G(\tau)_{m4}^{FB}$  or  $G(\tau)_{m4}^{MSB}$  has the higher influence on  $G(\tau)_{m4}^{allTPs}$ . For this, the percentage has to be taken into account, which is done later in this thesis. For  $JF646_{PBS\_V}$   $G(\tau)_{m4}^{MSB}$  is the main influence since the other two categories are lower than  $G(\tau)_{m4}^{allTPs}$ .

From Fig. 7.13, colour-coded in yellow, the dyes which has a  $G(\tau)_{ratio}^{RB}$  which is close to 1 also have a  $G(\tau)_{ratio}^{FB}$  close to 1. It is not possible to tell which category has the major influence on  $G(\tau)_{m4}^{allTPs}$ . To do this, the category percentages has to be compared, which is done later in this thesis.

### 7.3. Categorization of organic dyes in vitrified PBS in comparison

In this chapter the occurrence of the categories for each investigated dyes are compared. In Fig. 7.14 each bar represents one dye and each category is colour-coded: gray = always on, blue = fast blinking (FB), orange = multi state blinking (MSB), yellow = rare

blinking (RB). "Always on" describes the molecules or points in the recording where their fluorescence intensity are always above the 3 standard deviation as used by Böning *et al.*<sup>68</sup>

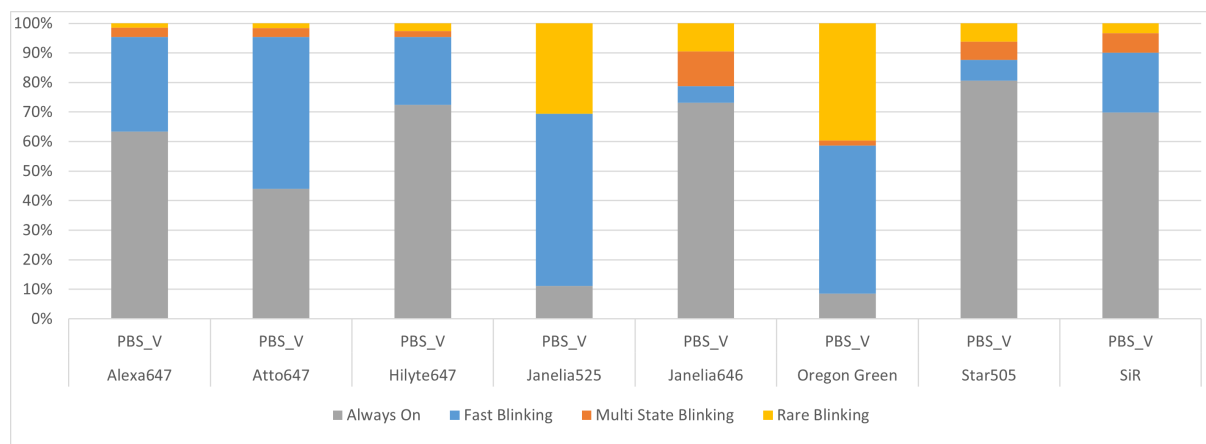


**Fig. 7.14.** Percentage of all categories from the organic dyes. Each bar represent one dye. Different categories are colour-coded: gray = always on, blue = fast blinking (FB), orange = multi state blinking (MSB), yellow = rare blinking (RB).

To compare the different blinking categories with themselves it is easier to leave out the "always on" category. This is shown in Fig. 7.15. For the most dyes the FB category dominates with 50% to over 90%. Indicating their suitability for cryo-SOFI. For JF646<sub>PBS\_V</sub> and Star505<sub>PBS\_V</sub> it is below 50%. The MSB and RB categories dominates for JF646<sub>PBS\_V</sub>. For Star505<sub>PBS\_V</sub> all categories equally distributed. OG<sub>PBS\_V</sub> has a really low percentage of MSB and the highest percentage of RB. This might indicate that it might be suitable for cryo-SMLM.

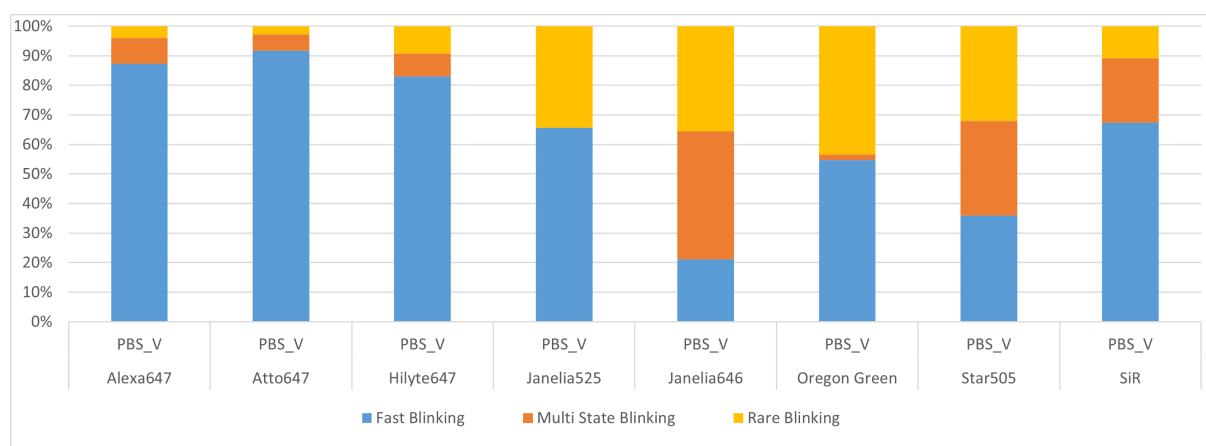


**Fig. 7.15.** Only the FB, MSB and RB categories from Fig. 7.14 are shown and are colour-coded: blue = FB, orange = MSB and yellow = RB. The FB category is the most occurring category.

By combining the data from Fig. 7.12 with the data from Fig. 7.15 a new metric can be calculated:

$$G(\tau)_{m4}^{\text{weighthed}} = G(\tau)_{m4}^{\text{FB}} * N^{\text{FB}} + G(\tau)_{m4}^{\text{MSB}} * N^{\text{MSB}} + G(\tau)_{m4}^{\text{RB}} * N^{\text{RB}} \quad (7.2)$$

with  $N$  the number of TPs in the category,  $G(\tau)_{m4}$  the mean value of the correlations coefficient of the category and  $G(\tau)_{m4}^{\text{weighthed}}$  the weighted mean value of the correlations coefficient of all blinking categories.

This is shown in Fig. 7.16. The  $G(\tau)_{m4}^{\text{weighthed}}$  is close to  $G(\tau)_{m4}^{\text{allTPs}}$ . This suggests that the influence of the non-blinking signals in the stack do not have a significant influence on  $G(\tau)_{m4}^{\text{allTPs}}$  and therefore either  $G(\tau)_{m4}^{\text{allTPs}}$  or  $G(\tau)_{m4}^{\text{weighthed}}$  can be used to estimate the suitability for cryo-SOFI.

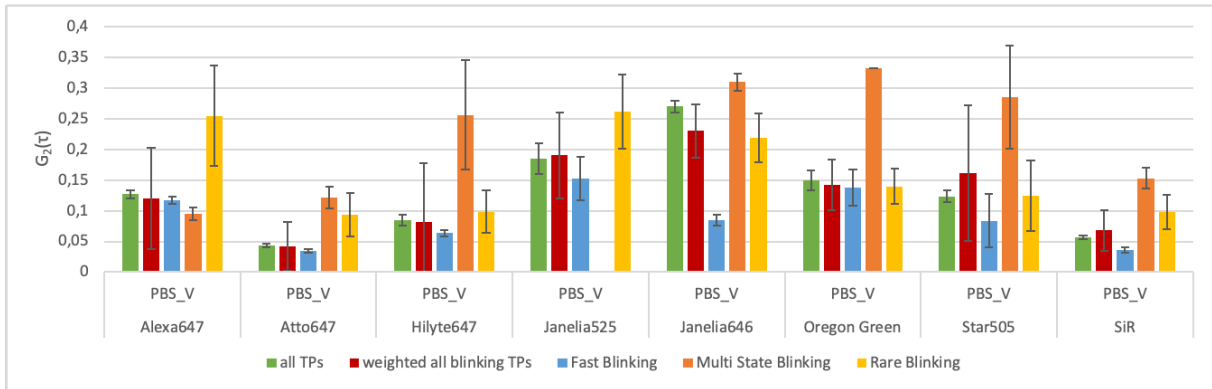


**Fig. 7.16.** Weighted mean of  $G(\tau)_{m4}$  of the ACs (Fig. 7.12) from all blinking categories (Fig. 7.15). For this the percentage of the categories was used to calculate the mean of  $G(\tau)_{m4}$  for all the blinking categories. Different blinking categories are colour-coded: green = all TPs, red = weighted  $G(\tau)_{m4}$  of all blinking categories, blue = FB TPs, orange = MSB TPs and yellow = RB TPs. The error bars show the SEM.

## 7.4. Determination of on and off times for the FB category

In this chapter the FB category is investigated further. From the preceding methods the  $t_{\text{on}}$  and  $t_{\text{off}}$  can not be determined. Initially the threshold method from Böning *et al.*<sup>68</sup> used to determine the  $t_{\text{on}}$  and  $t_{\text{off}}$ . For this threefold standard deviation is used as a threshold to determine when a molecule is considered in its on-state or off-state. One example of this is shown in Fig. 7.17 and a zoom-in in Fig. 7.18. The developed Matlab script also obtains the length of each on or off event.

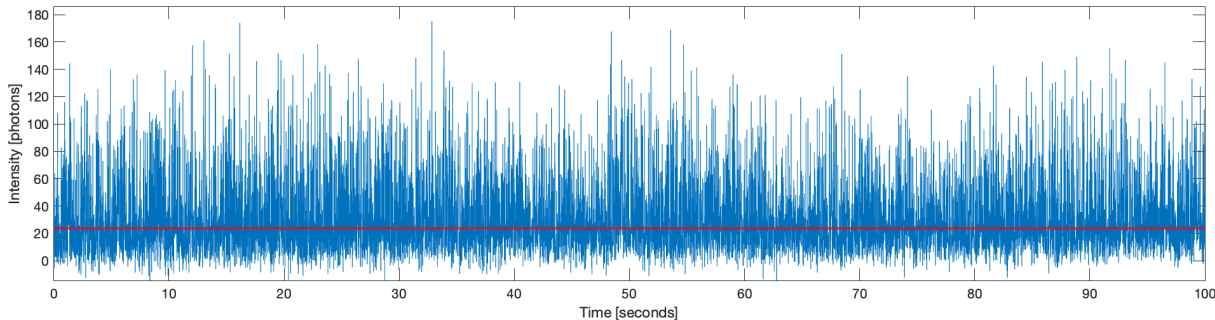


**Fig. 7.17.** One example TP from the FB category with the threshold of 3 standard deviations drawn in. The temporal resolution is 10 ms.

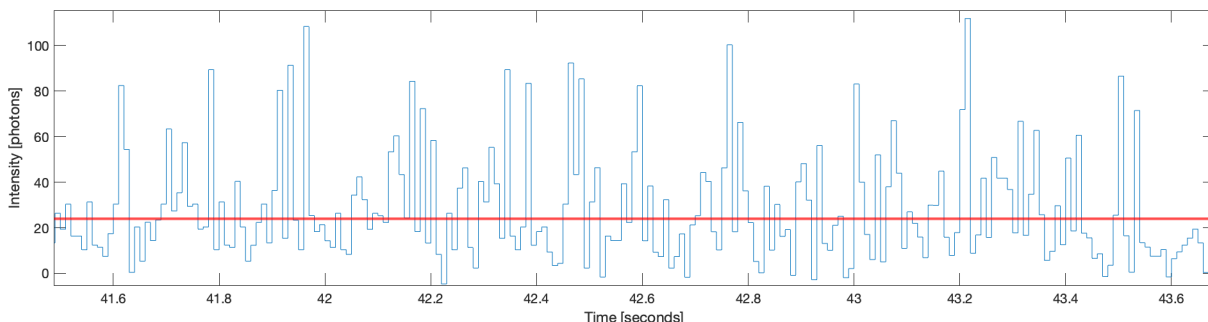


**Fig. 7.18.** One example TP from the FB category with the threshold of 3 standard deviations drawn in. The temporal resolution is 10 ms.

To obtain the on-times and off-times from the on-frames and off-frames a biexponential fitting on the on on-frames and off-frames was done. The resulting on-times and off-times are shown in Tab. 7.1.

**Tab. 7.1:** On-time and off-times of Alexa647<sub>PBS\_V</sub> determined by the threshold method. The errors show the standard deviation.

$t_1^{\text{on}}$	$t_2^{\text{on}}$	$t_1^{\text{off}}$	$t_2^{\text{off}}$
$18.65 \pm 0.94$	$60.1 \pm 4.11$	$38.45 \pm 1.35$	$94.32 \pm 2.97$

To confirm if the method is working properly and the obtained times are correct, a few different TPs were simulated and the same workflow as for the experimental single molecule data was used to obtain the on-times and off-times from the simulated data. The results are shown in Tab. 7.2.

**Tab. 7.2:** On-time and off-times of simulated TPs determined by the threshold method. Two different sets of signal intensity  $I_{\text{signal}}$  and background intensity  $I_{\text{BG}}$  was used to estimate the suitability of the method. The errors shows the standard deviation.

	$I_{\text{signal}}$	$I_{\text{BG}}$	$t^{\text{on}}$ [ms]	$t^{\text{off}}$ [ms]
input	60	7	20	50
output			$24.4 \pm 0.2$	$61.6 \pm 0.3$
input	37	9	20	50
output			$19.0 \pm 0.3$	$83.7 \pm 0.3$

For the first input parameters both times were overestimated by the threshold method. If the signal to noise ratio (SNR) is worse the estimate for  $t^{\text{off}}$  is getting worse. It shows that the threshold method produces reliable results for the kind of TP where there is only a single molecule with a clear FB behaviour. For molecules with a low signal to noise ratio, this method can introduce a systematic error in the determination of the on- and off-times as the noise might influence the detection of the on-states.

Instead of the threshold method a different method was developed. This new method use different on-times, off-times, signal intensity and background intensity to simulate TPs. The resulting intensity histograms are compared to the histograms of the measured TPs to find the best fit. This method is here called "histogram fit method". One example of the fit is shown in Fig. 7.19.

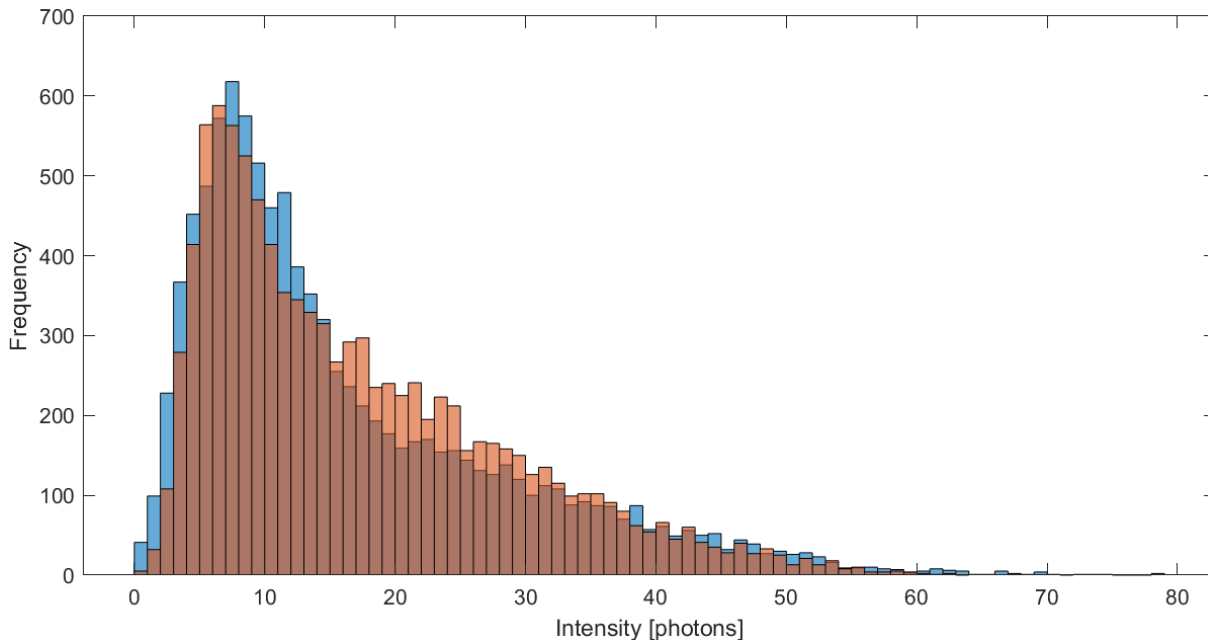


**Fig. 7.19.** One example of the histogram fit method. Overlaid are the histogram of fluorescence intensities from the measured TP (blue) and the histogram of the simulated TP (orange).

The parameters of the histogram with the best fit were extracted to estimate  $t_{\text{on}}$  and  $t_{\text{off}}$  of the measured TPs. This was repeated for all the measured TP and for all investigated dyes to obtain the average value for the parameters.

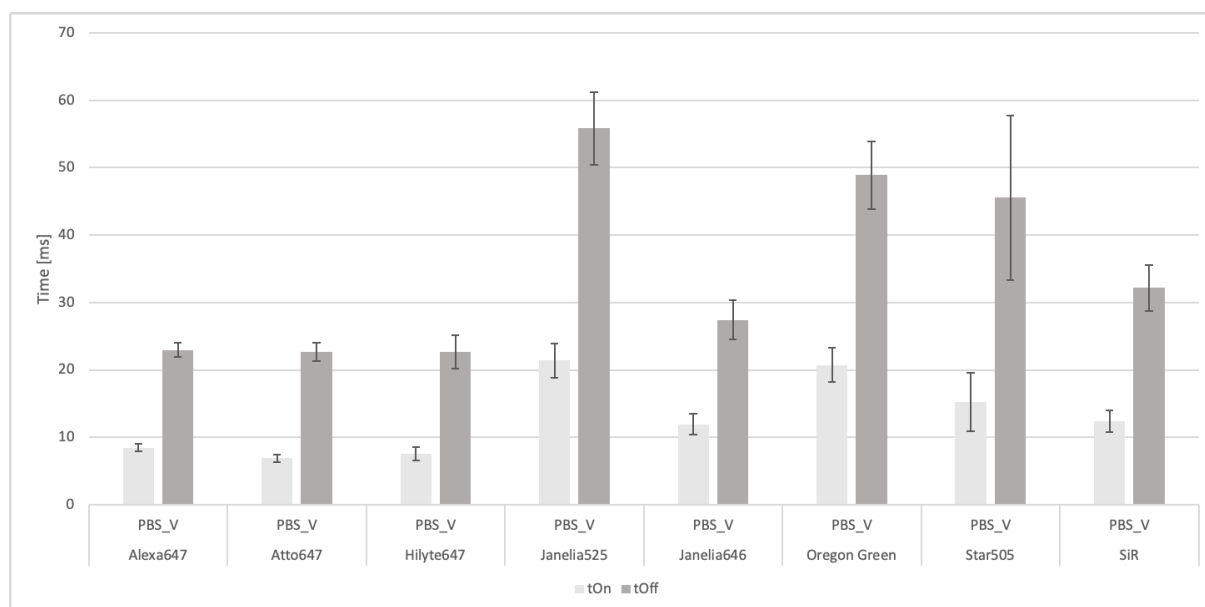


**Fig. 7.20.** On- and off-times of the FB category of different dyes.  $t_{\text{on}}$  and  $t_{\text{off}}$  determined from the histogram method in light gray and dark gray, respectively. All of the  $t_{\text{on}}$  are in the range of 6 to 32 ms and always smaller than  $t_{\text{off}}$  which is between 22 and 79 ms. The y-axis shows the time in ms. The error bars show the SEM.

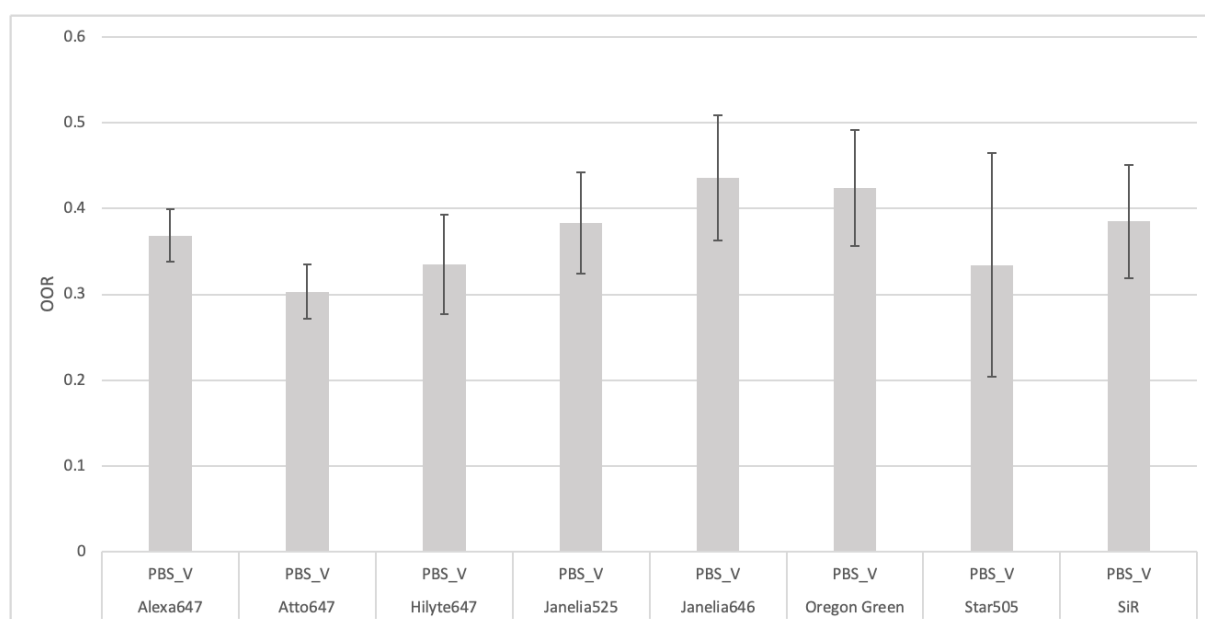


**Fig. 7.21.** OOR of the molecules of the FB category of all investigated dyes. The error bars show the SEM.



In Fig. 7.20 the determined  $t_{\text{on}}$  and  $t_{\text{off}}$  are shown for all investigated dyes in light gray and dark gray  $t_{\text{on}}$  and  $t_{\text{off}}$ , respectively. For every dye  $t_{\text{on}}$  is smaller than  $t_{\text{off}}$  and ranges from approx. 6 to 32 ms.  $t_{\text{off}}$  ranges from approx. 22 to 79 ms.

To achieve a better comparison of the dyes with each other regarding their suitability for cryo-SR-FM, the on-off-ratio (OOR) can be used. The OOR gives the ratio of  $t_{\text{on}}$  and  $t_{\text{off}}$ . A small OOR is desirable since it means that  $t_{\text{on}}$  is smaller than  $t_{\text{off}}$  which is beneficial for SOFI and SMLM. The OOR is given by:

$$\text{OOR} = \frac{t_{\text{on}}}{t_{\text{off}}} \quad (7.3)$$

The OOR of the molecules of the FB category of all investigated dyes are shown in Fig. 7.21. For all investigated dyes, the OOR of the FB category are in the range of 0.3-0.5.

## 7.5. Investigation of the effect of different environments on blinking and fluctuating fluorescent states for single Alexa Fluor 647 molecules

In this section the influence of conditions, in this case the media in which they were frozen and how they were frozen will be investigated. Those conditions are non-vitrified polyvinyl alcohol (PVA\_nonV), non-vitrified PBS (PBS\_nonV), vitrified PBS (PBS\_V) and vitrified heavy water PBS (dPBS\_V).

PVA was chosen since it is a common medium used in spectroscopy. PBS is a common buffer used in biological research and was therefore chosen as an environment for the dyes that comes close to their actual usage for cellular imaging. Lee *et al.*<sup>69</sup> showed that heavy water has a positive effect on the photo physics of dyes for room temperature (RT) SMLM methods. The fluorescence quantum yield is twice as high compared to water, which leads to the detection of twice as many photons, and therefore leads to an improvement of the mean localization precision.<sup>69</sup> Since it is also biocompatible it was also investigated. To examine if the ice arrangement of the frozen water molecules surrounding the fluorophore has an impact on the blinking behaviour PBS\_V was compared to non-vitrified samples.

### 7.5.1. Autocorrelation based comparison of different environments for Alexa Fluor 647 molecules

The  $G(\tau)_{m4}$  comparison of the different Alexa647 conditions are shown in Fig. 7.22. PVA\_nonV stands out since all of its  $G(\tau)_{m4}$  are significantly higher than the other conditions. For  $G(\tau)_{m4}^{\text{allTPs}}$  the other conditions are only approx. 1/2 or 1/4 of it. For PVA\_nonV

7.5. Investigation of the effect of different environments on blinking and fluctuating fluorescent states for single Alexa Fluor 647 molecules

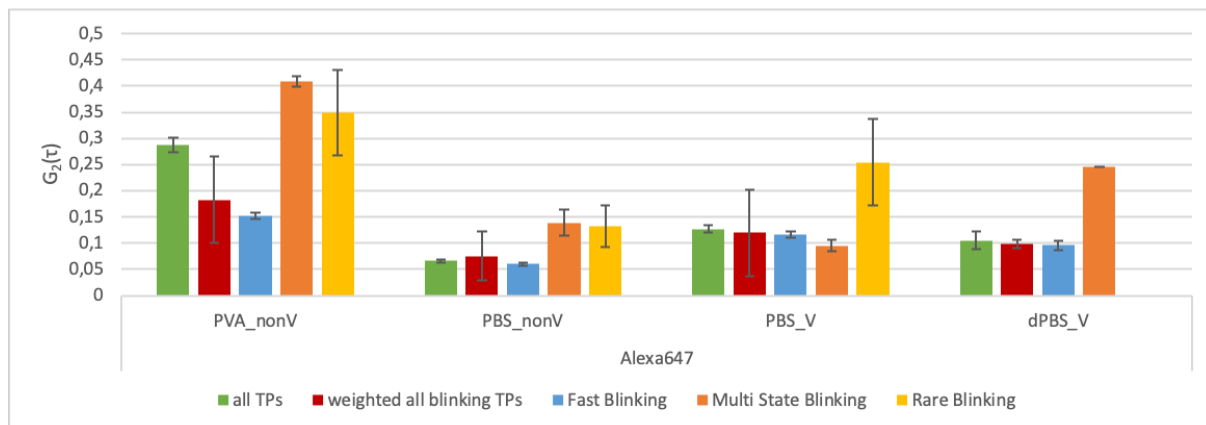


**Fig. 7.22.**  $G(\tau)_{m4}$  of each category for all conditions in which Alexa647 was investigated. Different blinking categories are colour-coded: green = all TPs, red = weighted  $G(\tau)_{m4}$  of all blinking categories, blue = FB TPs, orange = MSB TPs and yellow = RB TPs. The error bars show the SEM.

the  $G(\tau)_{m4}^{\text{weighted}}$  differs significantly from  $G(\tau)_{m4}^{\text{allTPs}}$ . This suggest that there is a major influence from the TPs which are not categorized as a clearly distinguishable blinking category. Overall PBS\_nonV has the lowest  $G(\tau)_{m4}$ s off all conditions, only  $G(\tau)_{m4}^{\text{MSB}}$  of PBS\_V is lower. dPBS\_Vs  $G(\tau)_{m4}$ s are quite similar to dPBS\_Vs. Only  $G(\tau)_{m4}^{\text{MSB}}$  differs by 0.15 and there is no occurrence of the RB category in the performed measurements.

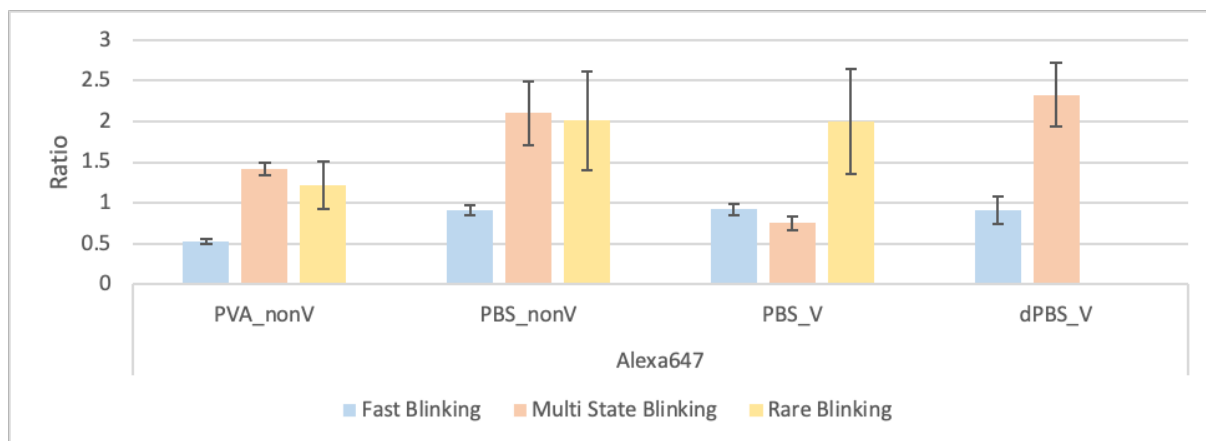


**Fig. 7.23.** Ratio of  $G(\tau)_{m4}$  of each category to  $G(\tau)_{m4}^{\text{allTPs}}$  for all conditions in which Alexa647 was investigated. The different categories are colour-coded: blue = FB, orange = MSB and yellow = RB. The error bars show the SEM.

In Fig. 7.23 the  $G(\tau)_{m4}$  ratios of each category to  $G(\tau)_{m4}^{\text{allTPs}}$  are shown, as defined in (7.1).  $G(\tau)_{ratio}^{\text{FB}}$  is close to 1 for all conditions but PVA\_nonV. Additionally,  $G(\tau)_{ratio}^{\text{MSB}}$  for all conditions are higher than PBS\_V.

### 7.5.2. Categorization comparison of Alexa Fluor 647 molecules in different environments

In this section the influence of different environments on Alexa647 blinking behaviour will be investigated.

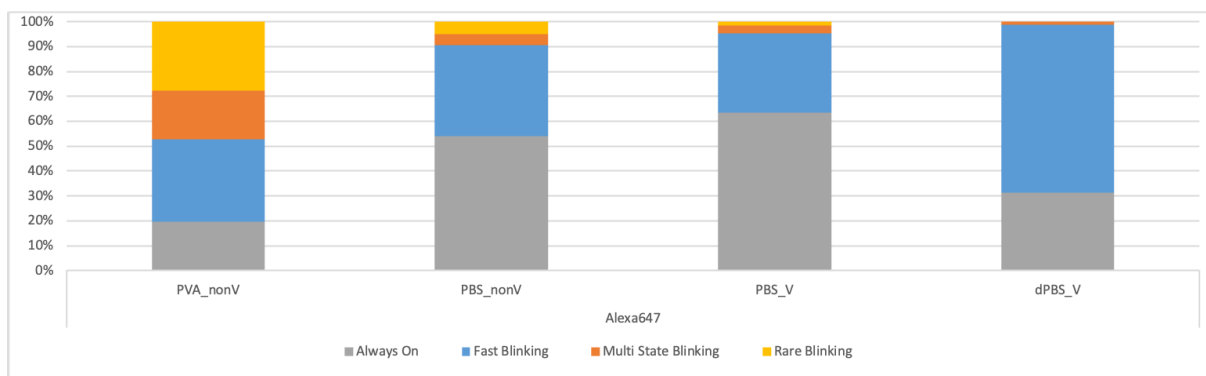


**Fig. 7.24.** Percentage of all categories from all conditions in which Alexa647 was investigated. Different categories are colour-coded: gray = always on, blue = fast blinking (FB), orange = multi state blinking (MSB), yellow = rare blinking (RB).

In Fig. 7.24 the percentage of all categories are shown. PVA\_nonV has the lowest "always on" percentage with aprox. 20% followed by dPBS\_V with aprox. 30%. The other two conditions are at 55-65%. In Fig. 7.25 only the FB, MSB and RB categories are shown. PVA\_nonV has the lowest percentage of FB but it still makes up the biggest part by just a few percent. For the other conditions the FB category dominates with least 80% and more.

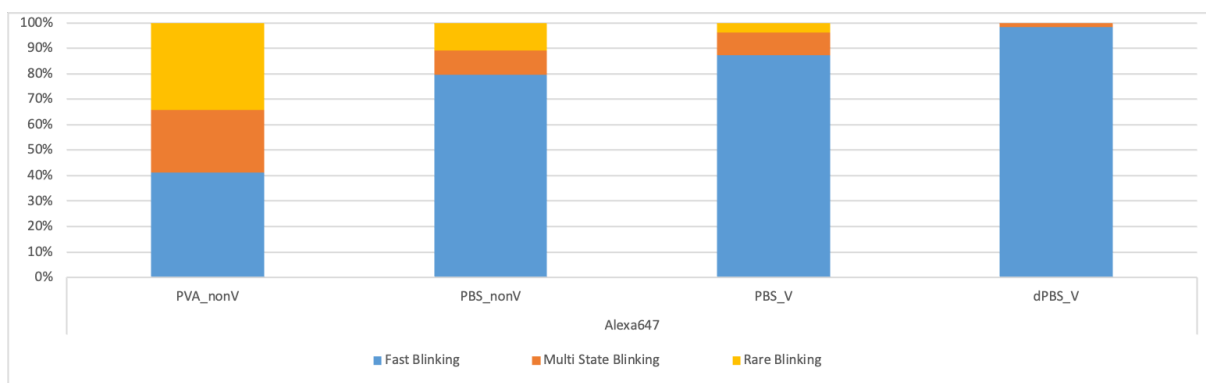


**Fig. 7.25.** FB, MSB and RB categories only from Fig. 7.24 are shown and are colour-coded: blue = FB, orange = MSB and yellow = RB. The FB category is the most occurring category.

### 7.5.3. Determination of on- and off-times of single Alexa Fluor 647 molecules for the FB category

The determined  $t_{on}$  and  $t_{off}$  are shown in Fig. 7.26. Compared to PBS\_V the  $t_{on}$  of the other conditions are higher by 1-3 ms but given the error the difference is not significant.  $t_{off}$  is for all the dyes in a similar range.

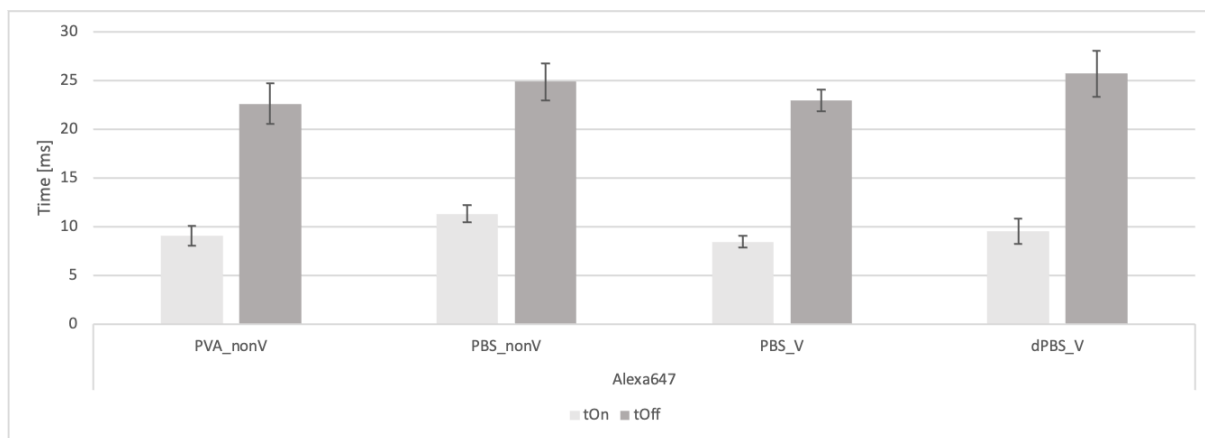


**Fig. 7.26.**  $t_{on}$  and  $t_{off}$  of the different conditions of Alexa647 determined from the histogram method in light gray and dark gray, respectively. The y-axis shows the time in ms. The error bars show the SEM.

In Fig. 7.27 the OOR are shown. Here PBS\_V has the lowest OOR. The other conditions are higher by at least 0.1 to 0.2. PBS\_nonV has the highest OOR with 0.4.

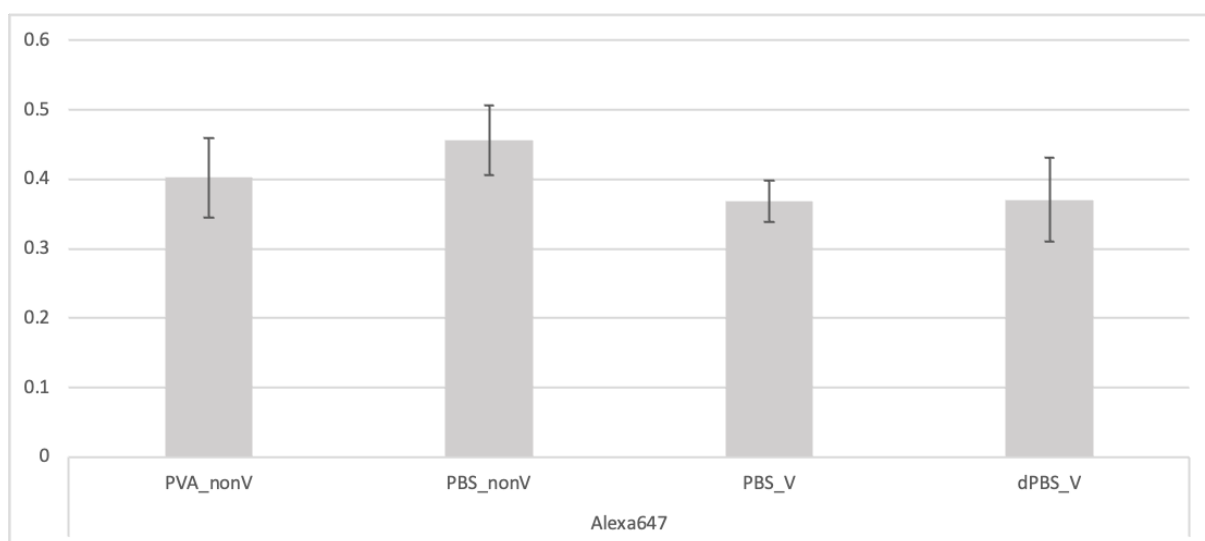


**Fig. 7.27.** OOR of the different conditions in which Alexa647 was investigated. The error bars show the SEM.

## 7.6. Influence of heavy water on photo-physics of organic dyes

In the previous section it was shown that PVA had an influence on the photo physical behaviour of Alexa647, but since it can not be used with living cells an interesting biocompatible alternative could be heavy water. As shown above there is an influence on Alexa647 caused by heavy water on the photo physical properties. Lee *et al.*<sup>69</sup> also showed that heavy water had an positive influence on RT SMLM. The fluorescence quantum yield is twice compared to water, therefore the detected photons are twice as many leading to an improvement in mean localization precision.<sup>69</sup> For this different dyes are compared which were vitrified in normal PBS and PBS made with heavy water (dPBS).

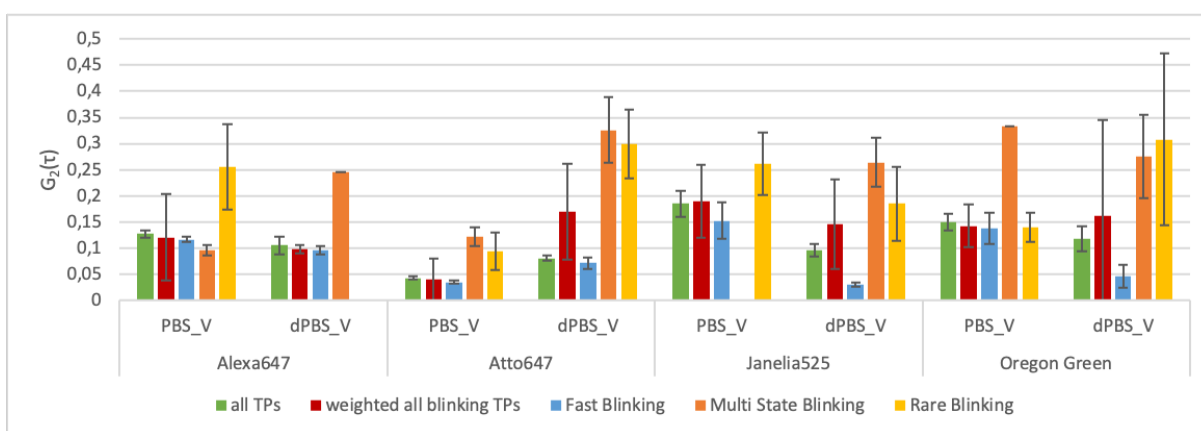


**Fig. 7.28.**  $G(\tau)_{m4}$  of each category for all dyes made in PBS and dPBS. Different blinking categories are colour-coded: green = all TPs, red = weighted  $G(\tau)_{m4}$  of all blinking categories (defined in (7.2)), blue = FB TPs, orange = MSB TPs and yellow = RB TPs. The error bars show the SEM.

In Fig. 7.28 the  $G(\tau)_{m4}$ s of all the dyes made with dPBS were shown. For Alexa647 the  $G(\tau)_{m4}$ s are quite similar. Only  $G(\tau)_{m4}^{\text{MSB}}$  is nearly twice as high in dPBS and there is no occurrence of the RB category but might be due to statistical inaccuracies, as also for standard PBS the total number of RB events was relatively low. For Atto647 all  $G(\tau)_{m4}^{\text{MSB}}$  is higher in dPBS. In most cases twice to thrice compared to PBS.  $G(\tau)_{m4}^{\text{weighted}}$  differs by double the  $G(\tau)_{m4}^{\text{allTPs}}$ . Janelia525 shows a reduction of all  $G(\tau)_{m4}^{\text{MSB}}$ . For  $G(\tau)_{m4}^{\text{allTPs}}$  it is half of PBS,  $G(\tau)_{m4}^{\text{weighted}}$  is smaller by 0.05 and for  $G(\tau)_{m4}^{\text{RB}}$  it is smaller by 0.08.  $G(\tau)_{m4}^{\text{FB}}$  has the most dramatic change with value of 1/5 of PBS. The effect of heavy water on OG is mixed.  $G(\tau)_{m4}^{\text{allTPs}}$  and  $G(\tau)_{m4}^{\text{MSB}}$  are reduced by a bit.  $G(\tau)_{m4}^{\text{weighted}}$  on the other hand increased a bit. A more dramatic change is seen by  $G(\tau)_{m4}^{\text{FB}}$  where it is reduced to 1/3 of PBS and  $G(\tau)_{m4}^{\text{RB}}$  is doubled.

As shown in Fig. 7.29 there is a trend that the percentage of the "always on" molecules increases strongly with the use of dPBS but Alexa647 where it reduces by half.

In Fig. 7.30 only the FB, MSB and RB categories are shown. For Alexa647 the MSB and RB category reduces strongly. Atto647 contrastingly has an increase in the MSB and RB

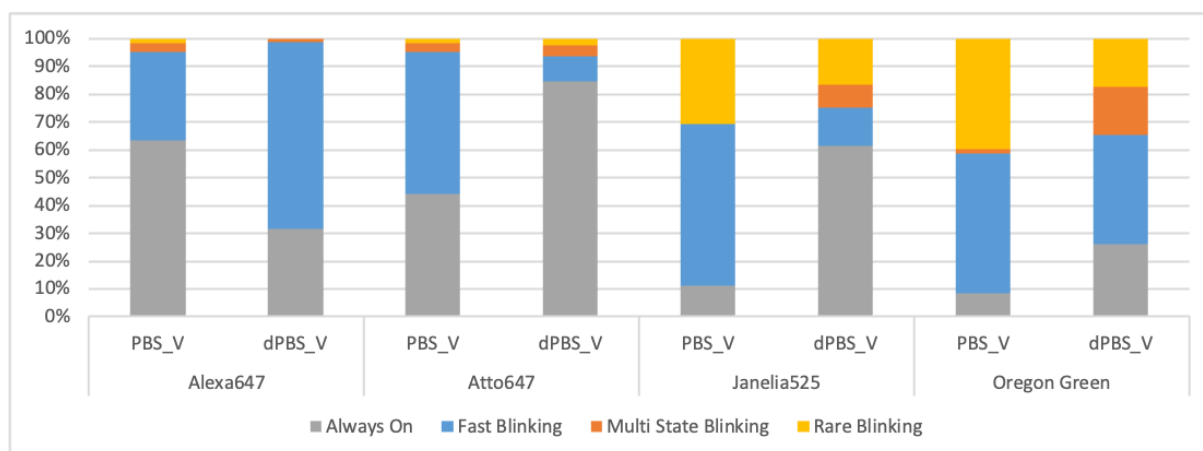


**Fig. 7.29.** Percentage of all categories for all dyes made in PBS and dPBS. Each bar represent one dye. Different categories are colour-coded: gray = always on, blue = fast blinking (FB), orange = multi state blinking (MSB), yellow = rare blinking (RB).

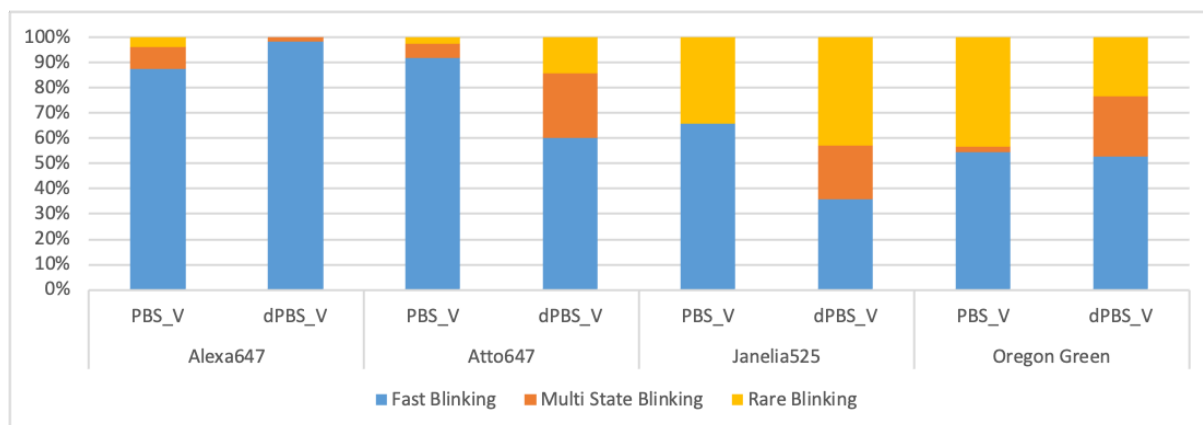


**Fig. 7.30.** Only the FB, MSB and RB categories from Fig. 7.29 are shown and are colour-coded: blue = FB, orange = MSB and yellow = RB. The FB category is the most occurring category.

category percentage, which is also true for Janelia525. For OG the FB category is similar only the proportion between the MSB and RB category changes. MSB increase to the same percentage as RB.

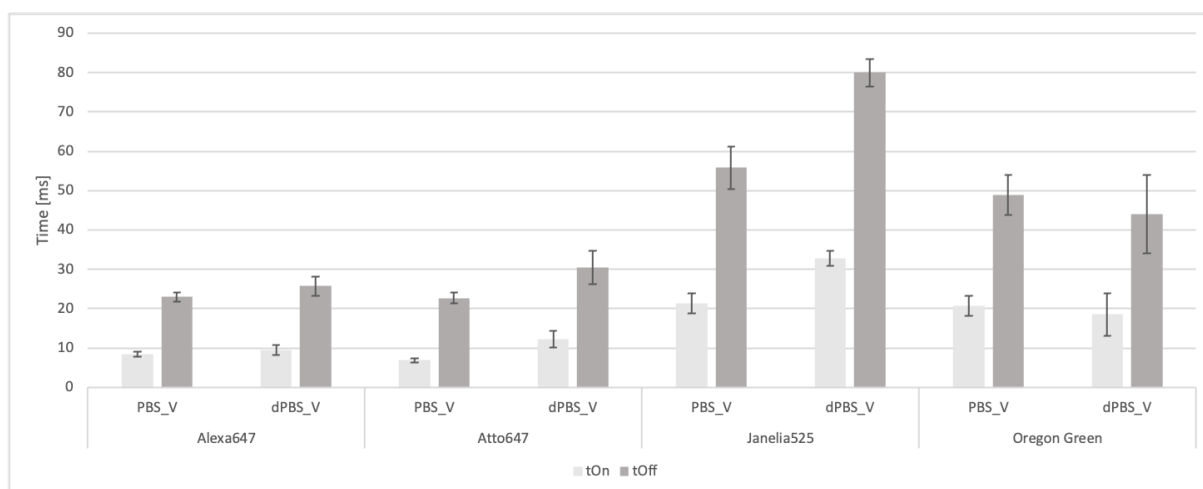


**Fig. 7.31.**  $t_{on}$  and  $t_{off}$  of the FB categories of all dyes made in PBS and dPBS determined from the histogram method in light gray and dark gray, respectively. The y-axis shows the time in ms. The error bars show the SEM.

The  $t_{on}$  and  $t_{off}$  of the FB categories of the investigated dyes determined by the histogram method are shown in Fig. 7.31. For Alexa647 no clear change in  $t_{on}$  and  $t_{off}$  can be observed if taking the error into account. For Atto647 and Janelia525 an increase for both  $t_{on}$  and  $t_{off}$  can be observed. Only for OG there is a trend that both  $t_{on}$  and  $t_{off}$  decreases. Overall, taking the error margins into account, the observed on- and off-times for the FB category seem to be not substantially influenced by using dPBS instead of standard PBS.

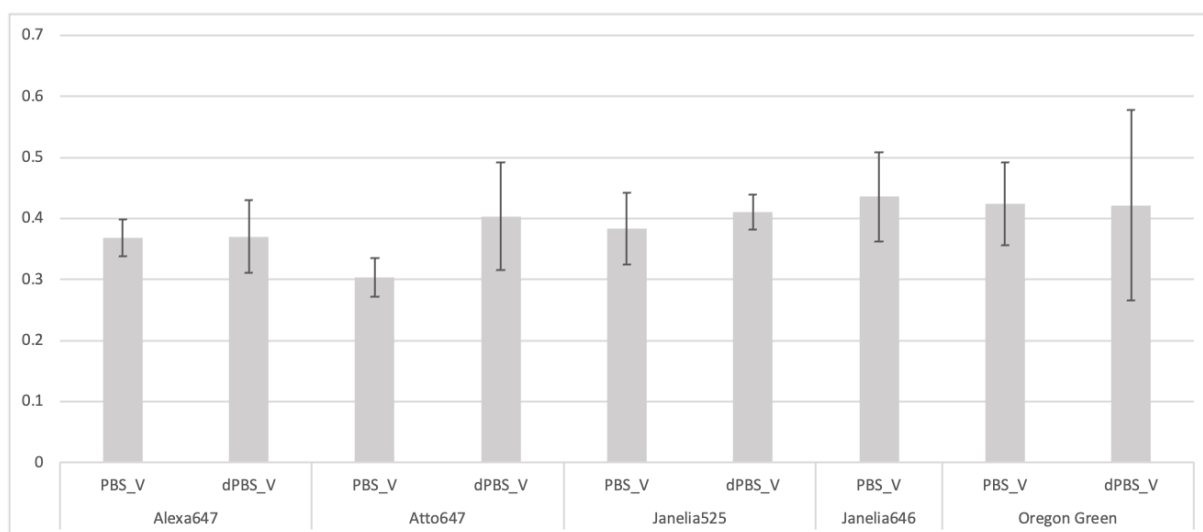


**Fig. 7.32.** OOR of all dyes made in PBS and dPBS. The error bars show the SEM.

In Fig. 7.32 the OOR of the investigated dyes made with standard PBS and heavy water PBS is shown. The OOR of most showed no clear change and lies within the error mar-

gins. Only Atto647 showed an increase of the OOR. Even though  $t_{\text{on}}$  and  $t_{\text{off}}$  of Atto647 increase as shown above, the difference between them is decreasing.

## 7.7. Qualitative analysis of multiple fluorescent states in individual single molecule time traces

In this chapter some specific molecules are analysed individually. This shows that the even though categorization might give a good overview and an easy way to characterize a dye, the molecules are more dynamic and complex if studied in detail.

In Fig. 7.33 the effect of different temporal binning is shown. For this a part from a TP from one Alexa647<sub>PVA<sub>nonV</sub></sub> molecule was chosen as an example. The TP starts at 50 s into the measurement. The original TP with an integration time of 10 ms is shown in the top panel. Three distinct sections can be observed: From the beginning of the time profile up to 70 s, from 70 s to 90 s and from 90 s to 100 s. In the first section the blinking behaviour is that of the FB category, spending more time in the off-state than in the on-state. At around 70 s it switches to an FB like behaviour where the molecule is mostly in the on-state and turns off occasionally but still considered fast blinking. In the third section the molecule switches back to FB, with the molecule spending more time in the off-state than in the on state. However, compared to the first section the frequency of switching into the on-states is higher. The constant intensity level of the on-state in all three sections and the returning to the background level in the off-switching, even for the second section, indicate that the TP indeed originates from only one molecule.

In the middle panel of Fig. 7.33 the same TP cut-out is shown with a 100 ms time binning. Here, the fast blinking in the first section looks like background with noise with a short on-state (similar to the RB category) at around 57 s. The second sections looks like the molecule turned into an on-state until it switches into an intermediate state in the third section where the intensity is fluctuating between a level that is higher than the background level in first section and an intensity level in the on state that is lower than the plateau in the second section. If the 10 ms time resolution data would not be available, one might conclude from the 100 ms binned TP that the intensity behaviour is originating from two (or more) molecules, as especially the change from the first to the second section looks like the result of a second molecule switching into the on-state. In the bottom the same panel of Fig. 7.33 TP cut-out is shown with a 1 s time binning. The first section looks more and more like background, with the on-state peaks visible in the 100 ms binning merged into one peak. The second section section is now just one continuous on state and the last section an appears like an intermediate state. Similar to the considerations for the 100 ms binning, Looking at this TP alone one would most likely assume that this is the result of two molecules where in the first section both are mainly in the off-state, in the second section both molecules in the on-state and in the



third section only one molecule in the on-state.

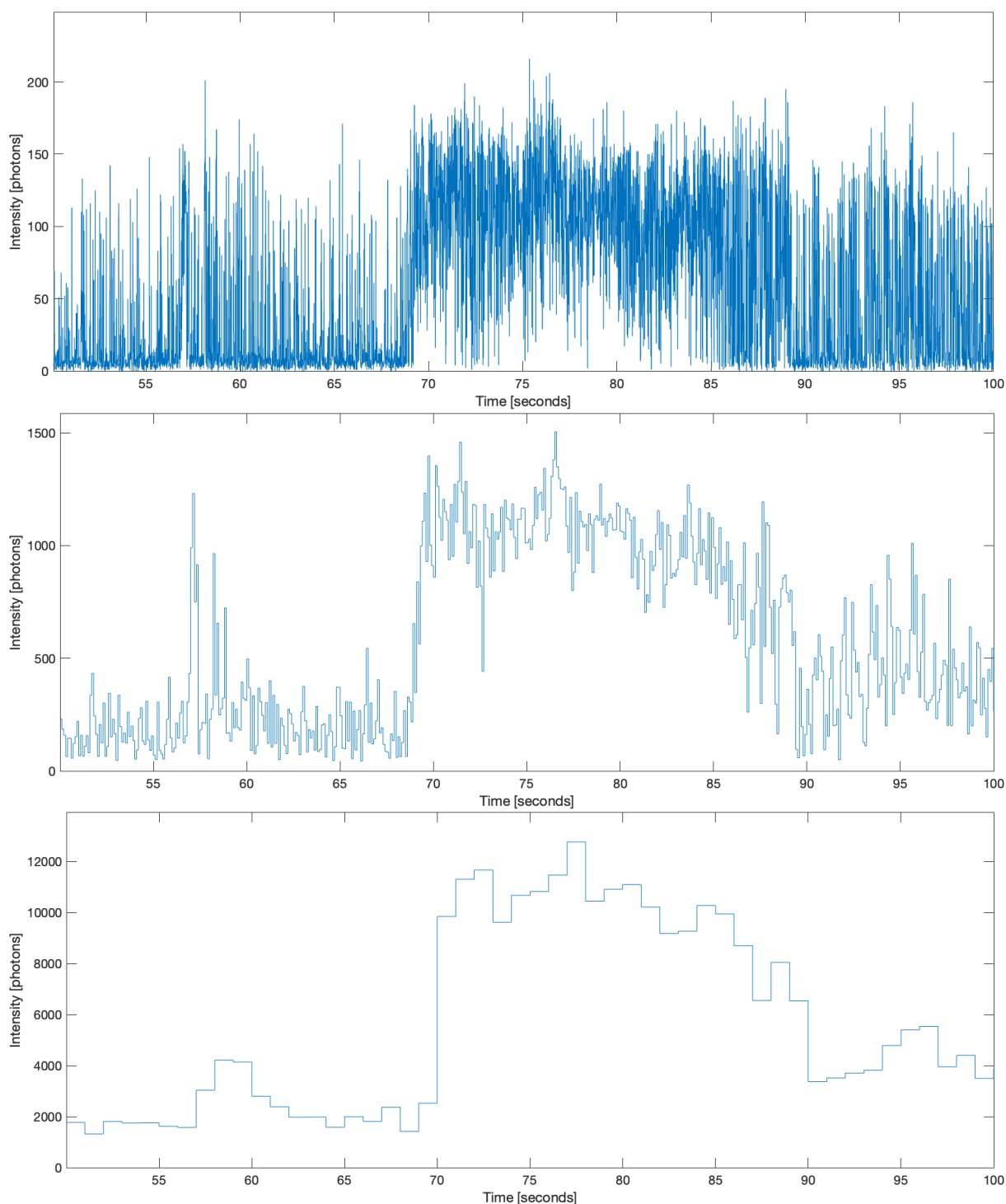


**Fig. 7.33.** Differently binned time profiles of one Alexa647<sub>PVA<sub>nonV</sub></sub> molecule. The time profile starts at 50 s into the measurement. Top: Original time profile with an integration time of 10 ms. Three distinct sections can be observed: From the beginning of the time profile up to 70 s, from 70 s to 90 s and from 90 s to 100 s. Middle and bottom: The same time profile cut-out with a 100 ms and 1 s time binning, respectively.

In Fig. 7.34 a TP from one Alexa647<sub>PBS<sub>V</sub></sub> molecule from the RB category is shown. With the same arguments as for the above discussed molecule, the TP at 10 ms temporal resolution shows that it is the result of a single molecule. Different sections of the TP are

marked which show changes in the blinking behaviour. The different sections are discussed in detail in Fig. 7.34, Fig. 7.35, Fig. 7.36, Fig. 7.37 and Fig. 7.38.

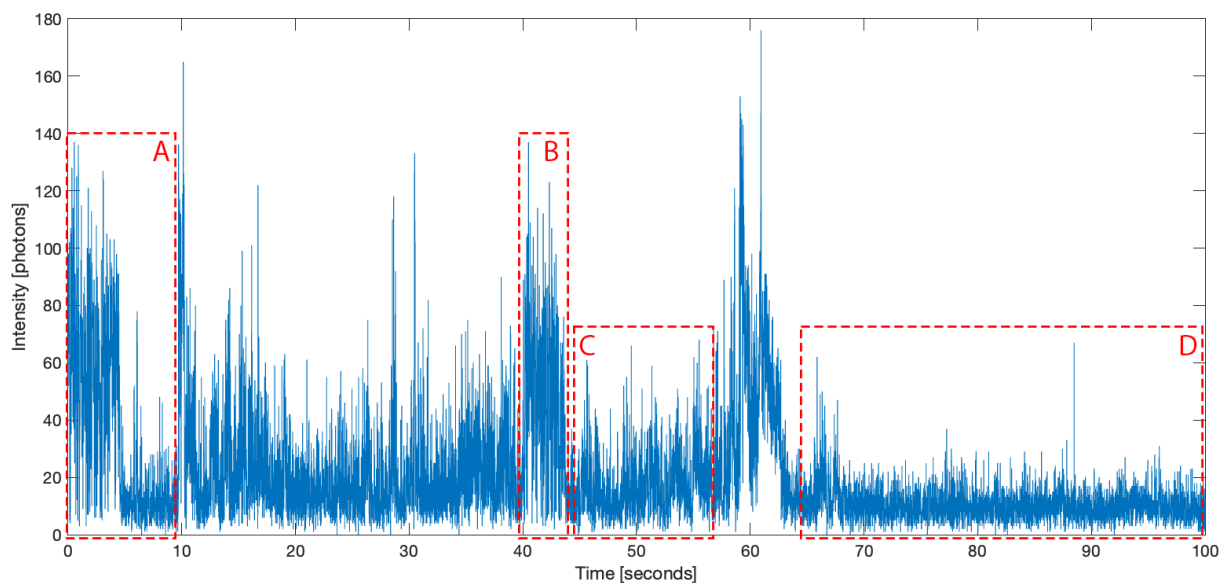


**Fig. 7.34.** TP of one Alexa647<sub>PBS\_V</sub> molecule from the RB category. On closer inspection different blinking behaviour can be observed in this one continuous recording of 100 seconds, which shows that the blinking behaviour is not limited to one category and can change over time. The integration time is 10 ms.

In Fig. 7.35 the first 9.5 seconds (section A) are shown. In the first 4.5 seconds the molecule is in a FB like behaviour where the molecule is more in the on-state than in the off-state. After that it changes into the RB category, where it mainly remains in the off-state and only occasionally switches into the on-state.

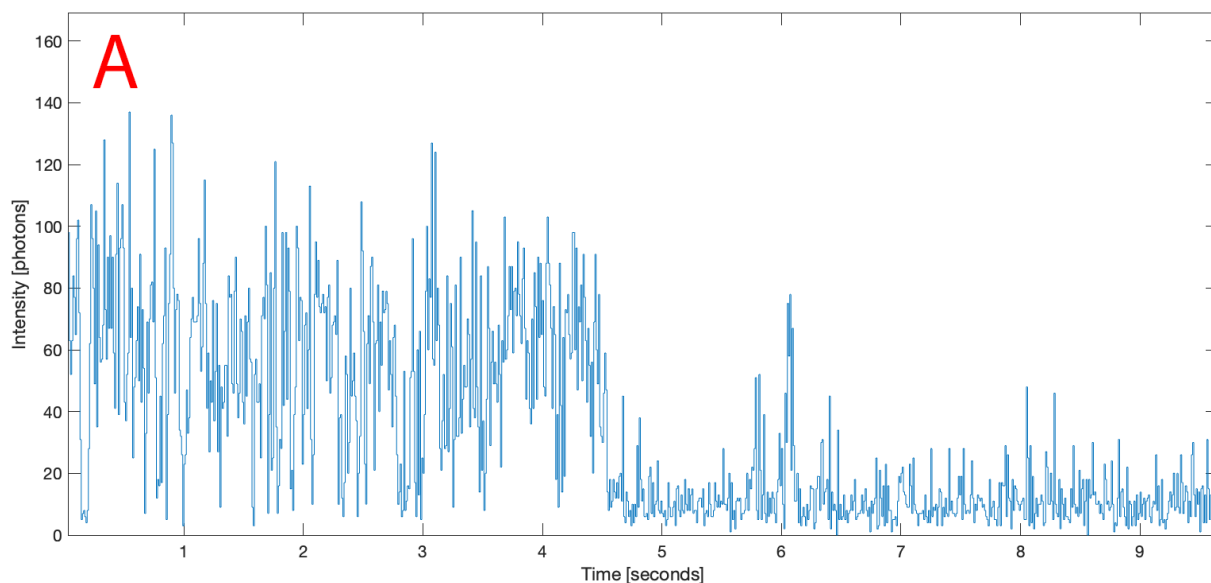


**Fig. 7.35.** Showing section A from Fig. 7.34. Here, in the first 4.5 seconds the molecule is in a mostly on-state, which would correspond to the FB category. Off-switching to the background level is observed. At around 4.5 seconds the behaviour changes to the RB category.

The section B is shown in Fig. 7.36 and includes the time range from 40 to 44 seconds. Like in the beginning of the TP it shows a FB like behaviour where the molecule is more in the on-state. At the beginning the off-state occurs less often and the molecule is more often in the on-state. Over the time span of 30 s the frequency of the off-states increases and the molecule tends to be less in the on-state. In orange the TP is shown with a time bin of 200 ms and shows the same section of the TP. In this figure it is possible to see the decrease in average intensity over the time span showing the change in on and off-state ratio. In the lower temporal resolution a slowly decreasing intensity is observable. Looking at the 10 ms temporal resolution the on and off-states can be clearly seen.

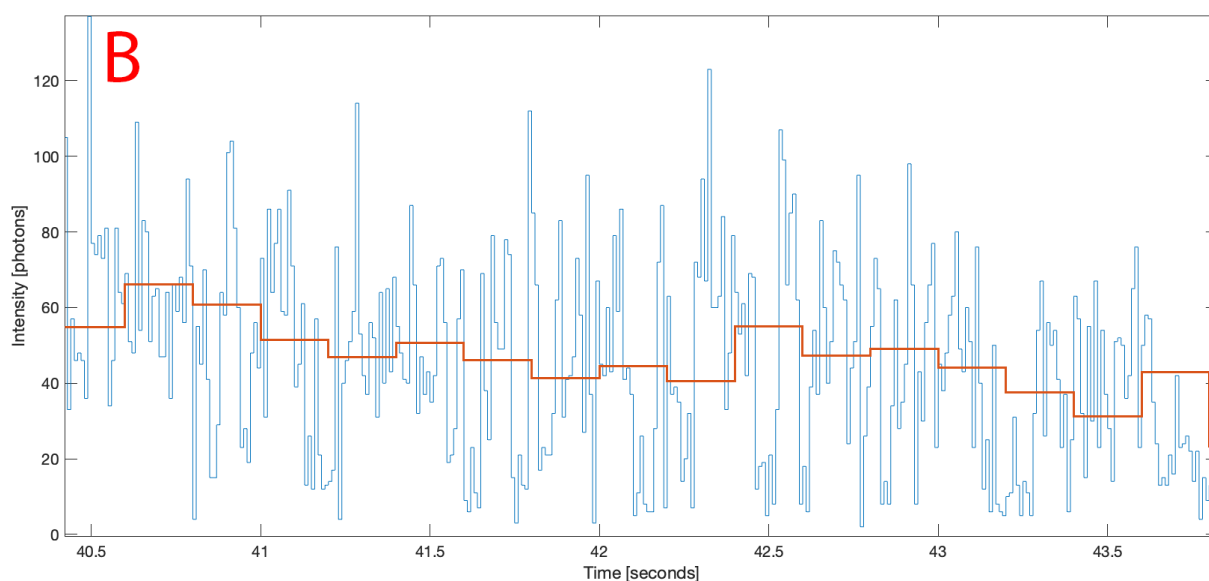


**Fig. 7.36.** Showing section B from Fig. 7.34 with two different time binnings. In blue the original integration time of 10 ms is shown, in orange 200 ms. It is possible to see that the frequency of the off-states increases leading to a drop in the average intensity which is clearly seen in the higher binning time color-coded in orange.

In Fig. 7.37 FB behaviour can be seen but with the difference that it tends to be more in the off-state.

Section D of the TP is shown in Fig. 7.38. In this section the molecules behaves like the second half of section A (Fig. 7.35) where it is mostly in the off-state and is similar to the FB and RB category.

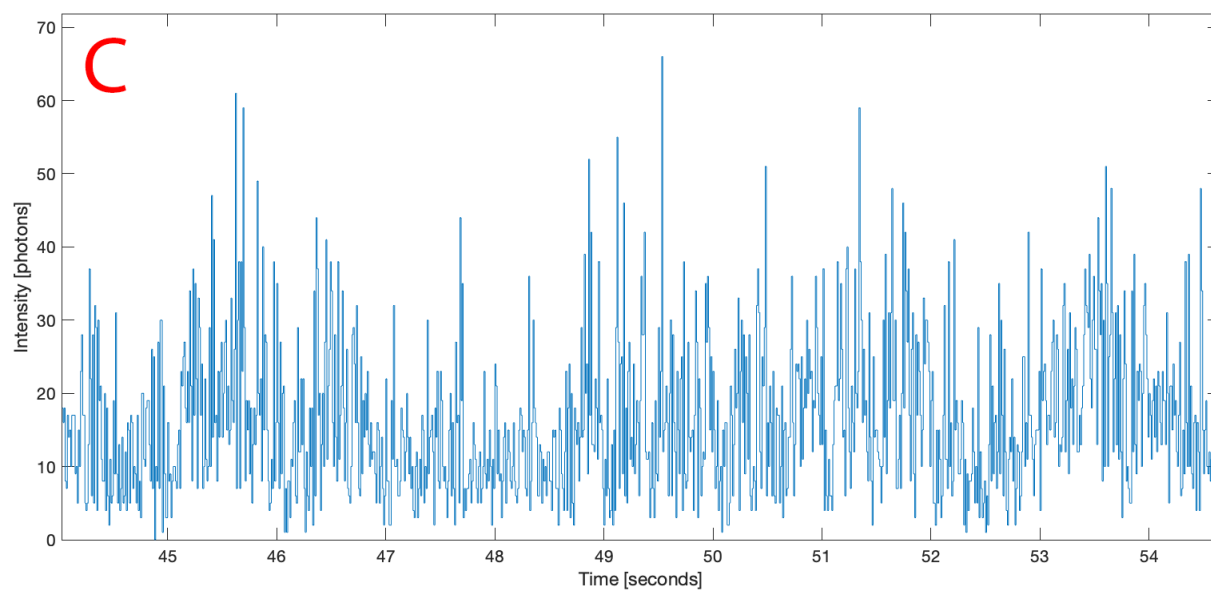


**Fig. 7.37.** Showing section C from Fig. 7.34. This section shows blinking behaviour the FB category but it tends to be more in the off-state.

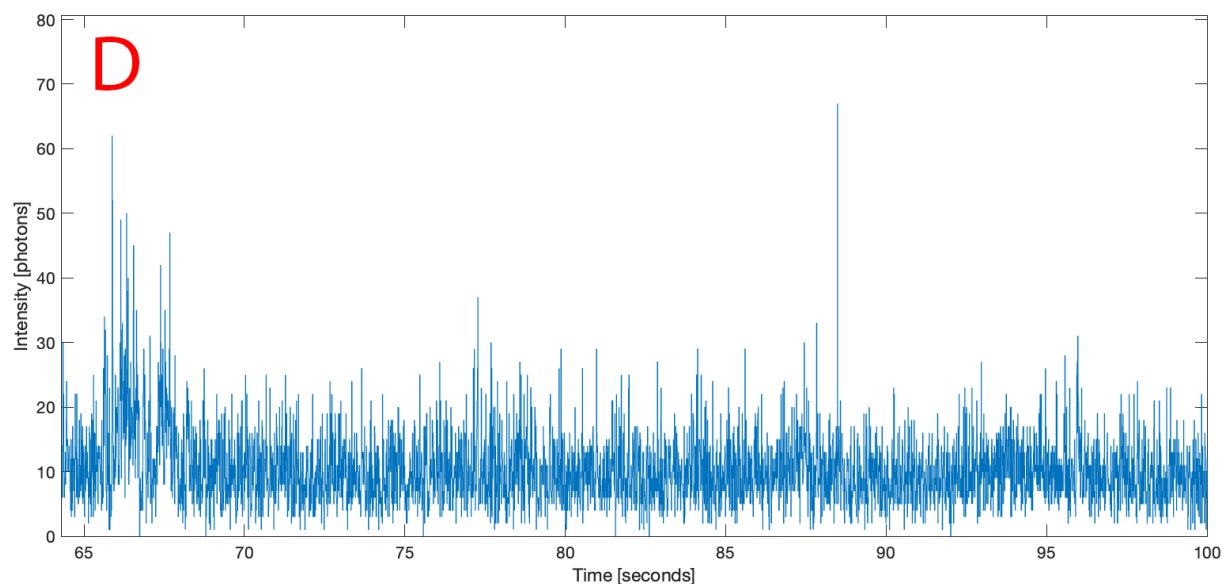


**Fig. 7.38.** Showing section D from Fig. 7.34. The last section of the time profile looks like the last half of section A, which is dominated by the off-state. The on-states are short but not as often and lies between FB and RB category.

## 7.8. Qualitative analysis of changes in single molecule switching on a time interval of hours

To see how the blinking behaviour of single molecules over a much longer time period (hours range) behaves and how intensity changes on the s-min range are connected to ms blinking/fluctuations, Alexa647<sub>PBS\_V</sub> was measured in the bespoke setup by Julian Falckenhayn. Two TPs are shown representatively in Fig. 7.39 and Fig. 7.41.

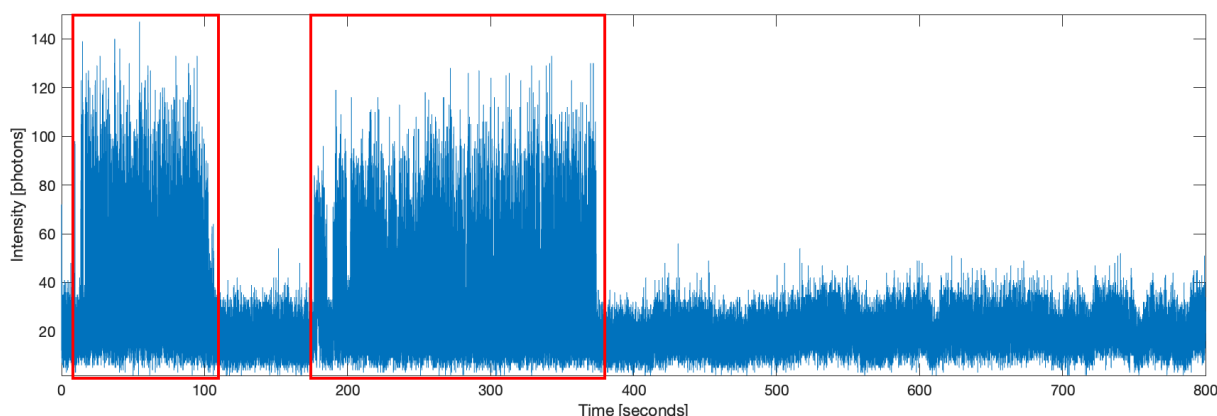


**Fig. 7.39.** TP from one Alexa647<sub>PBS\_V</sub> molecule over a time interval of 800 s. It shows a cut-out of a 35 min recording. After the switching at around 380 seconds the molecule did not change until the end of the recording. The integration time is 10 ms.

In Fig. 7.39 a TP of one molecule is shown where two different behaviours can be observed. The two boxes shows similar behaviour. FB with a high intensity over a time range of 90 seconds and 200 seconds. In Fig. 7.40 a zoom in from the transition at the end of the second box is shown. In the high intensity section the FB behaviour can be clearly observed and switched off afterwards.

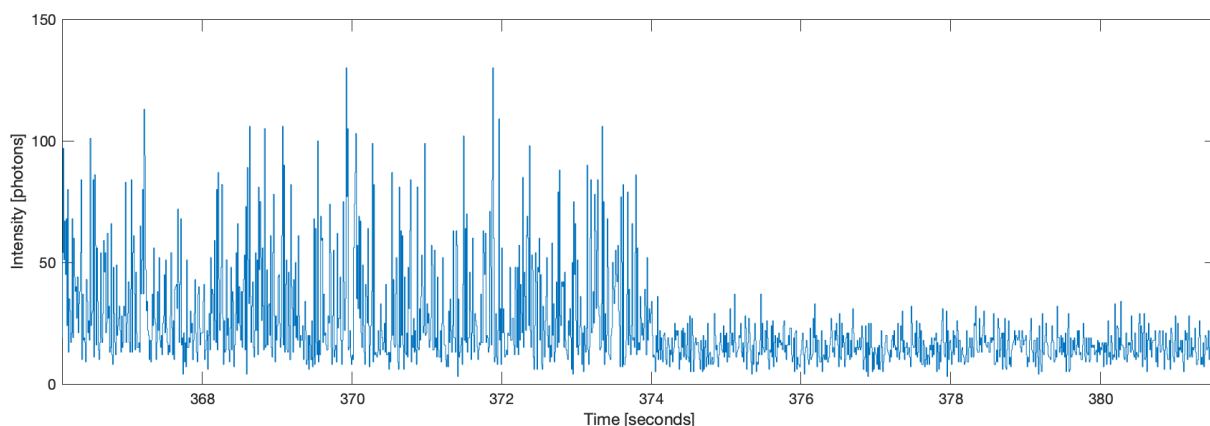


**Fig. 7.40.** Zoom in of the Alexa647<sub>PBS\_V</sub> molecule shown in Fig. 7.39. The transition from the on-state with FB behaviour to the off-state can be clearly seen. The integration time is 10 ms.

In Fig. 7.41 a TP of a Alexa647 molecule with a different blinking behaviour is shown. In the first 100 s the molecule is in an "always on" state with an intensity of aprox. 100

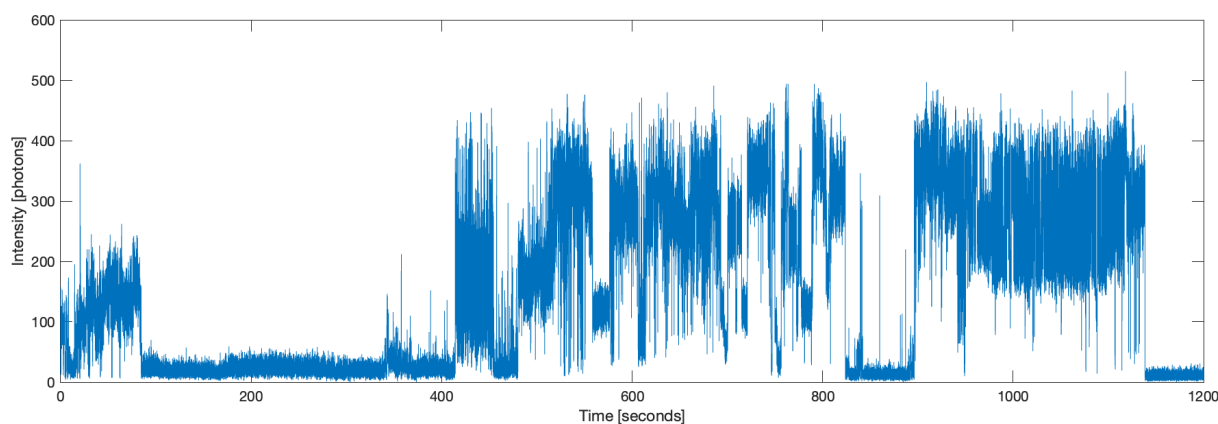


**Fig. 7.41.** TP from one Alexa647<sub>PBS\_V</sub> molecule over a time interval of 1200 s with a different blinking behaviour from the previous one in Fig. 7.39. It shows a cut-out of a 35 min recording. After about 1200 seconds the molecule switched into an off-state and did not switch back for the rest of the recording. The integration time is 10 ms.

to 200 photons. Which is about half the intensity of the following on-states. In this first section FB behaviour can be observed. If the measurement would be only 100 s long as the measurements for the quantitative characterization, it would be regarded as always on. Which means, that the shorter measurements can only show a "snapshot" of the TP and the molecule might be much more dynamic in its blinking behaviour. After this section for about 300 seconds the molecule is in an off-state. At the end of this section the molecule changes into a RB behaviour with intensities up to 200 photons. After this it changes into a different on-state. This on-state has a higher intensity of up to 500. From 400 to 800 s changes in the transition rates between an- and off-state can be observed. Additionally, there are intermediate intensity levels at 150 and 300 photons. Those intermediate states could be caused by the low temporal resolution. If the transition rate is faster than the temporal resolution the intensity looks like it is averaged. Between around 800 and 900 s it changes to a RB behaviour but with higher intensities of up to 400 photons. Between around 900 and 1100 s it changes into an on-state with rare off-switching until it changes back into an off-state for the rest of the recording.

## 7.9. UV recovery of different organic dye molecules

To investigate whether fluorescent molecules, which have transitioned to a long-lived off-state, can be actively brought back to the ground state to re-enter the fluorescence cycle, additional studies whether there is any photo reactivation/recovery by UV irradiation were made. For this Atto647 samples were plunge frozen on Protochips C-Flat copper grids with holey carbon. The samples were irradiated with 640 nm at 100 W/cm<sup>2</sup> and additional 405 nm at 10 and 20 W/cm<sup>2</sup> respectively for 1 second for recovery of the dye molecule. This was repeated for a recording time of 10 minutes. The collected series were post processed by a Matlab script which detected the UV irradiation and removed

these frames from the time series to compare single molecule blinking before and after. Afterwards all recorded and preprocessed TPs of individual fluorophores were collected and were analysed with another Matlab script which detects if each of the individual UV irradiation pulse activated or deactivated the fluorophores or had no effect. All the used Matlab scripts described above were developed as part of this thesis. The results of this analysis is shown in Tab. 7.3.

**Tab. 7.3:** UV recovery analysis of single Atto647 molecules in vitrified PBS. The data was generated from one grid from different grid squares. Each laser intensity was measured twice. The numbers shows the occurrence of on-switching and off-switching events as well as events that showed no observable effect on the fluorophores.

	10 W/cm <sup>2</sup>	10 W/cm <sup>2</sup>	20 W/cm <sup>2</sup>	20 W/cm <sup>2</sup>
on-switching	15 (1.2 %)	25 (1.5 %)	14 (1.0%)	2 (0.48%)
no effect	1211 (97.6 %)	1567 (96.5 %)	1323 (97.5%)	406 (98.3%)
off-switching	15 (1.2 %)	32 (2.0 %)	20 (1.5%)	5 (1.2%)
sum	1241	1624	1357	413

Most of the time the UV laser had no observable effect on the fluorophores and they remained on the same intensity level. The second most event was the switching off of the fluorophore which happened around 1-2 % of the time. A positive on-switching event were the least probable with around 1 %.

It was further investigated if fluorophores show a different switching behaviour if they are switch-able at all. To determine if a molecule is switch-able or not the intensity before and after the UV irradiation pulses were compared. If a change in intensity after each UV pulses could be detected it was labelled as "switched on", "switch off" or "no effect" if no change in intensity was detected. Another Matlab script used this labelling to sort the fluorophores whether the switched at least once during the recording and all the UV pulses for this molecule are considered. The statistics shown for those are shown in Tab. 7.4.

**Tab. 7.4:** UV recovery analysis of Atto647 molecules in vitrified PBS of only switch-able fluorophores. The data was generated from one grid from different grid squares. Each laser intensity was measured twice. The numbers shows the occurrence of on-switching and off-switching events as well as events that showed no observable effect on the fluorophores.

	10 W/cm <sup>2</sup>	10 W/cm <sup>2</sup>	20 W/cm <sup>2</sup>	20 W/cm <sup>2</sup>
on-switching	15 (2.0 %)	25 (2.1 %)	14 (1.4%)	2 (1.1%)
no effect	739 (96.1%)	1161 (95.3%)	969 (96.6%)	170 (96.0%)
off-switching f	15 (2.0 %)	32 (2.6 %)	20 (2.0%)	5 (2.8%)
sum	769	1218	1003	177

As one can see from the numbers about 96 % of the time the UV laser had no effect on the fluorophores.

Lastly, we have to check if the activation behaviour changes after it has been switched once. This is different to the investigation above, because for this only the UV pulses after the molecule has been switched on or off are considered are shown in Tab. 7.5

**Tab. 7.5:** UV recovery analysis of Atto647 molecules in vitrified PBS after they have been switched once before. Only the UV pulses after the switch are considered. The data was generated from one grid from different grid squares. Each laser intensity was measured twice. The numbers shows the occurrence of on-switching and off-switching events as well as no observable effect on the fluorophores.

	10 W/cm <sup>2</sup>	10 W/cm <sup>2</sup>	20 W/cm <sup>2</sup>	20 W/cm <sup>2</sup>
on-switching	7 (1.3 %)	20 (2.0 %)	8 (1.4 %)	3 (2.8 %)
no effect	538 (97.1 %)	976 (96.4 %)	544 (97.0 %)	101 ( 93.5 %)
off-switching f	9 (1.6 %)	16 (1.6 %)	9 (1.6 %)	4 (3.7 %)
sum	554	1012	561	108



## 7.10. Using fast fluorescence fluctuations for super-resolution cryo-FM imaging of shigella labelled with Alexa Fluor 647

In collaboration with Jelena Jeremic from the group of Michael Kolbe (CSSB Hamburg) Alexa647 was used in a biological application to demonstrate the usability of fluorescence blinking/fluctuations on the 10 ms time scale for super-resolution cryo-FM imaging in vitrified samples. The type 3 secretion system (T3SS) of shigella was modified to enable antibodies conjugated with Alexa647 to target them. The targeted region lies on the outside of the membrane. After the labelling the shigella were chemically fixed and plunge frozen shortly afterwards. The recordings were done with the same parameters as the single molecule investigation. In Fig. 7.42 one example of a shigella labelled with Alexa647 vitrified in PBS is shown.

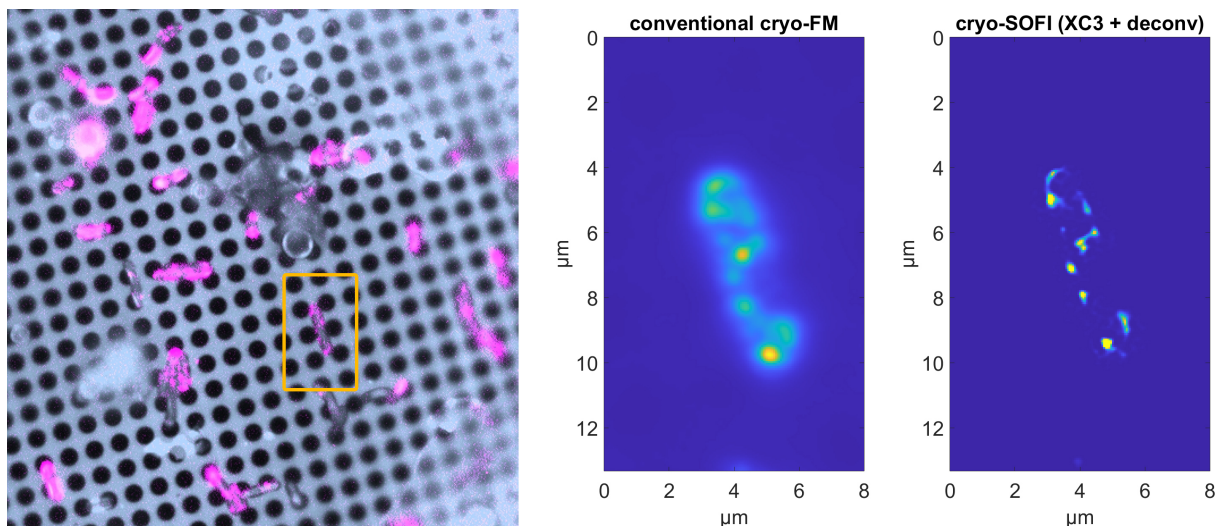


**Fig. 7.42.** Cryo-SOFI of AF647-labelled T3SS in Shigella. Left: Overlay of reflected light image (greyscale) and fluorescence signals (magenta) of Alexa647-labelled T3SS in Shigella. Right: Comparison of conventional cryo-FM and super-resolution cryo-FM (cryo-SOFI 3rd order cross-correlation including additional deconvolution).

On the left the overlay of reflected light and fluorescence signals of a Alexa647-labelled T3SS is shown. On the right a zoom-in of the shigella highlighted on the left showing a conventional cryo-FM image and a super-resolution cryo-FM in comparison. The super-resolution image was generated by a cryo-SOFI 3rd order cross-correlation including additional deconvolution. The background in the cryo-SOFI image is reduced and the resolution enhanced. Conventional cryo-FM show in the middle of the shigella only one spot whereas the cryo-SOFI signal shows to spots which are close to each other but still distinguishable.

## 7.11. Investigation of blinking in "super blinking nanoparticles"

Zong *et al.*<sup>70</sup> have described a rather simple procedure for synthesizing bio-compatible fluorescent "super blinking" nanoparticles (SBN) composed of multiple organic dyes and show at ambient temperatures that these nanoparticles have a different (more favourable for super-resolution FM) blinking characteristic than the sum of the individual dyes in one particle. In the bachelor thesis of Brian Jessen<sup>71</sup> conceived and co-supervised by me, SBN were investigated for its suitability for cryo super-resolution imaging. The synthesis is based on the publication of Zong *et al.*<sup>70</sup> They synthesised nanoparticles out of BSA with dye molecule conjugated to the BSA. The SBN could be successfully synthesised yielding 18,3 nm and 24,6 nm particles.

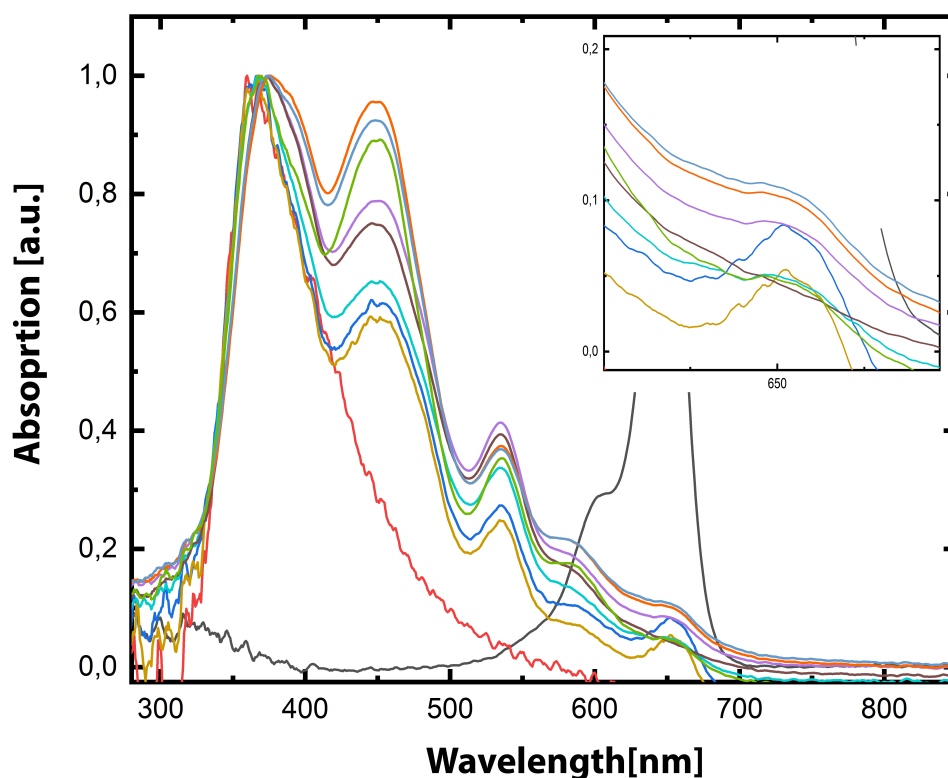


**Fig. 7.43.** Absorption spectra from pure Alexa647 color-coded in black, pure BSA color-coded in red and the synthesised SBN with Alexa647. The pure BSA nanoparticles without dyes are color-coded in brown, SBN<sub>1</sub> color-coded with purple at RT and cyan at cryogenic conditions, SBN<sub>2</sub> color-coded in blue at RT and ochre at cryogenic conditions. The other curves are not further examined in this thesis. The values are normalized. Modified from Jessen.<sup>71</sup>

In Fig. 7.43 the absorption spectra of pure Alexa647, pure BSA and the synthesised SBN<sub>1</sub> and SBN<sub>2</sub> with Alexa647 are shown. The BSA concentration of SBN<sub>2</sub> was double

that of SBN<sub>1</sub>. For more detailed information on the samples refer to the bachelor thesis of Jessen.<sup>71</sup> Compared to BSA which has a peak at around 380 nm the SBNs have additional peaks at around 450 nm and 530 nm. Those additional peaks also appear in pure BSA nanoparticles synthesized without Alexa647. The difference to the other samples are apparent in zoom-in to the wavelength around 650 nm in Fig. 7.43. Only the pure BSA nanoparticles show no peak at around 650 nm.

**Tab. 7.6:**  $t_{on}$  and  $t_{off}$  of SBN doted with Alexa647 at different temperatures.

Sample		$t_{on}$ [ms]	$t_{off}$ [ms]
Room temperature	SBN <sub>1</sub>	61.3	120
	SBN <sub>2</sub>	113	55.0
Cryogenic conditions	SBN <sub>1</sub>	20.0	115
	SBN <sub>2</sub>	69.4	46.3

As shown in Tab. 7.6 a change in  $t_{on}$  and  $t_{off}$  can be observed. To obtain the  $t_{on}$  and  $t_{off}$  the histogram method was used. For sample 005  $t_{on}$  decreases to 1/3 and for sample 009  $t_{on}$  nearly halved.  $t_{off}$  for both samples do not change much in cryo.

## 7.12. Investigation of blinking and bleaching of fluorescent proteins in vitrified cells

In the master thesis of Nayab Majid Chaudhry,<sup>72</sup> which I co-supervised, fluorescent proteins (FPs) in cells under cryogenic conditions were investigated. For this the cells were grown on TEM grids and were vitrified to preserve the cells in a near native state. Since it is more difficult in a cellular context to be certain if only one protein is investigated Cahudhrys thesis focused on the investigation of the behaviour in an ensemble. Notably three FPs are shown in this thesis.

First the photobleaching of the red FP mScarlet was investigated. For this the cell was observed for 3 hours. In the first 60 minutes the cell was continuously irradiated with a 561 nm laser with an intensity of 100 W/cm<sup>2</sup>. Followed by 60 minutes of no exposure to the laser. Afterwards, the cell were irradiate for 30 minutes to see if the FPs recovered in the dark. After that, the cell was simultaneously irradiate by the 561 nm and 405 nm laser (100 W/cm<sup>2</sup>) to see if the UV can recover any fluorescence. To measure the bleaching several time series of 1,000 frames with an integration time of 100 ms were recorded. Each time series was summed up to obtain the intensity for one time point. The measurements are shown in Fig. 7.44 A.

For the first section shown Fig. 7.44 A the half life is  $8 \pm 2$  minutes. Neither the 60 minutes of darkness nor the additional 405 nm laser could recover the fluorescence intensity. Only additional photobleaching was observed during the 405 nm laser irradiation.

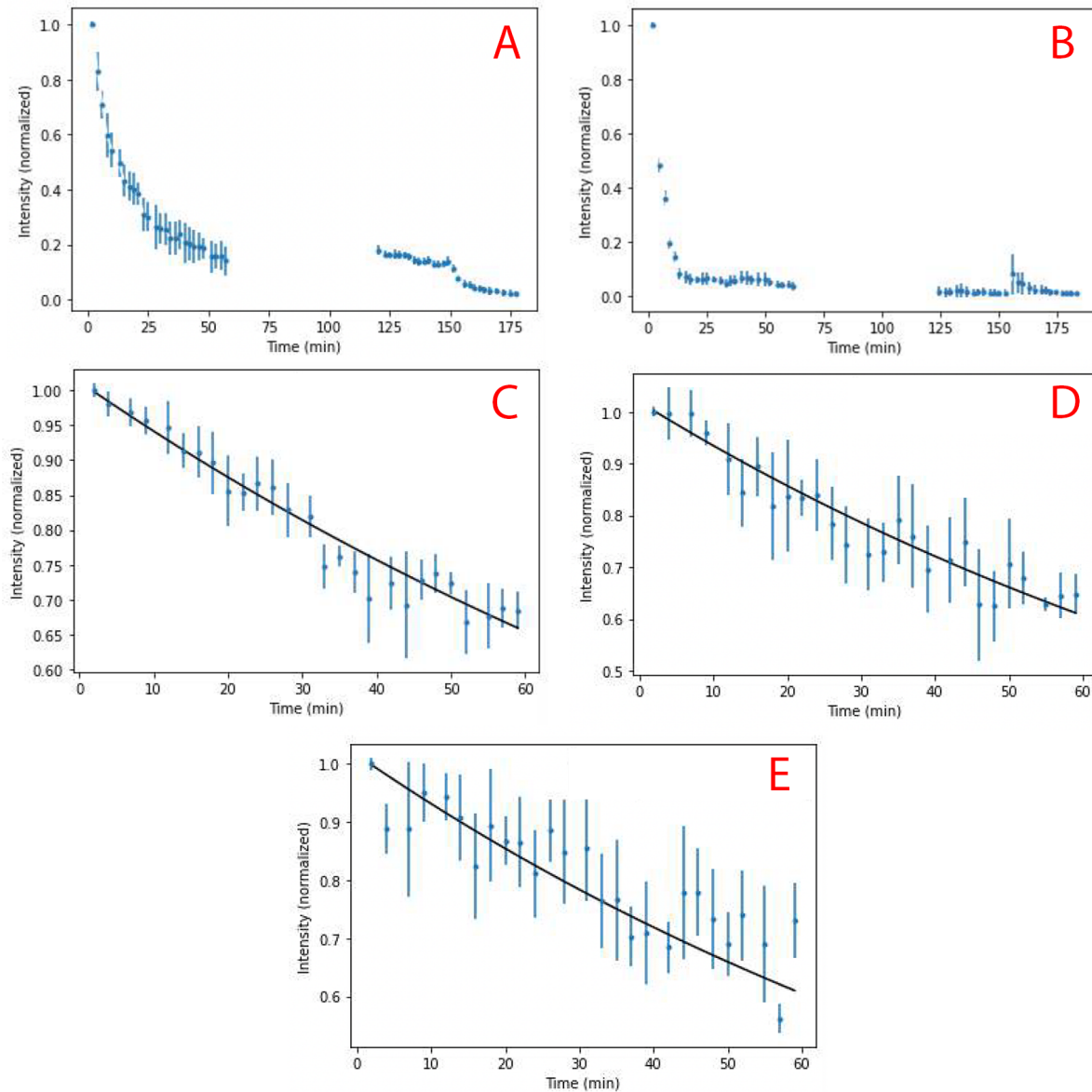


**Fig. 7.44.** Photobleaching measurement of the investigated FPs. A: mScarlet, shows of the complete measurement over 3 hours with a period of darkness of 60 minutes in the middle of the measurement. The used wavelength was 561 nm. The last 30 minutes a 405 nm laser was additionally. B: mEmerald. The same irradiation scheme like mScarlet. Used wave length for excitation was 488 nm and 405 for additional irradiation. C: emiRPF670. D: miRFP670nano. E: miRFP703. Only photobleaching measuring over a time range of 60 minutes for C, D and E. Used wavelength was 640 nm. Modified from Chaudhry.<sup>72</sup>

Next the photobleaching of one of the first green FPs mEmerald is investigated with the same parameter as mScarlet and is shown in Fig. 7.44 B. The cell was illuminated with a 488 nm laser. In the first 60 minutes the fluorescence intensity exponentially decreases with a half life of  $2.7 \pm 0.1$  minutes which is shorter than that of mScarlet. Like mScarlet there was no fluorescence intensity recovery after 60 minutes of darkness. Upon the additional irradiation of the cell with 405 nm there appears to be an increase in fluorescence intensity which also decreases exponentially.

For the measurement of photobleaching of the near-infrared FPs emiRFP670 which requires the cofactor biliverdin for fluorescence, miRFP670nano and miRFP703 the recording parameters were different. Each time series consist of 5,000 frames with an integration time of 20 ms. A 640 nm laser was used to irradiate the cells. The measurement is shown in Fig. 7.44 C, D and E respectively. The bleaching behaviour of the three near-infrared FPs were similar. The half life was much longer than that of the two FPs before with  $94 \pm 3$  minutes,  $79 \pm 2$  minutes and  $79 \pm 5$  minutes for emiRFP640, miRFP670nano and miRFP703 respectively.

Additionally to the bleaching experiments, the blinking behaviour of the five FPs was also investigated based on cryo-SOFI measurements in the master thesis of Chaudhry. For mScarlet no blinking was observed. For mEmerald on the other hand, blinking with on-states which are  $6 \pm 4$  seconds long could be observed. For emiRFP670 even longer on-states of  $20 \pm 5$  seconds with a higher blinking frequency after approximately 55 minutes of irradiation was observed. The observed on-states for miRFP670nano was  $24 \pm 6$  seconds. For miRFP703 no observation of blinking could be made. Regarding the suitability for cryo-SOFI only mScarlet and mEmerald fluorescence fluctuation was observed that was also observable in the AC curves. For the RFPs no final assertion of fluorescence fluctuation could be made since the measurement made during the master thesis were too noisy and the microscope was not stable enough.

## 8. Discussion

### 8.1. Autocorrelation and category analysis of blinking and fluctuating fluorescent states in single organic dyes

To achieve a resolution enhancement the blinking and fluctuating fluorescent states have a crucial impact on the resulting enhanced image. Studying the autocorrelation of the time profiles (TPs) under cryogenic conditions gives an insight on the suitability of the dyes for cryogenic single molecule localization microscopy (cryo-SMLM) and cryogenic super-resolution optical fluctuation imaging (cryo-SOFI). For cryo-SOFI the temporal fluctuation of the fluorescence intensity is important to obtain resolution enhancement. Only fluctuating or blinking fluorophores will have a high correlation and contribute to the enhanced image. Noise or constant fluorescence is not correlated and therefore will only indirectly contribute as noise in the final SOFI image. As seen in Fig. 7.1 there are a lot of different AC behaviours and they contribute to a varying degree to the image. It could be shown that it is possible to differentiate the TPs by their blinking behaviour. The resulting AC curves behave similar to each other in their respective categories as shown in Fig. 7.7, Fig. 7.8 and Fig. 7.11. All AC curves of the FB category have strong components of a typical AC curve of molecules of the FB category. They show a high correlation in the 10 ms range which agrees with the observed on- and off-states in the 10 ms range in the TPs.

The MSB category can show two different AC curve behaviours depending on the TPs as shown in Fig. 7.9 and Fig. 7.10. Both have a high correlation and both will contribute to the image since the mean value of the correlations coefficient  $G(\tau)_{m4}$  of the first four  $\tau$ , which is used in the cryo-SOFI image reconstruction, are contributing to the brightness of the pixel. This leads to two different classes in the MSB category which have different contribution to pixel brightness. From  $G(\tau)_{m4}$  it is not possible to discern if it is a result from multiple fluorophores or from a more pronounced of blinking of a single molecule.

Looking at the RB category there are two different possibility of AC curves. With a higher number of blinking events the correlation also increases which is observable in Fig. 7.11. If the number of blinking events is low the AC will be also low since there is not a lot of events for the AC to correlate with. This behaviour would be suitable for cryo-SMLM since SMLM utilises distinct on-states and off-states.

There is a high number of molecules which were considered in the analysis workflow



developed in this thesis as "always on" and were not included in the AC analysis. But since they are also in the image and will influence the quality of the enhanced image. In Fig. 8.1 only the AC curves resulting from TPs considered as "always on" are shown.

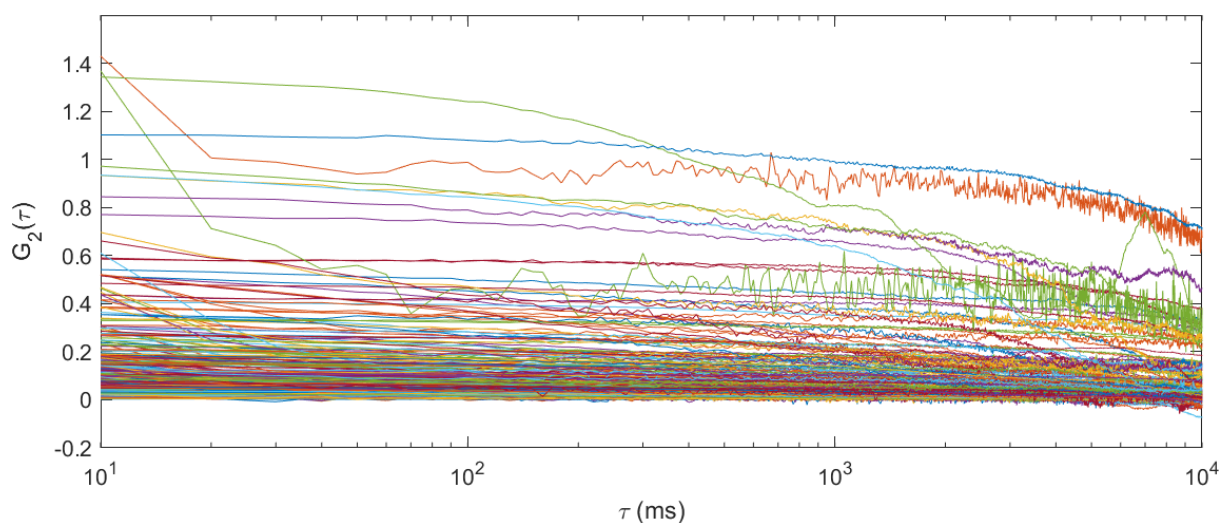


**Fig. 8.1.** AC curves of all TPs for Alexa647<sub>PBS\_V</sub> which are considered in the analysis workflow as "always on". Different AC behaviour can be seen, ranging from fast declining AC curves (indicating FB) to long plateaus (indicating long on-times ( $t_{on}$ )), but also including AC curves fluctuating around 0 (indicating no blinking or switching). The logarithmic x-axis shows  $\tau$  in ms. The temporal resolution is 10 ms.

The same AC behaviour from the other categories can be observed. The fast declining ACs like in the FB category, the plateaus like in the MSB and RB category and also AC curves with no correlation fluctuation around 0. It would be expected that the "always on" molecules would have a correlation close to zero since the molecule would only stay in their on-state. This is not the case, since the dyes are "always on" in regard of the threshold method where the fluorescence intensity stays above the threshold and do not switch off. But the molecules still can fluctuate in the on-state and therefore will have a correlation which is not 0. This shows that these TPs which are not possible to analyse in this workflow developed in thesis also contribute to the SOFI image and should be further investigated in future works. Additionally, there is a need to do more repetition of the samples to have a better statistical basis. Also, the  $t_{on}$  and  $t_{off}$  could be determined directly from the AC curves if the temporal resolution of the camera would be higher removing the need to use a computational expensive and indirect method like the histogram fit method Sec. 7.4 to calculate the  $t_{on}$  and  $t_{off}$ .

An ideal fluorophore for cryo-SOFI would have only one kind of blinking behaviour, because their AC curves would look similar and would produce a homogeneous image. In reality and shown in this thesis there are different blinking behaviours observable for one type of fluorescent molecule.

Only looking at the  $G(\tau)_{m4}$ , Alexa647<sub>PVA<sub>nonV</sub></sub> has the highest correlation in all categories. The  $G(\tau)_{m4}$  between the categories are quite different. For this dye, FB produces

the lowest correlation values and MSB and RB are more than double the value. But looking at the percentage the FB category dominates the blinking category and therefore one can assume that the resulting image would be quite homogeneous in its brightness distribution.

Since the FB category has the highest percentage for most of dyes, Alexa647<sub>PVA<sub>nonV</sub></sub>, Alexa647<sub>PBS<sub>V</sub></sub> and Alexa647<sub>dPBS<sub>V</sub></sub> would be the most suitable dye and solvent combination for homogeneous cryo-SOFI images. For the other dyes except Janelia646<sub>PBS<sub>V</sub></sub>, OG<sub>PBS<sub>V</sub></sub> and Star505<sub>PBS<sub>V</sub></sub> the  $G(\tau)_{m4}$  for the blinking categories are quite similar and therefore would result in good cryo-SOFI images.

For Janelia646<sub>PBS<sub>V</sub></sub>, OG<sub>PBS<sub>V</sub></sub> and Star505<sub>PBS<sub>V</sub></sub> the distribution of the blinking categories are equal. Combined with the strongly varying  $G(\tau)_{m4}$ , which would result in stronger brightness variability in the resulting SOFI image; the results for those three dyes indicated that they might not be best suited for cryo-SOFI. For cryo-SMLM on the other hand a higher number of molecules showing MSB or RB behaviour is better.

In the end, the blinking behaviour is complex and one dye does not only have one particular blinking behaviour but several which all contribute to the blinking behaviour. The analysis showed that even the TPs which could not be properly analysed in this thesis contribute to the cryo-SOFI image. With the AC and category analysis it was possible to distinguish between dyes which are suitable for cryo-SOFI, cryo-SMLM, or both. Further insight into the blinking behaviour could be obtained with a detector with higher temporal resolution.

## 8.2. Qualitative analysis of multiple fluorescent states in individual single molecule time traces

To get a better understanding of the blinking behaviour some TPs were further studied. This could not be automated in this thesis since it was out of scope to develop an algorithm which could distinguish between the different blinking behaviours. Looking at molecules in detail their TPs do not have only one blinking behaviour but might shift between different ones. As shown in Fig. 7.33 a shift in the off-times can be observed which leads to two different FB behaviours. The length of the on-frames typically does not change which is more apparent in Fig. 7.36. These changes in blinking behaviour make it hard to develop an automated analysis workflow. Since the algorithm has to detect the different blinking behaviour and then analyse the on- and off-states. Additionally, it was observed that the molecules show a faster blinking behaviour in tens of milliseconds scale at the same time as the long term blinking behaviour in the second to minutes time scale. Even though the molecule was in the "off-state" in the long term data fluorescence fluctuation could still be observed. Since both blinking behaviours, the fast blinking and the long term blinking, one dye is sufficient to obtain a "moderate" super-



resolution enhancement with cryo-SOFI in the range of about  $135 \text{ nm}^{64}$  with only a few minutes of recording or a nanometre spatial resolution with several hours of recording with cryo-SMLM.

An even higher temporal resolution would further enable the investigation of states that appear as higher intensity states like in the beginning of the TP shown in Fig. 7.5. Overall the blinking behaviour in one TP can change during the acquisition time. It was found that the on-states did not change their length but rather the off-states changes their length. Furthermore, it was observed that the molecules exhibit fast blinking and long term blinking at the same which which can both can be utilised for cryo-SOFI and cryo-SMLM and can be chosen depending on how high the resolution enhancement needs to be.

### 8.3. Determination of on and off times for the FB category

The histogram fit method, which was developed in this thesis to extract the lifetimes of on- and off-states, is an indirect method to estimate  $t^{\text{on}}$  and  $t^{\text{off}}$  since it needs to simulate the TPs, calculate their histograms and than compare it to the histograms of the measured TPs and will repeat it for each collected TP. This method is more reliable than the threshold based method from Böning *et al.*<sup>68</sup> - based on an exponential fit of the on- or off-time histogram to determine the times - since the signal to noise ratio (SNR) with this setup, the used fluorophores and sample preparation conditions is often too low and therefore prone to a systematic error. The overestimation of  $t^{\text{off}}$  for low SNR lies in the nature of the method. Since the threshold is calculated as the threefold standard deviation of the background, weak signals might get overshadowed by noise.  $t^{\text{on}}$  might get estimated correctly since the length of the on-states stays the same but are more rarely detected since the on-state have to be bright enough to be detected. Because of the "missed" on-state the off-states appears to be longer therefore the overestimation of  $t^{\text{off}}$ . Böning *et al.* determined for Alexa647<sub>PVA<sub>nonV</sub></sub> a  $t^{\text{on}} = 6.6 \text{ ms}$  and  $t_1^{\text{off}} = 2.5 \text{ ms}$  and  $t_2^{\text{off}} = 34.8 \text{ ms}$  with a laser intensity of  $1 \text{ kW/cm}^2$ . The determined times in this thesis using the same threshold method yielded  $t_1^{\text{on}} = 18.8 \pm 1.1 \text{ ms}$ ,  $t_2^{\text{on}} = 92.3 \pm 4.6 \text{ ms}$  and  $t_1^{\text{off}} = 49.0 \pm 1.4 \text{ ms}$  and  $t_2^{\text{off}} = 253.5 \pm 7.9 \text{ ms}$ . The used laser intensity was  $100 \text{ W/cm}^2$ , which is ten times smaller than the intensity used by Böning *et al.* The additional time results from an additional exponential function in the fit of the on- of off-time histogram which suggest that there are at least two transition rates into the bright and dark state respectively which governs the blinking behaviour of the molecules. This method can determine more than one exponential function but the low SNR introduce a systemic error as mentioned above limit its precision to determine the off-times. With the histogram fit method  $t^{\text{on}} = 9.1 \pm 1.0 \text{ ms}$  and  $t^{\text{off}} = 22.6 \pm 2.1 \text{ ms}$  were determined which is in much better agreement with the times determined by Böning *et al.* For this method only one on- and off-time was calculated since I could not successfully implemented an algorithm

to introduce two times for on- and off-times. With a faster detector the on- and off-times could be directly determined by the exponential fit based method. The algorithm from Marcel Leutenegg's `sofiSimulate`<sup>67</sup> used to simulate the TPs and their calculated histogram was modified to take into account read noise. Another possibility to estimate  $t^{\text{on}}$  and  $t^{\text{off}}$  would be to fit the AC curves with a Monte Carlo approach like in the thesis from Brandt<sup>73</sup> which was co-supervised by me.

Since the on-times and off-times themselves are not a good benchmark to estimate the suitability for cryo-SMLM the on-off-ratio is used. Atto647<sub>PBS\_V</sub> has the lowest on-off-ratio of the investigated dyes and therefore would be the most suitable for cryo-SMLM.

In the end, the histogram fit method can only be used to estimate the times since it only can simulate one on-time and off-time and also only one transition rate. But the data indicates that there are at least 2 on-times and therefore there have to be at least 2 different transition rates. Also the on-state have a broader intensity distribution that could not be simulated in the scope of this thesis. A detector with a higher temporal resolution would enable a direct determination of the on- and off-times.

## 8.4. Influence of heavy water on photo-physics of organic dyes

Even though PVA showed an improvement of  $G(\tau)_{m4}$  and reduced the amount of "always on" molecules, it is not suitable for live cell applications and therefore not compatible with cryo-immobilization of biological specimens with a focus on highest structural preservation or the compatibility with cryo-EM. Therefore, an alternative was investigated which in principle might have the possibility to change the photophysics of the dyes and is also biocompatible. Lee *et al.*<sup>69</sup> showed in their publication that heavy water have positive effect on RT super-resolution methods. The oxazine fluorophores had an fluorescence quantum yield twice as high compared to water and the fluorescence life time increased. A higher quantum yield leads to more photons which in turn leads to a higher localization precision. Looking at the four dyes investigated in heavy water under cryogenic conditions, there is no clear trend regarding the AC analysis. Alexa647 showed nearly no change. The AC curves increased for Atto647, decreased for Janelia525 and OG have a mixture of increase and decrease in  $G(\tau)_{m4}$ . Only Atto647 showed a positive change in AC curves. Only for Alexa647 the "always on" molecules decreased, the FB category increased and the two other categories decreased, whereas the other dyes behaves inversely: the "always on" part increased, the FB category decreased and the MSB category increased. There is also no pattern for  $t_{\text{on}}$  and  $t_{\text{off}}$ . For Alexa647, Atto647 and Janelia525  $t_{\text{on}}$  and  $t_{\text{off}}$  increases. For OG both times decrease. Regarding the OOR there is only a significant increase for Atto647. Overall, heavy water do not change the behaviour of the dyes in a common way. Only Atto647 had a positive change regarding

the AC and for Alexa647 in the blinking categories. The  $G(\tau)_{m4}$  of Atto647 doubled for all TPs, FB and MSB category, the mean of all blinking molecules is 4 times higher and the RB category tripled. For the other dyes a decrease in all aspects was observed.

## 8.5. UV recovery of different organic dye molecules

Some molecules can be recovered from the dark state by using UV irradiation. In this thesis the UV recovery of Atto647 in cryogenic conditions was investigated representatively which normally do not show UV recovery at ambient conditions. Additionally to the other investigations, the UV recovery of Atto647 in cryogenic conditions was studied. There was no or very small evidence found that Atto647 molecules could be recovered with UV irradiation after each 10 seconds of 640 nm laser irradiation. Only about 1-2% showed photo switching in either states. Even if only the molecules which showed any switching are considered most of the time there was no effect cause by the UV irradiation. There might be some really fast activation processes which are faster than 10 ms which we can not detect since the integration time we used is 10 ms. But even though the activation would be so short or low in intensity that we could not detect it with our setup. Also, other dyes have to be investigated since they might have different photophysics leading to UV recovery.

## 8.6. Using fast fluorescence fluctuations for super-resolution cryo-FM imaging of shigella labelled with Alexa Fluor 647

It could be shown that the fast fluorescence fluctuations observed in single Alexa647 molecules can be used for cryo-SOFI and enable a resolution enhancement even with a short recording time of the sample. Alexa647 and most other organic dyes are not cell permeable in living cells which limits their usability for structures inside cells. Oregon Green, Janelia Fluor and silicon rhodamine on the hand are organic dyes which are call permeable and need further investigation which could not be done in the scope of this thesis. Additionally, the microenvironment in the cells are different and might have an influence on the blinking behaviour of the dyes as shown in the investigation with different environment for Alexa647 with non-vitrified PVA, non-vitrified PBS, vitrified PBS, and with vitrified PBS made with heavy water. Furthermore, investigations with "super-blinking nanoparticles" also suggest that the environment changes the blinking behaviour. Additionally, there might be changes in the photo physics when the dye is conjugated to an antibody and/or conjugated to a bacteria, which needs to be further investigated.

To investigate if Alexa647 conjugated to an secondary antibody targeting a primary antibody for the type 3 secretion system, chemically fixed vitrified shigella were investigated under cryogenic conditions. Fast blinking was observed in the shigella samples and a resolution enhancement with the cryo-SOFI algorithm could be achieved as shown in Fig. 7.42.

## 8.7. Investigation of blinking in "super blinking nanoparticles"

To further investigate if the dyes studied in this thesis showed a different blinking behaviour in a microenvironment of BSA nanoparticles Brian Jessen successfully synthesised "super blinking nanoparticles" (SBN) with different parameters after Zong *et al.*<sup>70</sup> A strong decrease of  $t_{\text{on}}$  by 1/3 or 1/2 at low temperature could be observed compared to room temperature. SBN<sub>1</sub> has an OOR of 0.17 compared to 1.50 from SBN<sub>2</sub> which has twice the BSA concentration. Therefore, SBN<sub>1</sub> is usable for cryo-SMLM. The higher number of fluorescent dyes in on SBN create a much higher blinking frequency enabling a faster and better localization of the SBN compared to individual Alexa647 molecules since a higher number of photons and on- and off-states can be recorded in a shorter time. This is especially interesting if the individual dye only have unsatisfactory blinking behaviour for SMLM.<sup>70</sup> Jessen could show that the SBN had an positive influence on the blinking behaviour which made them more attractive for the use in cryo-SMLM even though it comes with the size limitation of the nanoparticles. Further investigations are needed to study the influence of the microenvironment on the blinking behaviour.

## 8.8. Investigation of blinking and bleaching of fluorescent proteins in vitrified cells

A different class of fluorophores which were not covered in the scope of thesis are fluorescent proteins (FPs) which was investigated by Nayab Majid Chaudhry. GFP already showed super resolution capabilities<sup>74</sup> at ambient conditions but no systemic study for cryogenic conditions were done. For her thesis she investigated the FPs in vitrified cells at an ensemble level and single molecule level. The investigation of FPs under cryo conditions showed that all the FPs instigated show exponential photobleaching. For mScarlet and mEmerald it was in the range of  $8 \pm 2$  minutes and  $2.7 \pm 0.1$  minutes and for the far red FPs emiRFP670, miRFP670nano and miRFP703 it was  $94 \pm 3$  minutes,  $79 \pm 2$  minutes and  $79 \pm 5$  minutes, respectively. No trend for the photobleaching could be observed since data from the group suggest that mCherry is also slowly photobleaching. mScarlet only show fluctuation in the fluorescence intensity and no blinking beyond

that making it only suitable for cryo-SOFI application. emiRFP670 on the other showed only blinking behaviour and no fast fluctuation of the fluorescence intensity making it suitable for cryo-SMLM but not cryo-SOFI. Lastly, mEmerald show fluctuation of the fluorescence intensity and showed blinking which making it suitable for both, cryo-SOFI and cryo-SMLM. Chaudhry could successfully investigate the FPs on their suitability for cryo-SOFI and cryo-SMLM. Still, more detailed investigation on the blinking behaviour of the FPs need to be done.

## 9. Conclusion

In this thesis a work flow to characterise fluorescent molecules at low temperatures was successfully developed. The developed algorithm and software automates the process as much as possible. The investigation of organic dyes showed that all of the dyes show fluorescence fluctuation which can be utilized by cryo-SOFI to achieve a resolution enhancement. Detailed investigation of some TPs revealed that the length of the on-states does not change. On the contrary the length of the off-states can change during the time series leading to a change in blinking frequency. Additionally, fast blinking and long term blinking was observed at the same time which enables the use of either cryo-SOFI or cryo-SMLM depending on the desired spatial resolution and time at hand. With the indirect histogram fit method the on- and off-times of the dyes could be determined which can be used as estimate. A detector with higher temporal resolution is needed to directly determine the on- and off-times especially since there are more than one on- and off-times which other measurements in this thesis has shown. The investigation of the UV recovery for Atto647 showed no significant recovery. Further dyes have to be investigated to gain a more complete image. It was also found that the environment of the dyes changes the blinking behaviour. PVA showed the highest positive effect on the cryo-SOFI suitability but PVA is not a suitable medium for live cells. Heavy water on the other hand is biocompatible but showed only a positive change for Atto647 in its suitability for cryo-SOFI and for Alexa647 had more favourable blinking behaviour category for cryo-SOFI. The other dyes showed no positive change in the blinking behaviour in heavy water. Furthermore, Alexa647 was successfully used to label chemically fixed vitrified shigella to obtain a resolution enhanced cryo-SOFI image. The investigation of this thesis gives more insight in the photophysics of fluorescent organic dyes and fluorescent proteins leading to a better understanding and ultimately an improvement in resolution in cryo super-resolution microscopy.

## 10. Outlook

This thesis started the investigation on some fundamental properties of fluorescent dyes but also found some limitations which limited more precise and direct determination of properties. With this work some resolution improvement already can be achieved especially the flexibility to use one dye for both, cryo-SOFI and cryo-SMLM with any change in the samples.

A detector with higher temporal resolution in the sub millisecond to milliseconds range would enable the direct determination of the on- and off-times of the dyes and possible enable the construction of model of the blinking behaviour. Also, it would be possible to investigate the change in off-times during of a single molecule. To further automate the analysis more elaborate algorithm can be developed to also include the time profiles which could not be analysed in the scope of this thesis.

Generally the influence of UV irradiation on live cells have to further investigated since the UV excites a number of different proteins in the cell. Additionally, more heat could be produced in the cell especially with dyes with a higher Stokes-shift, which might heat up the sample that one or two water molecule might move. This would not be a problem at shorter recording time but for longer time scales (days) this might be a problem.

If further dyes would be investigated it might be possible to might some predictions on the blinking behaviour based on the structure of the fluorescent molecules. And based on this knowledge new fluorophores could be designed taken into account the blinking behaviour found for the investigated dyes.

## Bibliography

- [1] ABBE, E.: Beiträge zur Theorie des Mikroskops und der mikroskopischen Wahrnehmung. In: *Archiv für Mikroskopische Anatomie* 9 (1873), Dezember, Nr. 1, S. 413–468. <http://dx.doi.org/10.1007/bf02956173>. – DOI 10.1007/bf02956173
- [2] FREUNDLICH, Martin M.: Origin of the Electron Microscope. In: *Science* 142 (1963), Oktober, Nr. 3589, S. 185–188. <http://dx.doi.org/10.1126/science.142.3589.185>. – DOI 10.1126/science.142.3589.185
- [3] DUBOCHET, Jacques: The physics of rapid cooling and its implications for cryoimmobilization of cells. In: *Methods in cell biology* 79 (2007), S. 7–21
- [4] RODRIGUEZ, Jose A. ; IVANOVA, Magdalena I. ; SAWAYA, Michael R. ; CASCIO, Duilio ; REYES, Francis E. ; SHI, Dan ; SANGWAN, Smriti ; GUENTHER, Elizabeth L. ; JOHNSON, Lisa M. ; ZHANG, Meng ; JIANG, Lin ; ARBING, Mark A. ; NANNENGA, Brent L. ; HATTNE, Johan ; WHITELEGGE, Julian ; BREWSTER, Aaron S. ; MESSERSCHMIDT, Marc ; BOUTET, Sébastien ; SAUTER, Nicholas K. ; GONEN, Tamir ; EISENBERG, David S.: Structure of the toxic core of  $\alpha$ -synuclein from invisible crystals. In: *Nature* 525 (2015), September, Nr. 7570, S. 486–490. <http://dx.doi.org/10.1038/nature15368>. – DOI 10.1038/nature15368
- [5] GLAESER, Robert M.: How good can cryo-EM become? In: *Nature Methods* 13 (2015), Dezember, Nr. 1, S. 28–32. <http://dx.doi.org/10.1038/nmeth.3695>. – DOI 10.1038/nmeth.3695
- [6] SARTORI, Anna ; GATZ, Rudolf ; BECK, Florian ; RIGORT, Alexander ; BAUMEISTER, Wolfgang ; PLITZKO, Juergen M.: Correlative microscopy: Bridging the gap between fluorescence light microscopy and cryo-electron tomography. In: *Journal of Structural Biology* 160 (2007), November, Nr. 2, S. 135–145. <http://dx.doi.org/10.1016/j.jsb.2007.07.011>. – DOI 10.1016/j.jsb.2007.07.011
- [7] SCHWARTZ, Cindi L. ; SARBASH, Vasily I. ; ATAULLAKHANOV, Fazoil I. ; MCINTOSH, J. R. ; NICASTRO, Daniela: Cryo-fluorescence microscopy facilitates correlations between light and cryo-electron microscopy and reduces the rate of photobleaching. In: *Journal of Microscopy* 227 (2007), August, Nr. 2, S. 98–109. <http://dx.doi.org/10.1111/j.1365-2818.2007.01794.x>. – DOI 10.1111/j.1365-2818.2007.01794.x



- [8] SCHELLENBERGER, Pascale ; KAUFMANN, Rainer ; SIEBERT, C. A. ; HAGEN, Christoph ; WODRICH, Harald ; GRÜNEWALD, Kay: High-precision correlative fluorescence and electron cryo microscopy using two independent alignment markers. In: *Ultramicroscopy* 143 (2014), August, S. 41–51. <http://dx.doi.org/10.1016/j.ultramic.2013.10.011>. – DOI 10.1016/j.ultramic.2013.10.011
- [9] CHANG, Yi-Wei ; CHEN, Songye ; TOCHEVA, Elitza I. ; TREUNER-LANGE, Anke ; LÖBACH, Stephanie ; SØGAARD-ANDERSEN, Lotte ; JENSEN, Grant J.: Correlated cryogenic photoactivated localization microscopy and cryo-electron tomography. In: *Nature Methods* 11 (2014), Mai, Nr. 7, S. 737–739. <http://dx.doi.org/10.1038/nmeth.2961>. – DOI 10.1038/nmeth.2961
- [10] KAUFMANN, Rainer ; SCHELLENBERGER, Pascale ; SEIRADAKE, Elena ; DOBBIE, Ian M. ; JONES, E. Y. ; DAVIS, Ilan ; HAGEN, Christoph ; GRÜNEWALD, Kay: Super-Resolution Microscopy Using Standard Fluorescent Proteins in Intact Cells under Cryo-Conditions. In: *Nano Letters* 14 (2014), Juni, Nr. 7, S. 4171–4175. <http://dx.doi.org/10.1021/nl501870p>. – DOI 10.1021/nl501870p
- [11] LIU, Bei ; XUE, Yanhong ; ZHAO, Wei ; CHEN, Yan ; FAN, Chunyan ; GU, Lusheng ; ZHANG, Yongdeng ; ZHANG, Xiang ; SUN, Lei ; HUANG, Xiaojun ; DING, Wei ; SUN, Fei ; JI, Wei ; XU, Tao: Three-dimensional super-resolution protein localization correlated with vitrified cellular context. In: *Scientific Reports* 5 (2015), Oktober, Nr. 1. <http://dx.doi.org/10.1038/srep13017>. – DOI 10.1038/srep13017
- [12] TUIJTEL, Maarten W. ; KOSTER, Abraham J. ; JAKOBS, Stefan ; FAAS, Frank G. A. ; SHARP, Thomas H.: Correlative cryo super-resolution light and electron microscopy on mammalian cells using fluorescent proteins. In: *Scientific Reports* 9 (2019), Februar, Nr. 1. <http://dx.doi.org/10.1038/s41598-018-37728-8>. – DOI 10.1038/s41598-018-37728-8
- [13] LICHTMAN, Jeff W. ; CONCHELLO, José-Angel: Fluorescence microscopy. In: *Nature Methods* 2 (2005), November, Nr. 12, S. 910–919. <http://dx.doi.org/10.1038/nmeth817>. – DOI 10.1038/nmeth817
- [14] DICKSON, Robert M. ; CUBITT, Andrew B. ; TSIEN, Roger Y. ; MOERNER, W. E.: On/off blinking and switching behaviour of single molecules of green fluorescent protein. In: *Nature* 388 (1997), Juli, Nr. 6640, S. 355–358. <http://dx.doi.org/10.1038/41048>. – DOI 10.1038/41048
- [15] ZONDERVAN, Rob ; KULZER, Florian ; ORLINSKII, Sergei B. ; ORRIT, Michel: Photoblinking of Rhodamine 6G in Poly(vinyl alcohol): Radical Dark State Formed through the Triplet. In: *The Journal of Physical Chemistry A* 107 (2003), August, Nr. 35, S. 6770–6776. <http://dx.doi.org/10.1021/jp034723r>. – DOI 10.1021/jp034723r

- [16] KASPER, Robert: *Optimierung von photophysikalischen Eigenschaften organischer Farbstoffe zur Auflösungserhöhung*, Diss., 2009
- [17] KAUFMANN, Rainer: *Entwicklung quantitativer Analysemethoden in der Lokalisationsmikroskopie*, Diss., 2011
- [18] RAYLEIGH: XXXI. Investigations in optics, with special reference to the spectroscopy. In: *The London, Edinburgh, and Dublin Philosophical Magazine and Journal of Science* 8 (1879), Oktober, Nr. 49, S. 261–274. <http://dx.doi.org/10.1080/14786447908639684>. – DOI 10.1080/14786447908639684
- [19] SPARROW, C. M.: On Spectroscopic Resolving Power. In: *The Astrophysical Journal* 44 (1916), September, S. 76. <http://dx.doi.org/10.1086/142271>. – DOI 10.1086/142271
- [20] KADERUPPAN, Shiraz S. ; WONG, Eugene Wai L. ; SHARMA, Anurag ; WOO, Wai L.: Smart Nanoscopy: A Review of Computational Approaches to Achieve Super-Resolved Optical Microscopy. In: *IEEE Access* 8 (2020), S. 214801–214831. <http://dx.doi.org/10.1109/access.2020.3040319>. – DOI 10.1109/access.2020.3040319
- [21] SCHERMELLEH, Lothar ; HEINTZMANN, Rainer ; LEONHARDT, Heinrich: A guide to super-resolution fluorescence microscopy. In: *The Journal of cell biology* 190 (2010), Nr. 2, S. 165–175
- [22] KLAR, Thomas A. ; JAKOBS, Stefan ; DYBA, Marcus ; EGNER, Alexander ; HELL, Stefan W.: Fluorescence microscopy with diffraction resolution barrier broken by stimulated emission. In: *Proceedings of the National Academy of Sciences* 97 (2000), Juli, Nr. 15, S. 8206–8210. <http://dx.doi.org/10.1073/pnas.97.15.8206>. – DOI 10.1073/pnas.97.15.8206
- [23] WESTPHAL, Volker ; HELL, Stefan W.: Nanoscale Resolution in the Focal Plane of an Optical Microscope. In: *Physical Review Letters* 94 (2005), April, Nr. 14, S. 143903. <http://dx.doi.org/10.1103/physrevlett.94.143903>. – DOI 10.1103/physrevlett.94.143903
- [24] HEINTZMANN, Rainer ; CREMER, Christoph G.: Laterally modulated excitation microscopy: improvement of resolution by using a diffraction grating. In: BIGIO, Irving J. (Hrsg.) ; SCHNECKENBURGER, Herbert (Hrsg.) ; SLAVIK, Jan (Hrsg.) ; SVANBERG, Katarina (Hrsg.) ; VIALLET, Pierre M. (Hrsg.): *SPIE Proceedings*, SPIE, Januar 1999
- [25] GUSTAFSSON, M. G. L.: Surpassing the lateral resolution limit by a factor of two using structured illumination microscopy. SHORT COMMUNICATION. In: *Journal of Microscopy* 198 (2000), Mai, Nr. 2, S. 82–87. <http://dx.doi.org/10.1046/j.1365-2818.2000.00710.x>. – DOI 10.1046/j.1365-2818.2000.00710.x

- [26] BURNS, David H. ; CALLIS, James B. ; CHRISTIAN, Gary D. ; DAVIDSON, Ernest R.: Strategies for attaining superresolution using spectroscopic data as constraints. In: *Applied Optics* 24 (1985), Januar, Nr. 2, S. 154. <http://dx.doi.org/10.1364/ao.24.000154>. – DOI 10.1364/ao.24.000154
- [27] BETZIG, E.: Proposed method for molecular optical imaging. In: *Optics Letters* 20 (1995), Februar, Nr. 3, S. 237. <http://dx.doi.org/10.1364/ol.20.000237>. – DOI 10.1364/ol.20.000237
- [28] BORNFLETH, H. ; SAETZLER, Kurt ; ELIS, R. ; CREMER, C.: High-precision distance measurements and volume-conserving segmentation of objects near and below the resolution limit in three-dimensional confocal fluorescence microscopy. In: *Journal of Microscopy* 189 (1998), S. 118–136. – ISSN 0022–2720
- [29] BETZIG, Eric ; PATTERSON, George H. ; SOUGRAT, Rachid ; LINDWASSER, O W. ; OLENYCH, Scott ; BONIFACINO, Juan S. ; DAVIDSON, Michael W. ; LIPPINCOTT-SCHWARTZ, Jennifer ; HESS, Harald F.: Imaging intracellular fluorescent proteins at nanometer resolution. In: *Science* 313 (2006), Nr. 5793, S. 1642–1645
- [30] HESS, Samuel T. ; GIRIRAJAN, Thanu P. ; MASON, Michael D.: Ultra-High Resolution Imaging by Fluorescence Photoactivation Localization Microscopy. In: *Biophysical Journal* 91 (2006), Dezember, Nr. 11, S. 4258–4272. <http://dx.doi.org/10.1529/biophysj.106.091116>. – DOI 10.1529/biophysj.106.091116
- [31] RUST, Michael J. ; BATES, Mark ; ZHUANG, Xiaowei: Sub-diffraction-limit imaging by stochastic optical reconstruction microscopy (STORM). In: *Nature Methods* 3 (2006), August, Nr. 10, S. 793–796. <http://dx.doi.org/10.1038/nmeth929>. – DOI 10.1038/nmeth929
- [32] LEMMER, P. ; GUNKEL, M. ; BADDELEY, D. ; KAUFMANN, R. ; URICH, A. ; WEILAND, Y. ; REYMANN, J. ; MÜLLER, P. ; HAUSMANN, M. ; CREMER, C.: SPDM: light microscopy with single-molecule resolution at the nanoscale. In: *Applied Physics B* 93 (2008), September, Nr. 1, S. 1–12. <http://dx.doi.org/10.1007/s00340-008-3152-x>. – DOI 10.1007/s00340-008-3152-x
- [33] BADDELEY, David ; JAYASINGHE, Isuru D. ; CREMER, Christoph ; CANNELL, Mark B. ; SOELLER, Christian: Light-Induced Dark States of Organic Fluochromes Enable 30 nm Resolution Imaging in Standard Media. In: *Biophysical Journal* 96 (2009), Januar, Nr. 2, S. L22–L24. <http://dx.doi.org/10.1016/j.bpj.2008.11.002>. – DOI 10.1016/j.bpj.2008.11.002
- [34] HEILEMANN, Mike ; LINDE, Sebastian van d. ; SCHÜTTPELZ, Mark ; KASPER, Robert ; SEEFELDT, Britta ; MUKHERJEE, Anindita ; TINNEFELD, Philip ; SAUER,

- Markus: Subdiffraction-Resolution Fluorescence Imaging with Conventional Fluorescent Probes. In: *Angewandte Chemie International Edition* 47 (2008), August, Nr. 33, S. 6172–6176. <http://dx.doi.org/10.1002/anie.200802376>. – DOI 10.1002/anie.200802376
- [35] FÖLLING, Jonas ; BOSSI, Mariano ; BOCK, Hannes ; MEDDA, Rebecca ; WURM, Christian A. ; HEIN, Birka ; JAKOBS, Stefan ; EGGELING, Christian ; HELL, Stefan W.: Fluorescence nanoscopy by ground-state depletion and single-molecule return. In: *Nature Methods* 5 (2008), September, Nr. 11, S. 943–945. <http://dx.doi.org/10.1038/nmeth.1257>. – DOI 10.1038/nmeth.1257
- [36] DERTINGER, T. ; COLYER, R. ; IYER, G. ; WEISS, S. ; ENDERLEIN, J.: Fast, background-free, 3D super-resolution optical fluctuation imaging (SOFI). In: *Proceedings of the National Academy of Sciences* 106 (2009), Dezember, Nr. 52, S. 22287–22292. <http://dx.doi.org/10.1073/pnas.0907866106>. – DOI 10.1073/pnas.0907866106
- [37] DOBRO, Megan J. ; MELANSON, Linda A. ; JENSEN, Grant J. ; MCDOWALL, Alasdair W.: Plunge Freezing for Electron Cryomicroscopy. Version:2010. [http://dx.doi.org/10.1016/s0076-6879\(10\)81003-1](http://dx.doi.org/10.1016/s0076-6879(10)81003-1). In: *Methods in Enzymology*. Elsevier, 2010. – DOI 10.1016/s0076-6879(10)81003-1, S. 63–82
- [38] TIVOL, William F. ; BRIEGEL, Ariane ; JENSEN, Grant J.: An Improved Cryogen for Plunge Freezing. In: *Microscopy and Microanalysis* 14 (2008), September, Nr. 5, S. 375–379. <http://dx.doi.org/10.1017/s1431927608080781>. – DOI 10.1017/s1431927608080781
- [39] MEJIA, Yara X. ; FEINDT, Holger ; ZHANG, Dongfeng ; STELTENKAMP, Siegfried ; BURG, Thomas P.: Microfluidic cryofixation for correlative microscopy. In: *Lab Chip* 14 (2014), Nr. 17, S. 3281–3284. <http://dx.doi.org/10.1039/c4lc00333k>. – DOI 10.1039/c4lc00333k
- [40] KAUFMANN, Rainer ; DUONG, Vi Q. ; FALCKENHAYN, Julian: Fluorescence cryo-microscopy. Version: Mai 2021. <http://dx.doi.org/10.1088/978-0-7503-3059-6ch6>. In: *Imaging Modalities for Biological and Preclinical Research: A Compendium, Volume 1: Part I: Ex vivo biological imaging*. IOP Publishing, Mai 2021. – DOI 10.1088/978-0-7503-3059-6ch6
- [41] McDONALD, Kent L.: Out with the old and in with the new: rapid specimen preparation procedures for electron microscopy of sectioned biological material. In: *Protoplasma* 251 (2013), November, Nr. 2, S. 429–448. <http://dx.doi.org/10.1007/s00709-013-0575-y>. – DOI 10.1007/s00709-013-0575-y

- [42] LUČIĆ, Vladan ; FÖRSTER, Friedrich ; BAUMEISTER, Wolfgang: STRUCTURAL STUDIES BY ELECTRON TOMOGRAPHY: From Cells to Molecules. In: *Annual Review of Biochemistry* 74 (2005), Juni, Nr. 1, S. 833–865. <http://dx.doi.org/10.1146/annurev.biochem.73.011303.074112>. – DOI 10.1146/annurev.biochem.73.011303.074112
- [43] LUČIĆ, Vladan ; RIGORT, Alexander ; BAUMEISTER, Wolfgang: Cryo-electron tomography: The challenge of doing structural biology in situ. In: *Journal of Cell Biology* 202 (2013), August, Nr. 3, S. 407–419. <http://dx.doi.org/10.1083/jcb.201304193>. – DOI 10.1083/jcb.201304193
- [44] MARKO, M. ; HSIEH, C. ; MOBERLYCHAN, W. ; MANNELLA, C. A. ; FRANK, J.: Focused ion beam milling of vitreous water: prospects for an alternative to cryo-ultramicrotomy of frozen-hydrated biological samples. In: *Journal of Microscopy* 222 (2006), April, Nr. 1, S. 42–47. <http://dx.doi.org/10.1111/j.1365-2818.2006.01567.x>. – DOI 10.1111/j.1365-2818.2006.01567.x
- [45] RIGORT, Alexander ; PLITZKO, Jürgen M.: Cryo-focused-ion-beam applications in structural biology. In: *Archives of Biochemistry and Biophysics* 581 (2015), September, S. 122–130. <http://dx.doi.org/10.1016/j.abb.2015.02.009>. – DOI 10.1016/j.abb.2015.02.009
- [46] UTAH, Advanced Microscopy U.: *Electron Microscopy Tutorial*. <https://advanced-microscopy.utah.edu/education/electron-micro/>. Version:2011
- [47] MOERNER, W. E. ; ORRIT, Michel: Illuminating Single Molecules in Condensed Matter. In: *Science* 283 (1999), März, Nr. 5408, S. 1670–1676. <http://dx.doi.org/10.1126/science.283.5408.1670>. – DOI 10.1126/science.283.5408.1670
- [48] KAUFMANN, Rainer ; HAGEN, Christoph ; GRÜNEWALD, Kay: Fluorescence cryo-microscopy: current challenges and prospects. In: *Current opinion in chemical biology* 20 (2014), S. 86–91
- [49] LAKOWICZ, Joseph R.: *Principles of Fluorescence Spectroscopy*. Springer-Verlag GmbH, 2007 [https://www.ebook.de/de/product/19111410/joseph\\_r\\_lakowicz\\_principles\\_of\\_fluorescence\\_spectroscopy.html](https://www.ebook.de/de/product/19111410/joseph_r_lakowicz_principles_of_fluorescence_spectroscopy.html). – ISBN 9780387463124
- [50] KEILIN, D. ; HARTREE, E. F.: Effect of Low Temperature on the Absorption Spectra of Hæmoproteins with Observations on the Absorption Spectrum of Oxygen. In: *Nature* 164 (1949), August, Nr. 4163, S. 254–259. <http://dx.doi.org/10.1038/164254a0>. – DOI 10.1038/164254a0

- [51] STÜBNER, Markus ; SCHELLENBERG, Peter: Low-Temperature Photochemistry and Photodynamics of the Chromophore of Green Fluorescent Protein (GFP). In: *The Journal of Physical Chemistry A* 107 (2003), Februar, Nr. 9, S. 1246–1252. <http://dx.doi.org/10.1021/jp027038d>. – DOI 10.1021/jp027038d
- [52] ENDERLEIN, Joerg ; TOPRAK, Erdal ; SELVIN, Paul R.: Polarization effect on position accuracy of fluorophore localization. In: *Optics Express* 14 (2006), Nr. 18, S. 8111. <http://dx.doi.org/10.1364/oe.14.008111>. – DOI 10.1364/oe.14.008111
- [53] GISKE, Arnold: *CryoSTED microscopy - a new spectroscopic approach for improving the resolution of STED microscopy using low temperature*, Universität Heidelberg, Diss., 2008. <http://dx.doi.org/10.11588/HEIDOK.00007969>. – DOI 10.11588/HEIDOK.00007969
- [54] MAO, B. ; TSUDA, M. ; EBREY, T.G. ; AKITA, H. ; BALOGH-NAIR, V. ; NAKANISHI, K.: Flash photolysis and low temperature photochemistry of bovine rhodopsin with a fixed 11-ene. In: *Biophysical Journal* 35 (1981), August, Nr. 2, S. 543–546. [http://dx.doi.org/10.1016/s0006-3495\(81\)84809-6](http://dx.doi.org/10.1016/s0006-3495(81)84809-6). – DOI 10.1016/s0006-3495(81)84809-6
- [55] CREEMERS, T. M. H. ; LOCK, A. J. ; SUBRAMANIAM, V. ; JOVIN, T. M. ; VÖLKER, S.: Photophysics and optical switching in green fluorescent protein mutants. In: *Proceedings of the National Academy of Sciences* 97 (2000), März, Nr. 7, S. 2974–2978. <http://dx.doi.org/10.1073/pnas.97.7.2974>. – DOI 10.1073/pnas.97.7.2974
- [56] FARO, Aline R. ; ADAM, Virgile ; CARPENTIER, Philippe ; DARNAULT, Claudine ; BOURGEOIS, Dominique ; ROSNY, Eve de: Low-temperature switching by photoinduced protonation in photochromic fluorescent proteins. In: *Photochemical & Photobiological Sciences* 9 (2010), Nr. 2, S. 254–262
- [57] ZONDERVAN, Rob ; KULZER, Florian ; KOL'CHENK, Mikhail A. ; ORRIT, Michel: Photobleaching of Rhodamine 6G in Poly(vinyl alcohol) at the Ensemble and Single-Molecule Levels. In: *The Journal of Physical Chemistry A* 108 (2004), Februar, Nr. 10, S. 1657–1665. <http://dx.doi.org/10.1021/jp037222e>. – DOI 10.1021/jp037222e
- [58] DEROSIER, David J.: Where in the cell is my protein? In: *Quarterly Reviews of Biophysics* 54 (2021). <http://dx.doi.org/10.1017/s003358352100007x>. – DOI 10.1017/s003358352100007x
- [59] M.A., Le G. ; MCDERMOTT, G. ; UCHIDA, M. ; KNOECHEL, C. G. ; LARABELL, C. A.: High-aperture cryogenic light microscopy. In: *Journal of Microscopy* 235 (2009), Juli, Nr. 1, S. 1–8. <http://dx.doi.org/10.1111/j.1365-2818.2009.03184.x>. – DOI 10.1111/j.1365-2818.2009.03184.x

- [60] NAHMANI, Marc ; LANAHAN, Conor ; DEROSIER, David ; TURRIGIANO, Gina G.: High-numerical-aperture cryogenic light microscopy for increased precision of super-resolution reconstructions. In: *Proceedings of the National Academy of Sciences* 114 (2017), März, Nr. 15, S. 3832–3836. <http://dx.doi.org/10.1073/pnas.1618206114>. – DOI 10.1073/pnas.1618206114
- [61] FAORO, Raffaele ; BASSU, Margherita ; MEJIA, Yara X. ; STEPHAN, Till ; DUDANI, Nikunj ; BOEKER, Christian ; JAKOBS, Stefan ; BURG, Thomas P.: Aberration-corrected cryoimmersion light microscopy. In: *Proceedings of the National Academy of Sciences* 115 (2018), Januar, Nr. 6, S. 1204–1209. <http://dx.doi.org/10.1073/pnas.1717282115>. – DOI 10.1073/pnas.1717282115
- [62] LI, Weixing ; STEIN, Simon C. ; GREGOR, Ingo ; ENDERLEIN, Jörg: Ultra-stable and versatile widefield cryo-fluorescence microscope for single-molecule localization with sub-nanometer accuracy. In: *Optics express* 23 (2015), Nr. 3, S. 3770–3783
- [63] WOLFF, Georg ; HAGEN, Christoph ; GRÜNEWALD, Kay ; KAUFMANN, Rainer: Towards correlative super-resolution fluorescence and electron cryo-microscopy. In: *Biology of the cell* 108 (2016), Nr. 9, S. 245–258
- [64] MOSER, Felipe ; PRAŽÁK, Vojtěch ; MORDHORST, Valerie ; ANDRADE, Débora M. ; BAKER, Lindsay A. ; HAGEN, Christoph ; GRÜNEWALD, Kay ; KAUFMANN, Rainer: Cryo-SOFI enabling low-dose super-resolution correlative light and electron cryo-microscopy. In: *Proceedings of the National Academy of Sciences* 116 (2019), Februar, Nr. 11, S. 4804–4809. <http://dx.doi.org/10.1073/pnas.1810690116>. – DOI 10.1073/pnas.1810690116
- [65] MARKO, Michael ; HSIEH, Chyongere ; SCHALEK, Richard ; FRANK, Joachim ; MANNELLA, Carmen: Focused-ion-beam thinning of frozen-hydrated biological specimens for cryo-electron microscopy. In: *Nature Methods* 4 (2007), Februar, Nr. 3, S. 215–217. <http://dx.doi.org/10.1038/nmeth1014>. – DOI 10.1038/nmeth1014
- [66] SCHERMELLEH, Lothar ; FERRAND, Alexia ; HUSER, Thomas ; EGGELING, Christian ; SAUER, Markus ; BIEHLMAIER, Oliver ; DRUMMEN, Gregor P. C.: Super-resolution microscopy demystified. In: *Nature Cell Biology* 21 (2019), Januar, Nr. 1, S. 72–84. <http://dx.doi.org/10.1038/s41556-018-0251-8>. – DOI 10.1038/s41556-018-0251-8
- [67] GIRSAULT, Arik ; LUKES, Tomas ; SHARIPOV, Azat ; GEISSBUEHLER, Stefan ; LEUTENEGGER, Marcel ; VANDENBERG, Wim ; DEDECKER, Peter ; HOFKENS, Johan ; LASSER, Theo: SOFI Simulation Tool: A Software Package for Simulating and Testing Super-Resolution Optical Fluctuation Imaging. In: *PLOS ONE* 11 (2016), September, Nr. 9, S. e0161602. <http://dx.doi.org/10.1371/journal.pone.0161602>. – DOI 10.1371/journal.pone.0161602

- [68] BÖNING, Daniel ; WIESER, Franz-Ferdinand ; SANDOGHDAR, Vahid: Polarization-encoded co-localization microscopy at cryogenic temperatures. (2020)
- [69] LEE, Steven F. ; VÉROLET, Quentin ; FÜRSTENBERG, Alexandre: Improved Super-Resolution Microscopy with Oxazine Fluorophores in Heavy Water. In: *Angewandte Chemie International Edition* 52 (2013), Juli, Nr. 34, S. 8948–8951. <http://dx.doi.org/10.1002/anie.201302341>. – DOI 10.1002/anie.201302341
- [70] ZONG, Shenfei ; PAN, Fengmei ; ZHANG, Ruohu ; CHEN, Chen ; WANG, Zhuyuan ; CUI, Yiping: Super blinking and biocompatible nanoprobe based on dye doped BSA nanoparticles for super resolution imaging. In: *Nanotechnology* 30 (2018), Dezember, Nr. 6, S. 065701. <http://dx.doi.org/10.1088/1361-6528/aaf03b>. – DOI 10.1088/1361-6528/aaf03b
- [71] JESSEN, Brian: *Synthese von BSA-Nanopartikeln dotiert mit organischen Farbstoffmolekülen und deren Charakterisierung unter kryogenen Bedingungen*, Universität Hamburg, Diplomarbeit, 2021
- [72] CHAUDHRY, Nayab M.: *Investigation of photo-physical properties of fluorescent proteins under cryo conditions in a biological context*, Universität Hamburg, Diplomarbeit, 2022
- [73] BRANDT, Yannik: *Autokorrelationsanalyse transienter Fluoreszenzzustände einzelner Moleküle unter kryogenen Bedingungen*, Universität Hamburg, Diplomarbeit, 2021
- [74] RIES, Jonas ; KAPLAN, Charlotte ; PLATONOVA, Evgenia ; EGHLE, Hadi ; EWERS, Helge: A simple, versatile method for GFP-based super-resolution microscopy via nanobodies. In: *Nature Methods* 9 (2012), April, Nr. 6, S. 582–584. <http://dx.doi.org/10.1038/nmeth.1991>. – DOI 10.1038/nmeth.1991



## A. Danksagung

Ich möchte mich bei allen bedanken, die zu dieser Arbeit beigetragen haben:

Prof. Dr. Rainer Kaufmann, der mich als Doktorand aufgenommen hat und immer geduldig und unterstützend, egal was war.

Prof. Dr. Arwen Pearson, die ohne zu zögern das Zweitgutachten für diese Arbeit übernommen hat.

Prof. Dr. Kay Grünewald, ohne ihn das Projekt so nicht möglich gewesen wäre.

Julian Falckenhayn, meinen Arbeitskollegen, wodurch die Zeit viel anregender war.

Rene Rosch und Karin Ruban, die zusammen mit mir durch dick und dünn gegangen sind.

Julia Sandberg, mit der ich auch über die schweren Zeiten lachen konnte.

Tim Laugks, der genauso enthusiastisch ist wie ich.

Brian und Nayab, mit denen ich eine wundervolle Zeit verbracht hat.

Jelena und Fereshta, für die gute Zusammenarbeit.

Tien Truong für die Unterstützung.

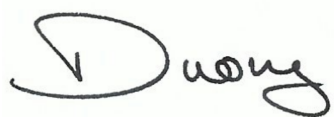
Dr. med. Lisa Schmitz, ohne die ich nicht mehr wäre.

Hanna, weil sie die beste Schwester der Welt ist.

Und meinen Eltern, ohne deren Unterstützung es nie möglich gewesen wäre.

## B. Erklärung

Hiermit versichere ich an Eides statt, die vorliegende Dissertationsschrift selbst verfasst und keine anderen als die angegebenen Hilfsmittel und Quellen benutzt zu haben.



Hamburg, 26th October 2023